POLITECNICO DI TORINO

Collegio di Ingegneria Chimica e dei Materiali

Corso di Laurea Magistrale

in Ingegneria dei Materiali

Tesi di Laurea Magistrale

Multiple graphene synthesis from pre-dissolved carbon resource in CuNi alloy

Relatori

prof. Marco Sangermano

prof. Jie Sun

Candidato

Andrea Fazi

Ottobre 2018

Index

List of Figures

List of Tables

List of Abbreviations

CVD	Chemical Vapour Deposition
EG	Epitaxial Graphene
FCC	Face-Centred Cubic
GO	Graphene Oxide
HCP	Hexagonal Closed-Packed
ITO	Indium-Tin Oxide
LIB	Lithium Ions Battery
MOSFET	Metal Oxide Silicon Field Effect Transistor
PECVD	Plasma Enhanced Chemical Vapour Deposition
QED	Quantum Electro Dynamic
QHE	Quantum Hall Effect
RGO	Reduced Graphene Oxide
SIMS	Secondary Ions Mass Spectroscopy
UHV	Ultra-High Vacuum

Sommario

Introduzione

Il grafene, rappresentato in Figura 1, è un singolo strato di atomi di carbonio organizzati in una struttura esagonale a nido d'ape (ibridizzazione sp2), questa struttura teorizzata già negli anni cinquanta fu isolata e caratterizzata per la prima volta nel 2004[1]. Immediatamente dopo la sua scoperta, grazie alle sue straordinarie proprietà meccaniche[2], elettroniche[3] e chimiche[4], attirò l'attenzione dell'intera comunità scientifica. Ad oggi, rimane uno dei materiali più studiati dell'ultimo decennio[5,6] e sono molte le applicazioni in cui questo materiale sembra essere in grado di portare innovazione e miglioramento delle performance. Il principale campo di applicazione è quello dell'elettronica dove è stato dimostrato che è possibile fabbricare dispositivi con caratteristiche superiori, ad esempio transistor basati sul grafene[7], touchscreen[8], dissipatori di calore per circuiti integrati[9,10], LED[11], pannelli solari[12] e molti altri. In aggiunta al campo dell'elettronica, il grafene promette di rivoluzionare anche altri campi, come quello dei materiali compositi e dei biomateriali[13,14].

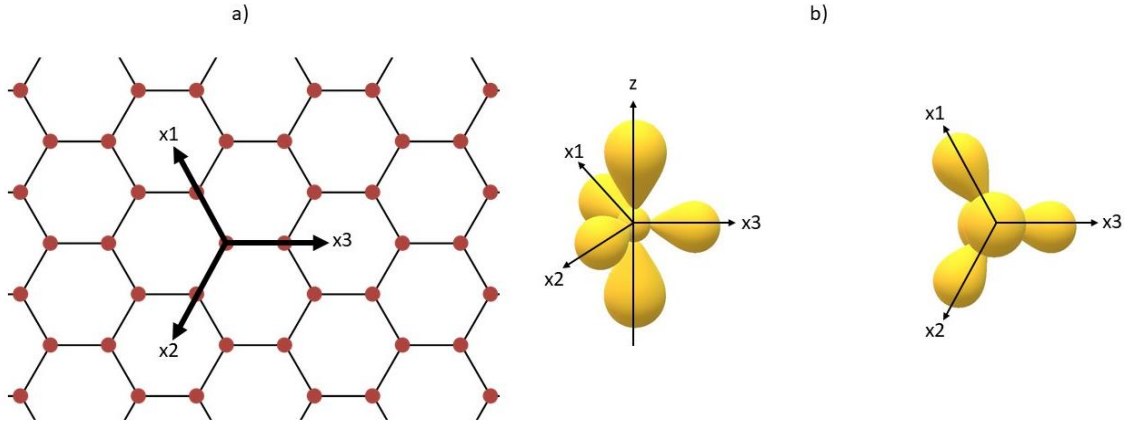

Figura 1: (a) Reticolo cristallino esagonale del grafene. (b) Ibridizzazione sp^2 degli orbitali elettronici degli atomi di carbonio che formano il monostrato di grafene.

Diversi metodi di deposizione del grafene sono stati ideati negli anni, tra questi si possono citare il cleavage meccanico, la sublimazione di SiC, chemical vapor deposition (CVD) e l'esfoliazione in fase liquida di grafite. Il metodo CVD permette di depositare grafene di alta qualità, con elevata riproducibilità e controllo del numero di strati e dimensione dei grani cristallini[15]. Per ottenere questo livello di controllo sul processo di deposizione, spesso, vengono utilizzati catalizzatori solidi nella forma di substrati metallici come Cu[16], Ni[17] e Pt[18], ogni metallo permette di ottenere caratteristiche diverse nel risultante grafene. Il rame, ad esempio, permette una deposizione controllata di 1-2 strati atomici di grafene[19], mentre il nickel ed il platino[20] catalizzano la crescita di grafene multistrato. Questi metalli possono anche essere utilizzati in leghe per ottenere caratteristiche intermedie

a quelle dei metalli puri. Alcuni esempi sono leghe Cu-Ni e Cu-Pt le quali permettono la rapida deposizione di grafene monocristallino con spessore controllabile [21,22].

In questo lavoro, una lega Cu-Ni è stata selezionata come substrato catalitico per la deposizione di grafene. La lega adottata combina la capacità del rame di catalizzare mono-strati di grafene[16] con la più elevata solubilità di carbonio nel nickel[23] che permette di immagazzinare atomi di carbonio all'interno del substrato metallico. In questo modo si studia la possibilità di depositare grafene multiple volte utilizzando lo stesso campione di foglio metallico ed un unico processo CVD. Il processo CVD viene utilizzato per immagazzinare atomi di carbonio all'interno della lega metallica, la quale viene poi successivamente sottoposta a trattamento termico ad alta temperatura. Il trattamento termico permettere a questa risorsa di atomi di carbonio immagazzinata nel foglio metallico di migrare verso la superfice a formare il grafene obbiettivo dello studio. Grazie alla elevata solubilità di carbonio nel nickel, il processo può essere ripetuto fino a quando la risorsa di carbonio non si esaurisce, permettendo di depositare grafene con successo fino a 5 volte.

Metodo

Uno schema del processo è mostrato in Figura 2. Il primo passo del metodo proposto in questo studio prevede di sottoporre un campione metallico di CuNi ad un processo CVD (Figura 2 (a) e (b)). L'obiettivo di questo step è quello di diffondere carbonio all'interno del catalizzatore metallico in modo da formare la risorsa di atomi di carbonio necessaria alla successiva produzione di grafene. Durante il processo CVD parte del carbonio proveniente dal precursore gassoso andrà a formare grafene sulla superficie del catalizzatore, è da notare che questo grafene non è di diretto interesse in questo studio ma che è stato comunque studiato come riferimento. Una volta concluso l'iniziale processo CVD, il risultante grafene è stato trasferito su di un substrato Si-SiO_2 in modo da liberare la superficie del catalizzatore metallico per i successivi step e da permettere la caratterizzazione del grafene ottenuto durante la deposizione CVD (Figura 2 (c)). Dopo aver rimosso il grafene dalla superficie del foglio metallico in CuNi, questo è pronto ad essere sottoposto al primo trattamento termico (Figura 2 (d)). Durante il trattamento termico di annealing non viene utilizzato alcun precursore gassoso del carbonio e l'unica fonte di atomi di carbonio è costituita dagli atomi in soluzione solida interstiziale nel reticolo del CuNi. Il grafene ottenuto sulla superficie del catalizzatore metallico è stato poi trasferito su un substrato in Si-SiO_2 lasciando la superficie del foglio di CuNi libera per i successivi trattamenti termici e per permettere l'analisi del grafene ottenuto (Figura 2 (e)). Questo set di operazioni è poi ripetuto nello stesso modo fino al raggiungimento del quinto trattamento termico di annealing (Figura 2 (f) e (g)).

Il processo CVD è stato condotto ad 850°C, a 6 mbar di pressione, per una durata di 10 minuti, in una atmosfera di acetilene, argon e idrogeno nel seguente rapporto: 25 sccm di H_2, 1000 sccm di Ar e 40 sccm di C_2H_2.

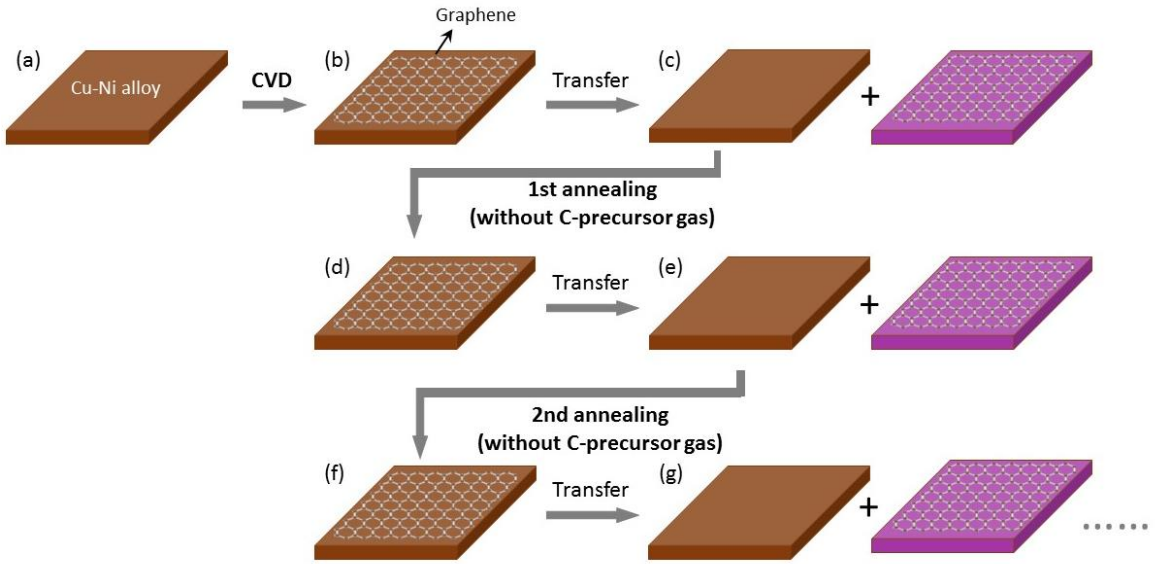

Figura 2: Rappresentazione schematica delle procedure sperimentali: (a) substrato catalitico in CuNi prima di essere processato; (b) dopo il processo CVD, il campione di CuNi risulta essere arricchito di carbonio e presenta uno strato di grafene sulla superficie; (c) il grafene viene trasferito su un substrato Si-SiO_2 (in viola), la superficie del campione di CuNi è ora libera dalla presenza del grafene ed è pronta ad essere sottoposta al primo trattamento termico; (d) durante il 1° annealing, nuovo grafene si forma sulla superficie del catalizzatore (nessun precursore gassoso del carbonio è utilizzato nel processo di annealing, gli atomi di carbonio che formano il grafene provengono dal bulk del catalizzatore); (e) dopo l'annealing, il grafene viene trasferito su un substrato Si-SiO_2 (in viola) in modo da liberare nuovamente la superficie del catalizzatore metallico; (f) il 2° annealing può essere condotto durante il quale si forma nuovamente grafene sulla superficie del catalizzatore; (g) il grafene può essere nuovamente trasferito preparando la superficie del catalizzatore metallico per i successivi trattamenti termici; la procedura viene ripetuta seguendo questo schema fino a raggiungere il 5° trattamento termico.

I trattamenti termici di annealing sono stati condotti a 850°C, 6 mbar di pressione, per una durata di 10 minuti, in una atmosfera di argon e idrogeno nel seguente rapporto: 25 sccm di H_2 e 1000 sccm di Ar. Il processo di trasferimento del grafene dai campioni di CuNi al substrato di Si-SiO_2 è stato condotto utilizzando la tecnica del electrochemical bubbling transferring[24], tecnica che ha permesso di preservare l'integrità dei campioni metallici di CuNi in modo da permettere i successivi annealing.

I campioni di catalizzatore metallico sono stati ottenuti da un figlio metallico dello spessore di 0,05 mm, tagliati in rettangoli di misura 3 cm x 4 cm. I substrati di Si-SiO_2 su cui il grafene è stato trasferito per le analisi sono stati ottenuti tramite ossidazione controllata di wafer di silicio dello spessore di 0,54 mm, lo strato di silice interessava entrambi i lati del wafer e risultava essere spesso 300 nm. Prima del processo CVD e prima di ogni step di annealing i campioni metallici utilizzati come catalizzatore per la formazione del grafene sono stati puliti dello strato di ossido superficiale e dalla presenza di altri componenti organici attraverso un bagno in acido acetico per 5 minuti seguito da un bagno in acetone per 5 minuti, risciacquo con isopropanolo e asciugatura con azoto.

I campioni di grafene ottenuti sono stati analizzati al microscopio ottico, con spettroscopia Raman e sottoposti ad una misurazione della resistività. Le immagini ottenute con la microscopia ottica sono state analizzate con ImageJ, un software di image processing che

ha permesso di valutare quantitativamente la percentuale di area coperta da grafene nei vari campioni ottenuti. Analisi al SIMS è stata effettuata sui campioni di catalizzatore metallico allo scopo di determinare il profilo di concentrazione di carbonio nel bulk del foglio di CuNi.

Risultati e discussione

Microscopia ottica

Quando trasferito su un substrato di Si-SiO_2 dove l'ossido ha uno spessore di 300 nm, il grafene diventa visibile pur essendo di spessore atomico[25]. Il contrasto di colore prodotto da ogni singolo strato di grafene è dovuto ad un effetto di interferenza tipico dei film sottili nei quali a causa di questo fenomeno, in base al loro spessore, riflettono selettivamente una specifica lunghezza d'onda. Nel caso del grafene e del substrato selezionato la variazione di colore varia dal rosa pallido, al viola ed in fine al blu ed al bianco, rispettivamente a partire da monostrato di grafene andando verso grafene multistrato e nano piastrine di grafite. Figura 3 contiene le immagini al microscopio ottico a basso ingrandimento utilizzate per ottenere informazioni sulla qualità, uniformità e distribuzione del grafene ottenuto nei vari step dell'esperimento. Colonna A contiene le immagini ottiche catturate ad ingrandimento di 5x1 senza alcuna modifica, Colonna B mostra le immagini elaborate con ImageJ per ottenere la percentuale di superficie coperta da grafene multistrato mentre Colonna C mostra le stesse immagini analizzate per evidenziare la parte di superficie non coperta da alcun film a base di carbonio. Figura 4, in aggiunta, riassume graficamente il contenuto di Figura 3. Per trarre le conclusioni sulla natura di ogni regione dei vari campioni, la spettroscopia Raman è stata usata in combinazione con la microscopia ottica in modo da poter associare uno spettro Raman ad ogni intensità di colore.

Come può essere dedotto dalle Figure 3 e 4, il processo CVD è risultato in una copertura praticamente completa (~90%) in grafene multistrato e nano placche di grafite. Il risultato era bene o male previsto, infatti il Ni è noto per catalizzare la crescita di grafene multistrato[17], inoltre le condizioni di processo erano state scelte in modo da produrre la più alta concentrazione di carbonio possibile alla superficie del catalizzatore e da garantire un elevato flusso di carbonio verso il bulk del catalizzatore metallico; andando a fornire alla superficie del catalizzatore molto più carbonio di quello necessario alla formazione di grafene monostrato. A partire dal primo annealing invece, è possibile vedere chiaramente come la diffusione sulla superficie di grafene multistrato si riduce ad una piccola porzione di superficie mentre la maggiorparte del campione risulta essere coperto da 1-3 strati di grafene. La percentuale di grafene multistrato si riduce ulteriormente con il secondo annealing fino a sparire completamente con il terzo annealing. In contrapposizione, a partire dal terzo annealing, alcune zone dei campioni analizzate risultavano non coperte da alcun grafene. L'ammontare di superfice scoperta rimane stabile per il quarto annealing ma raggiunge circa il 25% con il quinto e ultimo annealing.

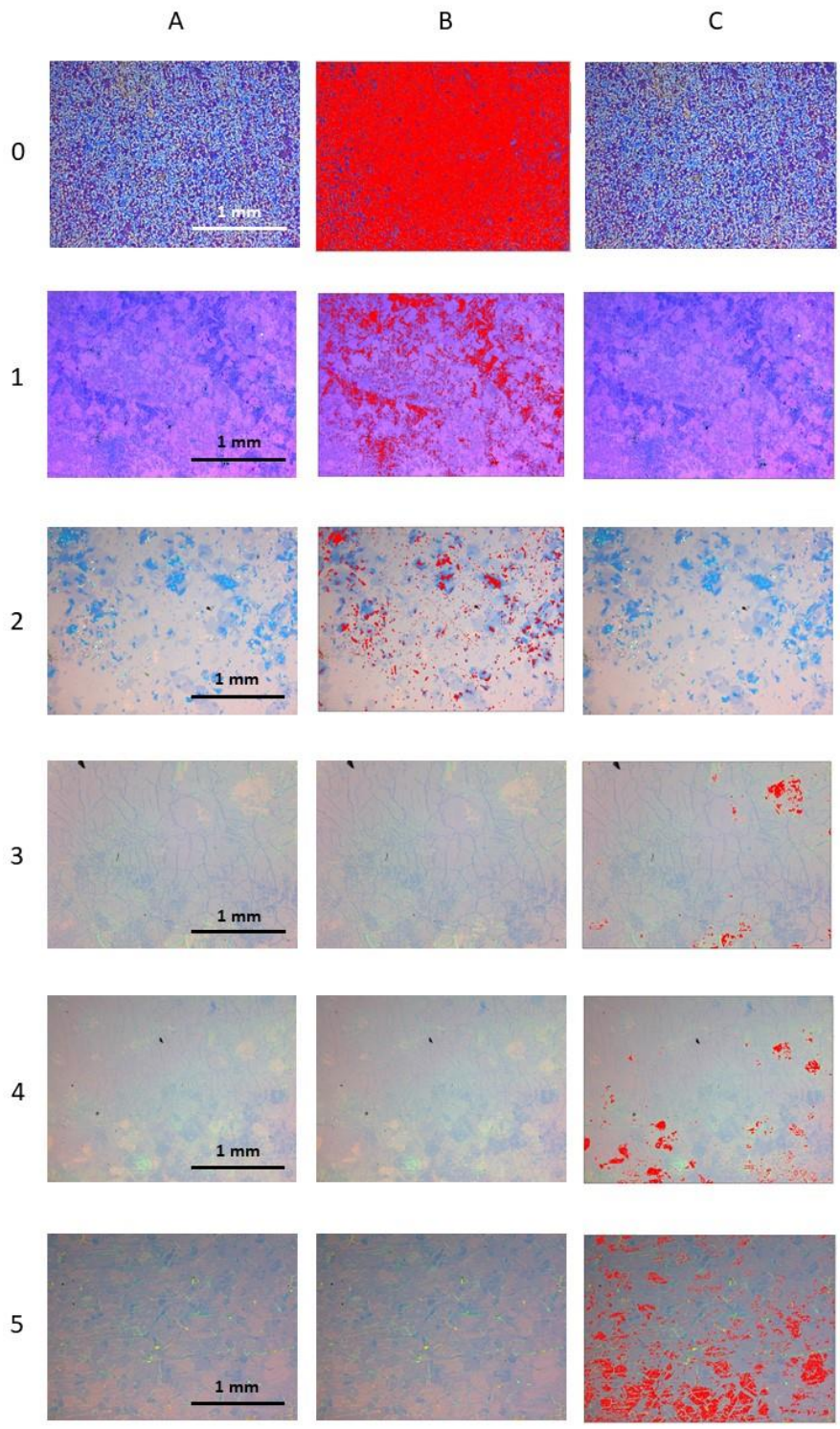

Figura 3: Colonna A: Immagini al microscopio ottico (ingrandimento 5x1) dei campioni di grafene trasferiti su Si-SiO_2. Colonna B: Immagini analizzate con ImageJ, le aree evidenziate in rosso rappresentano zone coperte da un multistrato di grafene. Colonna C: Immagini analizzate con ImageJ, le aree evidenziate in rosso rappresentano le zone prive di grafene. Riga 0: Immagini di grafene ottenuto durante il processo CVD. Rige 1 a 5: Immagini del grafene ottenuto durante i trattamenti termici, rispettivamente dal primo a quinto annealing.

In Figura 4 in particolare, può essere individuato un andamento, dal primo al quinto annealing l'area coperta da grafene multistrato diminuisce fino a sparire, in contemporanea con il terzo annealing la deposizione inizia a risultare incompleta.

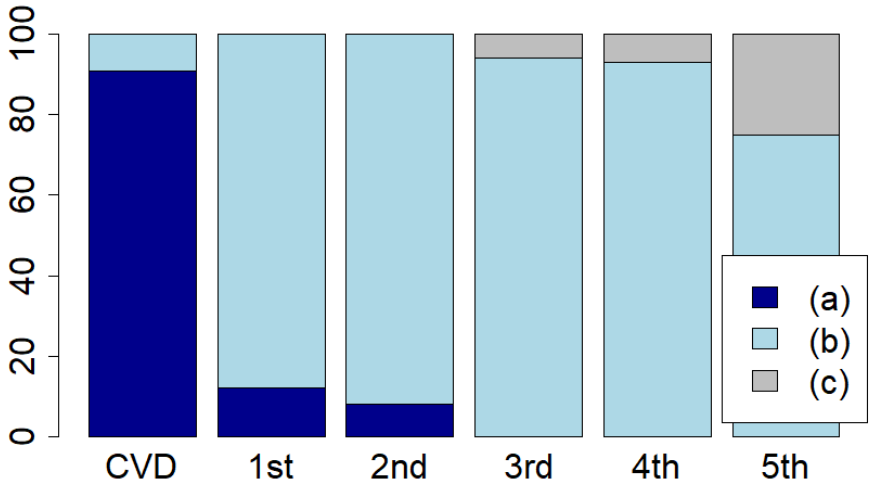

Figura 4: Grafico contenente le percentuali di superficie dove può essere trovato grafene multistrato (a), grafene monostrato (b) e superficie senza alcun grafene (c).

Questi risultati sembrano suggerire che il carbonio disponibile per la formazione di grafene sulla superficie del catalizzatore diminuisca dopo ogni trattamento termico fino al punto di non essere più in grado di fornire una deposizione di grafene completa su tutta la superficie. In particolare, raggiunto il quinto annealing, la disponibilità di carbonio sulla superficie del catalizzatore risulta insufficiente e, come si può notare in Figura 3 - Riga 5, una significativa parte della superficie non è coperta da grafene. Un'altra cosa interessante che può essere dedotta da questi dati è che, CVD a parte, ogni processo di annealing ha prodotto una deposizione omogenea di 1-3 strati di grafene e che prima del quinto annealing il film appare di alta qualità e uniforme.

Spettroscopia Raman

Per confermare la natura del grafene ottenuto e per valutarne la qualità e difettosità, ogni campione di grafene ottenuto dai vari step del processo è stato analizzato con la spettroscopia Raman. In Figura 5 è possibile vedere gli spettri relativi al grafene ottenuto durante la CVD (Figura 5 (a)) e durante ogni trattamento termico (Figura 5 da (b) a (f)). Ogni spettro presenta i picchi tipici del grafene o più in generale dei materiali a base carbonio: banda G, D e 2D, rispettivamente relative al grafene, ai difetti reticolari e al numero di strati analizzati[26]. Confrontando i risultati ottenuti dal grafene CVD e dal grafene prodotto durante il primo annealing è immediato notare come si tratti di due tipologie completamente diverse. Il grafene CVD ha una banda G molto intensa, una banda D appena visibile ed un rapporto 2D/G ~ 0,5. Queste caratteristiche si possono trovare di solito in grafene multistrato o in nano piastrine di grafite. In aggiunta, la banda 2D ha un piccolo picco secondario a sinistra del picco principale, tipico della grafite. Grazie a queste

informazioni è possibile affermare che il risultato del processo CVD è uno strato di background di grafene multistrato coperto quasi interamente da nano placche di grafite. Analizzando lo spettro del grafene prodotto durante il primo annealing è invece possibile notare come la banda 2D sia decisamente più intensa della banda G, con un rapporto 2D/G molto elevato, questo spettro è tipico di un monostrato di grafene. Si può dunque ottenere un primo dato interessante: utilizzando lo stesso substrato catalitico, il processo CVD e il proposto trattamento termico producono film completamente diversi; si dimostra inoltre che il processo di annealing fornisce grafene monostrato di alta qualità e con bassissima difettosità (picco D appena visibile).

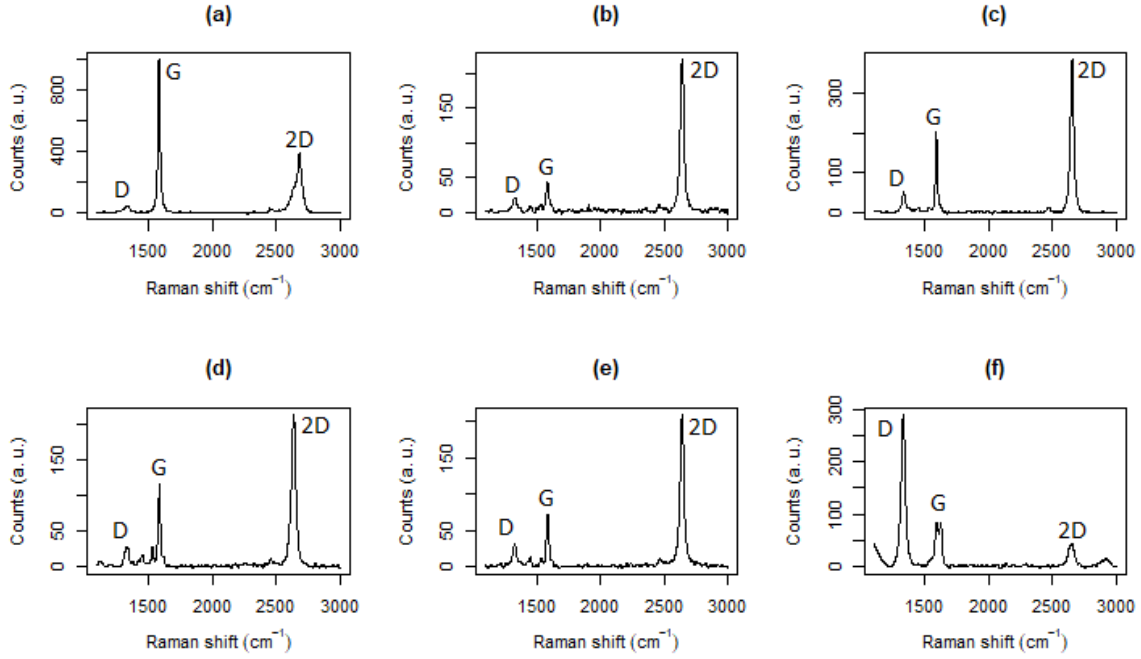

Figura 5: Risultati della spettroscopia Raman condotta su campioni di grafene trasferiti su substrato di Si-SiO_2. Il grafene analizzato è stato ottenuto durante il processo di CVD (a) e durante ogni trattamento termico, dal primo al quinto rispettivamente da (b) fino a (f).

Passando ora al confronto tra grafene ottenuto nei diversi trattamenti di annealing è possibile notare come gli spettri Raman rilevati dal primo a quarto annealing sono pressoché identici. Questo significa che lo stesso campione di substrato catalitico in CuNi è in grado di fornire un monostrato di grafene di alta qualità per più di una volta, attingendo dal solo carbonio inserito nella lega durante l'iniziale CVD. In aggiunta, la qualità del grafene rimane omogenea annealing dopo annealing fino alla quarta ripetizione del processo. Diverso è il caso del quinto annealing. Come si può notare in Figura 5, il grafene risultate dal quinto trattamento termico ha uno spettro Raman completamente diverso dai precedenti. In questo caso, è la banda D ad essere la più intensa, mentre i picchi G e 2D risultano essere di intensità molto inferiore. Questo risultato fa pensare alla presenza di un film di carbonio sulla superficie ma con difettosità cristalline estremamente elevate. Il grafene risultante dal quinto annealing è probabilmente incompleto ed altamente danneggiato.

In generale questi risultati sembrano essere in completo accordo con le immagini al microscopio ottico. I processi di annealing sono in grado di produrre grafene ripetutamente ma la risorsa di carbonio si consuma ciclo dopo ciclo, fino a quando non risulta praticamente esaurita alla quinta ripetizione.

La mappatura Raman è stata invece utilizzata per verificare sulla piccola scala, all'interno di uno stesso grano cristallino, la qualità e la omogeneità del grafene ottenuto. Figura 6 contiene i risultati della mappatura Raman condotta su un campione di grafene ottenuto durante la CVD e su un campione di grafene prodotto durante il quinto annealing. Sulla sinistra è riportata la mappatura del rapporto D/G e si può vedere che, nonostante la diversità di valori già riscontrata in precedenza, entrambi i campioni analizzati siano pressoché omogenei sull'area analizzata. Lo stesso vale per i rapporti 2D/G riportati a destra, in questo caso però possiamo notare come il campione di grafene ottenuto nel quinto trattamento termico sia leggermente meno omogeneo. In conclusione, si può dire che il grafene depositato risulta essere omogeneo, ma va notato che il grafene depositato nell'ultimo annealing risulta avere maggiori disomogeneità se confrontato con il resto dei campioni. Il risultato è in accordo con la spettroscopia Raman e la microscopia ottica. I risultati della spettroscopia Raman hanno permesso di determinare la presenza di grafene su tutti i campioni e di valutarne l'elevata qualità ed omogeneità.

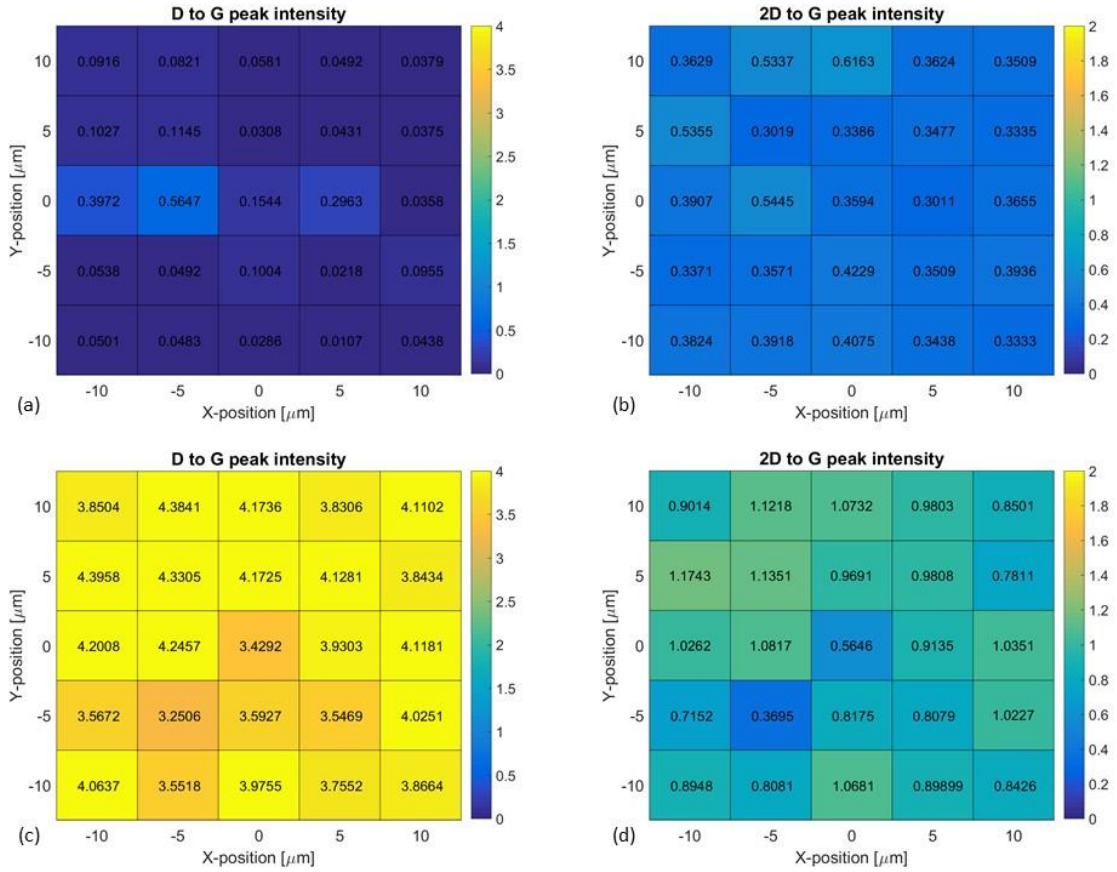

Figura 6: Risultati della mappatura Raman. (a) e (b) riportano rispettivamente i rapporti D/G e 2D/G per il grafene ottenuto durante il processo CVD; (c) e (d) riportano rispettivamente i rapporti D/G e 2D/G per il grafene ottenuto durante il quinto trattamento termico di annealing.

Resistività di superficie

Molte delle applicazioni del grafene sono in elettronica, di conseguenza, la resistività elettrica di questo film è una delle caratteristiche più importanti da misurare e da conoscere quando si analizza il grafene. Il metodo utilizzato analizzava un'area di 4mm x 1mm fornendo informazioni su un'area relativamente grande. I risultati di queste misurazioni sono contenuti in Figura 7. Ancora una volta è possibile individuare una chiara tendenza. Il grafene CVD, che dalle analisi combinate al microscopio e spettroscopia Raman possiamo ora affermare essere un discontinuo film sottile di grafite depositato sopra un continuo multistrato di grafene, è risultato avere una resistività di superficie di ~ 0,6 kΩ. Il grafene estratto durante i trattamenti termici invece, essendo molto più sottile, ha una resistività di superficie di circa ~ 25kΩ. La differenza di conduttività è ragionevole specialmente se si considera il ruolo dello spessore del film: il film depositato durante la CVD ha un numero di strato di grafene qualche decina di volte superiore al mono- o bistrato di grafene ottenuto durante gli annealing. La resistività misurata per il monostrato di grafene ottenuto nei primi tre annealing è tipica di un grafene di qualità medio-alta.

In aggiunta, è possibile notare come la resistività rimanga costante attorno ai 25 kΩ fino al terzo annealing. A partire dal quarto processo, la resistività del film inizia a salire fino a duplicarsi nel caso del grafene ottenuto nel quinto annealing. Questo risultato è una ulteriore conferma alla presunta dinamica di processo: durante i primi trattamenti termici l'abbondanza di atomi di carbonio è sufficiente a garantire la formazione di strati completi di grafene, avvicinandosi al quinto annealing però il carbonio inizia a scarseggiare fino ad essere insufficiente; nell'ultimo annealing infatti la deposizione di grafene risulta essere incompleta.

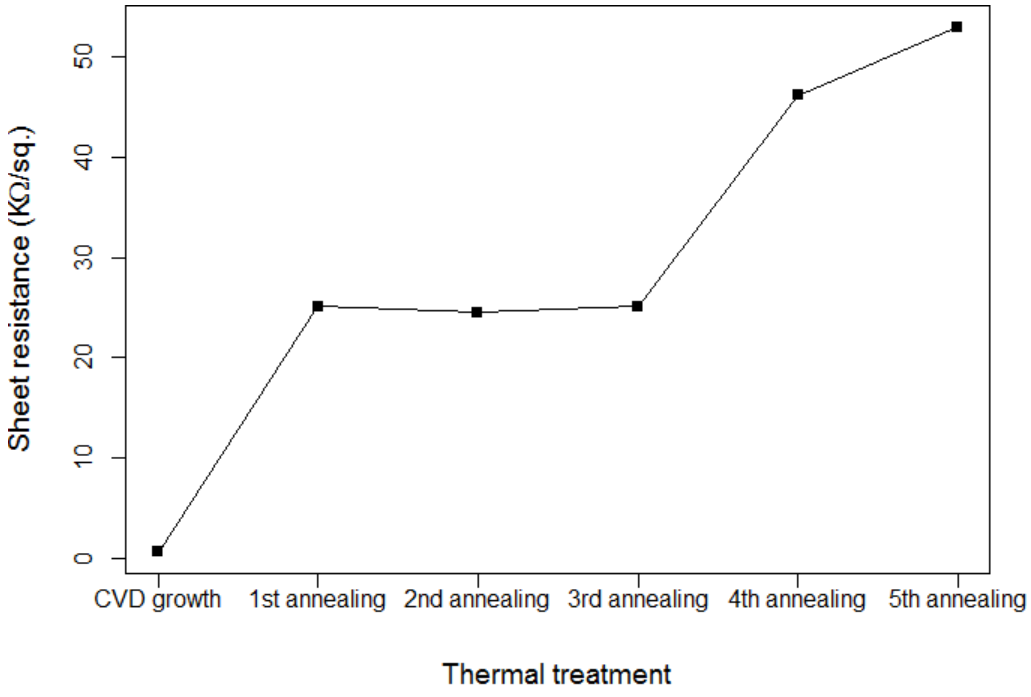

Figura 7: Risultati della misura di resistività elettrica del film di grafene ottenuto durante il processo CVD e durante ogni annealing step.

Analisi SIMS (Secondary ions mass spectroscopy)

Dall'analisi dei campioni di grafene è stato possibili identificate un trend tra i vari step di annealing. Da tutte le analisi è apparso che il metodo di sintesi del grafene attraverso annealing di una lega CuNi pre-arricchita di carbonio produce grafene di alta qualità, che può essere ripetuto più volte, ma che dopo un certo numero di ripetizioni l'esaurimento della risorsa di carbonio impedisce una deposizione completa. Per studiare il processo di esaurimento della risorsa di carbonio, dopo ogni step, uno dei campioni di catalizzatore CuNi è stato prelevato ed analizzato al SIMS. L'obiettivo di questa analisi era quello di individuare l'andamento della concentrazione di carbonio all'interno del catalizzatore metallico attraverso l'intero processo e verificarne il consumo. Il risultato dell'analisi al SIMS è riportato in Figura 8. Come è possibile notare dal grafico, la concentrazione di carbonio dopo il trattamento CVD risulta essere di 0,58 at.%, questa concentrazione iniziale decresce linearmente con il numero di annealing a cui il foglio metallico è sottoposto fino a raggiungere 0,42 at.% dopo la terza ripetizione. Una volta raggiunto questo valore, la concentrazione di carbonio si stabilizza raggiungendo un plateau.

La solubilità teorica di carbonio a 1000°C nel Cu e nel Ni è rispettivamente di 0,0027 at.%[19] e di 1,26 at.%[23]. La lega utilizzata (50% Cu e 50% Ni) ha quindi una solubilità teorica di carbonio a 1000°C di 0,6313 at.% (1,26 x 0,5 + 0,0027 x 0,5). Il processo CVD è stato condotto a 850°C e la solubilità a quella temperatura è leggermente inferiore. A temperatura ambiente la solubilità sarà ulteriormente inferiore. Considerando però il rapido raffreddamento, le condizioni non saranno di equilibrio.

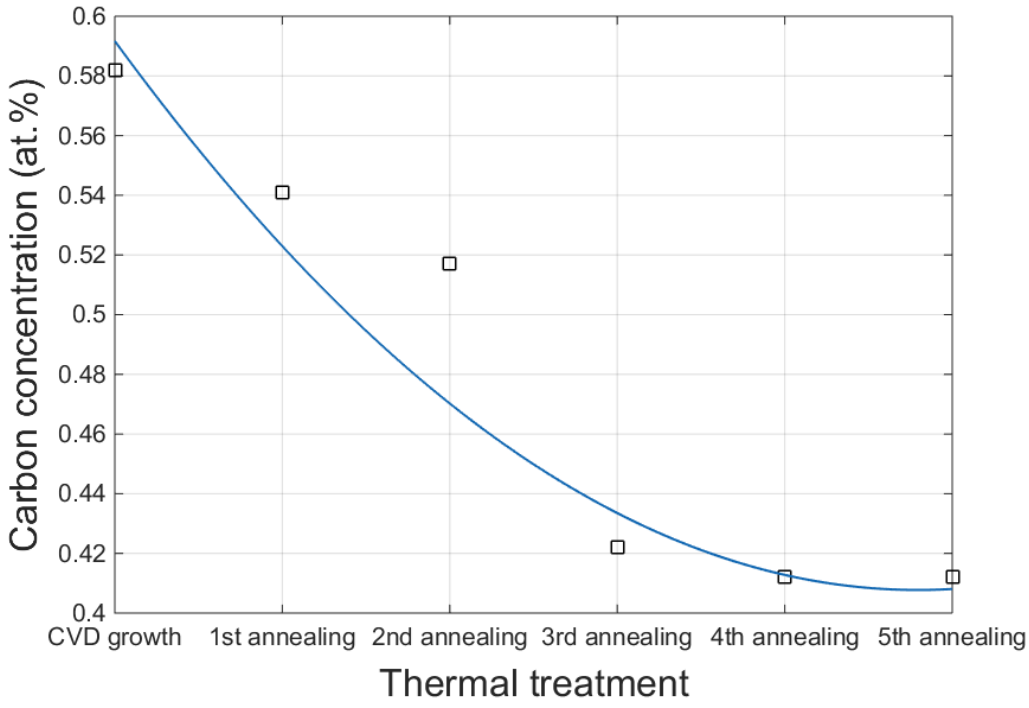

Figura 8: Risultati dell'analisi al SIMS, il grafico riporta l'andamento della concentrazione di carbonio nel catalizzatore metallico sottoposto ai vari step del processo.

Tenendo in considerazione i risultati del SIMS e la solubilità teorica, è possibile proporre un modello per il processo di deposizione durante gli annealing. Dopo il processo CVD la concentrazione di carbonio è 0,58 at.%, prossima a quella di saturazione nella lega di 0,63 at.%, il rapido raffreddamento che segue il processo CVD congela il reticolo cristallino intrappolando il carbonio all'interno della foglio metallico. Quando il foglio metallico viene scaldato nuovamente a 850°C gli atomi di carbonio sono nuovamente in grado di diffondere, durante l'annealing però, la solubilità di carbonio nella lega è sufficientemente alta e la soluzione solida non risulta essere sovrasatura, il flusso di atomi di carbonio sarà unicamente dovuto alla differenza di concentrazione tra il bulk e la superficie (che può essere considerato non troppo elevato). Durante il raffreddamento, la solubilità del carbonio nella lega inizia a diminuire ed il carbonio è spinto verso l'esterno del foglio metallico provocando un grande afflusso di atomi di carbonio alla superficie. Questi atomi di carbonio sulla superficie si organizzano a formare grafene, catalizzati dallo stesso substrato catalitico. Una volta raggiunta una temperatura sufficientemente bassa da impedire la diffusione, la situazione viene nuovamente congelata. Ad ogni ciclo, la concentrazione di carbonio nella lega diminuirà, come mostrato dall'analisi al SIMS, fino a raggiungere un livello prossimo alla solubilità del carbonio nella lega a temperatura ambiente. Una volta raggiunto questo valore, come riscontrato nell'esperimento riportato, durante il raffreddamento non vi sarà più alcuna forza spingente a provocare il flusso di carbonio verso l'esterno del foglio metallico, l'unica forza spingente sarà la differenza di concentrazione tra superficie e bulk. Un modello semplificato di questo fenomeno è rappresentato in Figura 9. In conclusione, i risultati del SIMS confermano che la forza spingente che permette al carbonio di diffondere verso l'esterno del foglio metallico di CuNi è una sovrasaturazione della soluzione solida interstiziale. In aggiunta, una volta raggiunto il plateau di concentrazione, il flusso di atomi di carbonio che diffonde verso la superficie è ancora presente (a causa della differenza di concentrazione) ma non è sufficiente a garantire una deposizione completa di grafene.

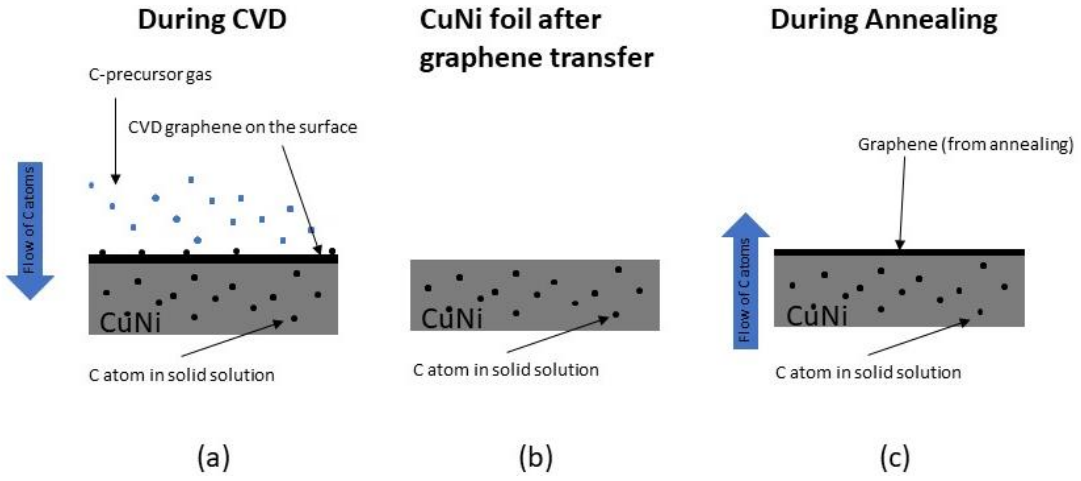

Figura 9: Modello proposto per il meccanismo di crescita del grafene durante i vari trattamenti termici. (a) Durante il processo CVD il precursore gassoso si decompone sulla superficie del catalizzatore metallico e gli atomi di carbonio diffondono nella lega di Cu-Ni andando a formare una risorsa di atomi di carbonio (b). Durante il processo di annealing termico (c), l'elevata temperatura permette agli atomi di carbonio di diffondere verso la superficie del catalizzatore metallico dove si riorganizzano a formare grafene.

Conclusioni

Si è dimostrato che sottoponendo una lega di CuNi precedentemente arricchita di carbonio ad un trattamento termico di annealing è possibile depositare ripetutamente grafene di alta qualità.

Questa tecnica è innovativa e potrebbe cambiare il modo in cui la produzione di grafene è generalmente concepita, rendendo più facile lo stoccaggio a lungo termine di grafene ed il suo utilizzo in un contesto industriale. Uno dei problemi principali del grafene è che non è possibile passivarlo efficacemente, la mancanza di passivazione rende il grafene suscettibile a modifiche delle sue proprietà e caratteristiche nel tempo attraverso adsorbimento chimico e fisico di molecole provenienti dall'atmosfera e dall'ambiente circostante. Il metodo proposto in questo studio renderebbe possibile ad una ditta che si concentra sulla produzione di grafene la preparazione di fogli metallici sottili precedentemente arricchiti di carbonio. Questi fogli potrebbero poi essere venduti singolarmente o nella forma di coil, stoccati in normali magazzini senza grosse limitazioni né sul deterioramento nel tempo e tantomeno sulle condizioni ambientali. Quando necessario, la compagnia che si occupa della produzione di dispositivi basati sul grafene avrebbe unicamente da prelevare la quantità necessaria di foglio metallico, sottoporlo a trattamento termico per poi trasferire il grafene ottenuto sul substrato di interesse. La possibilità di ripetere il processo di annealing permette inoltre di ottenere maggiori quantitativi di grafene dalla stessa quantità di foglio metallico riducendo lo spazio necessario per lo stoccaggio ed il costo associato al catalizzatore metallico. In aggiunta, lo stesso processo potrebbe teoricamente funzionare a pressione ambiente in atmosfera controllata, rendendo il trattamento termico ancora più economico e scalabile.

Da un punto di vista scientifico, questo studio permette di comprendere in modo più approfondito la dinamica di formazione del grafene sulla superficie di catalizzatori metallici, fornendo interessanti informazioni sul ruolo del catalizzatore e delle condizioni di processo. In linea teorica, questo metodo può essere applicato facilmente a molti altri substrati catalitici e a diversi materiali 2D aprendo molte possibilità per studi futuri.

Abstract

In recent years graphene has been one of most studied materials, it has drawn the attention of many scientist and research groups and the European Union has also funded a research flagship[27] on it in order to incentivise and speed up research and improvements on graphene science. Its properties have attracted specialists from almost all research field, it seems to be one of the most promising materials ever discovered in the last years[5] and there is even who hypnotises the coming of the Graphene Era[28].

As will be treated in detail in Chapter 1 of this work, graphene has many incredible and outstanding properties, but it has also few flaws that are delaying its commercialization and its actual use in everyday applications and technologies. One of the main issues is the absence of a stable passivation layer [29,30], this passivation layer is needed for many application and a lot of studies are being done on it, but no perfect solution has yet been found. In addition and in consequence to this lack, graphene storage is somehow challenging, graphene is itself chemically stable but moisture or other chemicals from the environment might be adsorbed on its surface changing its properties[31–33] making long-term preservation of graphene somehow difficult.

In this work graphene is obtained from a carbon-enriched copper-nickel alloy through high-temperature annealing. This process, described in Chapter 2, allows the deposition of graphene without the direct use of a carbon precursor gas in a simplified chemical vapour deposition process which involves the use of heat, inert gas and reducing gas only. To achieve this result, CuNi alloy is selected as catalytic substrate for graphene deposition in order to combine the ability of Cu to grow large area mono- or bi-layer graphene[16] with the capability of Ni to store carbon atoms inside the alloy substrate[23]. In this way, graphene thin films are extracted multiple times by annealing repeatedly the same metallic sample which has undergone a single initial CVD process as shown in the figure below. The obtained graphene is then transferred with bubbling transfer method[31] on a SiO_2-Si substrate and analysed.

The proposed method requires only a pre-treated CuNi foil and an annealing chamber to work. CuNi foil is easily stored and can survive unmodified for years in almost any common warehouse before being processed to produce graphene. The pre-treated CuNi foil could be sold in the form of a coil by the graphene production company to a devices manufacturer without the risk of compromising graphene quality. Storing the coil would not need special care. When required, the manufacturer could take as much of the foil as it needs for its production, it could anneal the CuNi foil *in loco* and use the obtained graphene freshly after production. To transfer the graphene obtained with this method any technique can be used, in this work bubbling transfer has been selected. Bubbling transfer method, in addition to transferring the deposited film, preserves the metallic foil allowing it to be used multiple

times, greatly increasing the quantity of graphene that can be obtained from a fixed amount of CuNi foil.

In conclusion this work demonstrates that is possible to synthetize graphene annealing a pre-enriched metallic foil made of copper-nickel alloy. This result provides deep insight in graphene formation dynamics and offer a solution to graphene long-term storage.

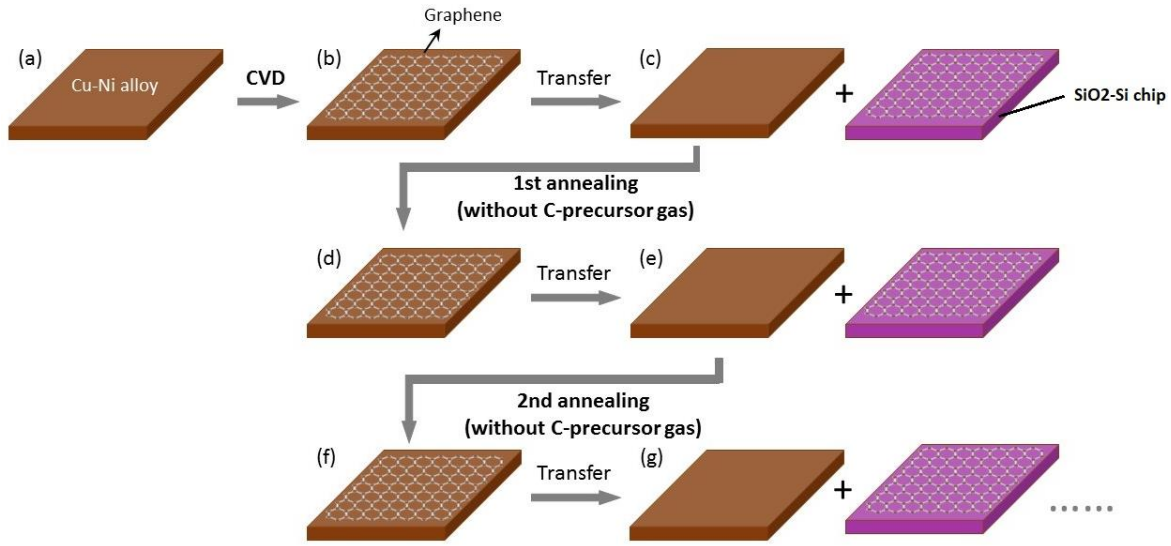

Sketch of the experimental procedures: (a) CuNi metal foil before any process; (b) CuNi metal foil covered by graphene after the thermal CVD; (c) The graphene film has been transferred on SiO2-Si substrate (purple), Now the CuNi foil is ready for the 1st annealing; (d) After the 1st annealing the CuNi foil is covered by graphene anew; (e) Again, the graphene has been transferred from CuNi to SiO2-Si substrate to prepare the CuNi metal foil for the 2nd annealing; (f) After the 2nd annealing new graphene is grown; (g) The graphene is transferred again and the whole process is repeated until the 5th annealing is reached.

1. Graphene: properties, applications and synthesis

1.1 Graphene and its properties

Graphene is a single layer of carbon atoms with sp^2 hybridization organized in a hexagonal 2D honeycomb lattice. Each layer has crystalline periodicity along the plane but, due to the sp^2 hybridization of its carbon atoms, has no primary chemical bonds on other planes or directions. Beside the absence of a covalent 3D structure, secondary bonds (van der Waals forces) might occur between different layers granting the existence of an ordered 3D crystalline structure made of stacked layers: the result is graphite. The term "graphene" describes the single layer of C-atoms, but since many variations of graphene and graphene derived materials and composites exist, the name might also be used to represent a family of materials. The remarkable properties of this material lay in the hexagonal structure (see Figure 1.1 (a)) where all carbon atoms are bonded to three neighbours, each at a 120° angle with a bond length of 1.42 Å. The sp^2 hybridization among two *p* orbitals and one *s* orbital allows the formation of three σ bonds in the three x directions shown in Figure 1.1 (b) which form a closed-shell band responsible of the robustness of the single layer. The remaining unhybridized *p* orbital of each carbon atom is oriented perpendicularly to the graphene plane and can interact with the neighbours only through a π bond to form a π band half filled with delocalized electrons, the electrons contained in this band can easily migrate along the honeycomb plane but not among different layers. In addition, graphene can be seen as the building block to form other structures, by rolling a section of a graphene plane for example it is possible to obtain other allotropes as carbon nanotubes or fullerenes and by arranging sections of graphene planes perpendicularly to a substrate vertical aligned graphene is obtained. Every form has its own peculiarity which allows the graphene-based material family to offer many different tuneable features.

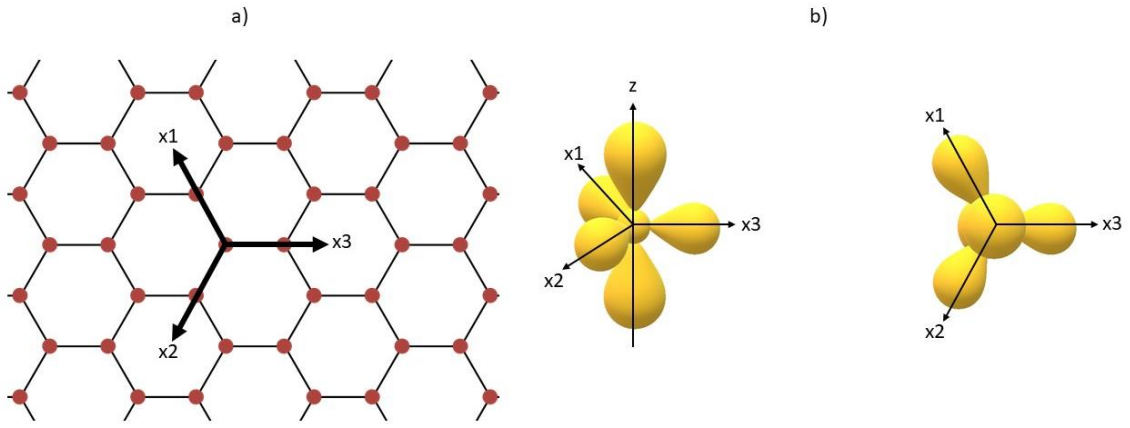

Figure 1.1: (a) Top view of a graphene honeycomb, each of the red point represent a carbon atom while the black lines corresponds to covalent bonds. (b) Representation of sp2 hybridised electron wavefunction.

From an historical point of view, the properties of the stacked crystalline structure of graphene layers has been used since the XVI century to allow writing with pencils[34]. While using a pencil, a shear force is applied to the lead, the lead is made of graphite crystals and when the shear force loads the Van der Waals bonds among graphene planes these weak bonds break and stacks of graphene are deposited on the writable surface. However, the real nature of graphite and the existence of graphene was theorized only in 1947 in a study about graphite band structure[35] and the first isolation and measurement of graphene electrical properties were made in 2004 by Andre Geim and Kostya Novoselov[1] using micromechanical cleavage to transfer graphene from a graphite crystal to a SiO2 substrate. Before 2004, the scientific community though of graphene as a theoretical material highly unstable that could not exist. Besides, after the development of the micromechanical cleavage technique and the isolation of the first 2D crystalline lattice an avalanche of discoveries in 2D materials triggered the interest of the scientific community. Graphene drawn special interest becoming one of the most studied materials of the current era. To follow in this section, the main properties of graphene are illustrated, these are then compared with other common materials to highlight why graphene is being talked so much in the scientific community in the last decade.

1.1.1 Electronic properties of pristine graphene

Graphene peculiar electrical properties were first studied in 1946 by Wallace[35], where the band structure of graphene was calculated in order to better understand graphite conductivity. These calculations, confirmed both experimentally and theoretically in the following decades[36–41], showed the unique semi-metallic characteristics of graphene and allowed to obtain band structure and electronic dispersion for this material. In Figure 1.2 a simplified version of the electronic dispersion of a single layer of graphene is depicted, of main interest is the evolution of the curve around $\mathrm{E(k)} = 0$, this region of the E vs. k space shows a linear dispersion and contains the so-called Dirac point which make graphene a peculiar semiconductor with a band gap virtually equal to zero. In graphene, the fact that there is a linear electronic dispersion means the electrons are massless. Thanks to this feature, graphene electrons resembles “relativistic” particles that moves at the fermi velocity instead of the speed of light. They can be described by the massless Dirac equation[3] opening an unique chance to probe quantum electron dynamics (QED) phenomena. As consequence of graphene QED, many interesting effects emerge, among all, those which have caught the greatest interest are the Quantum Hall Effect (QHE)[42,43] and the Klein tunnelling[3,44,45]; both effects helped to understand the physics of graphene electron transport and to further explore quantum mechanics.

At room temperature, the scarce quantity of carriers in common semiconductors is coupled with a strong electron-phonon scattering (interaction between optical phonons and electrons) which cause a sharp decrease of carrier mobility and therefore a decrease of conductivity. In graphene, the energies of optical phonons are too high to interact with the carriers and the electrons can move through the lattice with minimal momentum loss[46,47]. The small electron-phonon interactions and the fact that graphene electrons are massless

allows graphene to have an incredibly high carrier mobility[48,49] making it a perfect material for electronics and transistors.

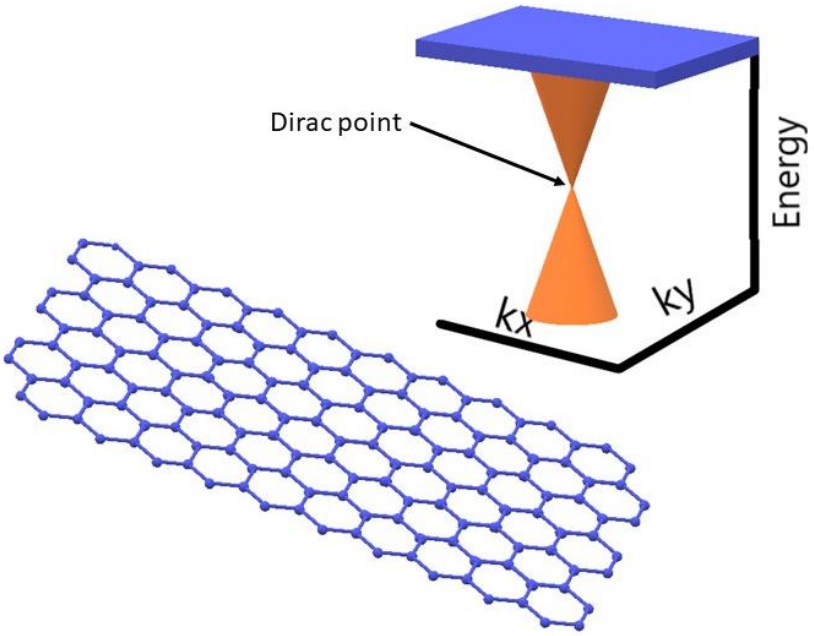

Figure 1.2: Schematic representation of graphene electron dispersion, the fermi level for graphene electrons is at the Dirac point where the two cones meet. Thanks to these peculiarity, graphene behave as a gapless semiconductor where electrons are massless.

1.1.2 Chemical and biological properties

What distinguish graphene from other materials are its 2D geometry and the atomic thickness. The confinement to the two dimensions greatly increases the surface area per unit of volume, when a 2D material reaches thicknesses of less than a nanometre, as for graphene case, all the atoms contained in the crystalline lattice are exposed to the surface and can react with the environment at which the material is exposed. In these conditions the chemistry of the surface is all that matters and physisorption, chemisorption, surface reactivity and bioreactivity become extremely important. The crystalline lattice of graphene has a 2D structure and for this reason it cannot host 3D defects, beside this fact, as all other crystalline lattices it has region or higher reactivity in correspondence of defects as single or multiple vacancies, edges of graphene layer, substitutional atoms and dislocation-like defects (See Figure 1.3)[50–53]. Defective areas represent the perfect binding site for adsorption and reactions, they provide a keyhole to an otherwise stable structure. Their presence, abundance and typology are mostly related to the method used to synthesise the films and affect the reactivity and bioreactivity of the film affecting the electronic properties as well. In addition to crystal defects, the carbon-based chemistry of graphene permits to functionalise the film with almost any kind of organic or inorganic chemical. Surface chemistry and the addition of functional groups are related to presence of heteroatoms as oxygen, nitrogen or hydrogen that work as binding site for many organic functional groups

such as carboxylic acids, lactones, phenols, aldehydes, ethers, amines and nitro compounds. In addition, more complex biochemical groups can be bounded to the surface of the graphene. These groups can be acidic, basic or neutral and strongly influence graphene chemistry and surface interactions opening many possibilities in design and optimization for catalysis, gas adsorption, drug delivery and other applications [13,50,54].

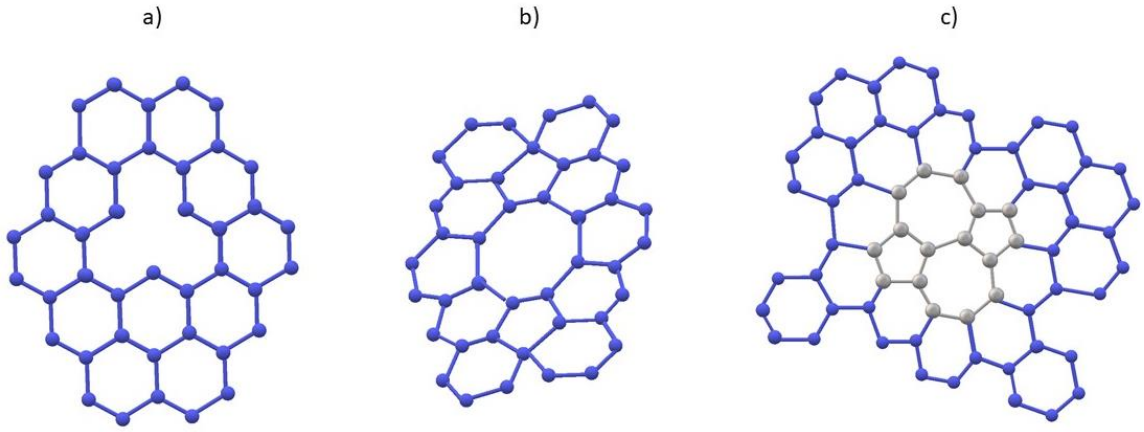

Figure 1.3: Example of most common point defects in a graphene plane. (a) Monovacancy, (b) divacancy, (c) Stone-Wales defect.

1.1.3 Mechanical, Thermal and Optical Properties

Beyond electronic and chemical properties, the atomic structures and the chemical nature of graphene express them-selves in impressive macroscopic properties as well. From the mechanical point of view graphene has a high elastic module that can vary from 0.5 to 1 TPa depending on the quality and the morphology of graphene[2], ultimate strength near the theoretical value of 126 GPa[55] and elongation before failure that can reach 20% (almost all of the elongation is due to elastic deformation) [55,56]. These outstanding properties collocate graphene among the strongest materials ever measured, in fact, the strong covalent C-C atomic bond is aligned with the graphene plane and all mechanical loads are transferred on it allowing ultimate strength 100 times higher than steel, Young's module typical of the most rigid ceramics and final elongations that compete with some polymers. However, it is crucial to keep in mind that all these mechanical properties are normalized on the thickness of the material and graphene is atomically thin. At that scale, what it is measured are the properties of a perfect single crystal without grain boundaries or other defects which help to provide exceptional properties.

In addition to outstanding mechanical properties, graphene has an extremely high thermal conductivity (3080 to 5150 W/mK) due mostly to high phonon mean free path with a small dependence from electron contribution (electron contribution to thermal conductivity is less

than 1%) [57,58]. Obviously, the high thermal conductivity is referred to in-plain heat transfer and the same feature measured transversally to the graphene layers is various order of magnitude lower.

To complete the profile of this material, one last consideration has to deal with its optical transparency: depending on the method used to produce the atomic films, their transparency ranges from 60% up to 97.7%[59,60]. This feature is rarely found in conductors and it is mainly related to the infinitely small thickness of the material, in fact, each layer of high quality graphene has an absorbance of 2.3% that stacks linearly when piling more layers[60]. Compared with other transparent conductors, graphene shows the highest transmittance, and above all, its transmittance is wavelength independent allowing for less design restrains.

1.2 Graphene applications

Graphene has many wonderful properties and it has drawn the attentions of experts from many fields for its possible applications: its uses range from electronics to composite materials and energy applications. Among all features, what makes graphene hypothetically a great material for all fields of applications is that it is potentially extremely cheap[6]. It is a carbon-based material and can be obtained from abundant and affordable resources as methane and graphite, resources that can be found in almost unlimited amounts. Its toxicity for biological beings is still in debate, but there are no dangerous chemical and biochemical reactions associated with carbon materials and, setting process residues apart, graphene biocompatibility seems to be flawless[6,61]. Both the exposed traits are fundamental when commercializing a new material and graphene might become a substitute of silicon in electronics, a reinforcement for the strongest composite materials ever designed and the foundation for brand new technologies. In the following lines some of the most important applications of graphene will be briefly described focusing on why graphene is a material of interest and what might be holding the commercialization of some of the proposed applications.

1.2.1 Graphene-based transistors

Electronic devices have become a vital part of human life and the respective market one of the more important of modern economy. At the core of this technology there is silicon and silicon-based transistors. A transistor is basically a switching unit and, in digital electronics, silicon-based complementary MOSFETs play this role and are the base unit for all integrated circuits (See Figure 1.4 (a)). They are made in fabrication laboratories that costs more than 1 billion USD to build. Huge investments were made in order to scale this technology and integrate an always higher number of transistors in miniaturised chip, but they also have some limitations. Continuing scaling the size of the transistors the on-off ration gradually reduces, the off current (static power) grows and power dissipation increase bringing to battery-life and heat management issues [62,63]. There is a significant effort in finding a new transistor design that can solve these issues and graphene appears to be a valid candidate. Graphene has higher carrier mobility that allows faster switching, it is atomically

thin which make it easier to control the gate voltage and it can be used for interconnections instead of copper reducing resistivity and circuit capacitance. All considering, a graphene transistor (Figure 1.4 (b)) would theoretically perform better and have better interconnected performances[64–66]. Graphene based electronics might substitute the current silicon-based devices [7,67,68] and the future of this application seems to be bright, but to compete with silicon-based electronics, graphene transistor design has to mature and confirm its feasibility but. On this subject, IBM scientists have shown the potential of graphene field-effect transistors building a device with an operational frequency of 10 GHz that might reach 26 GHz[69] and a lot of work is being done on the subject. Therefore, the future of electronics might be not so far.

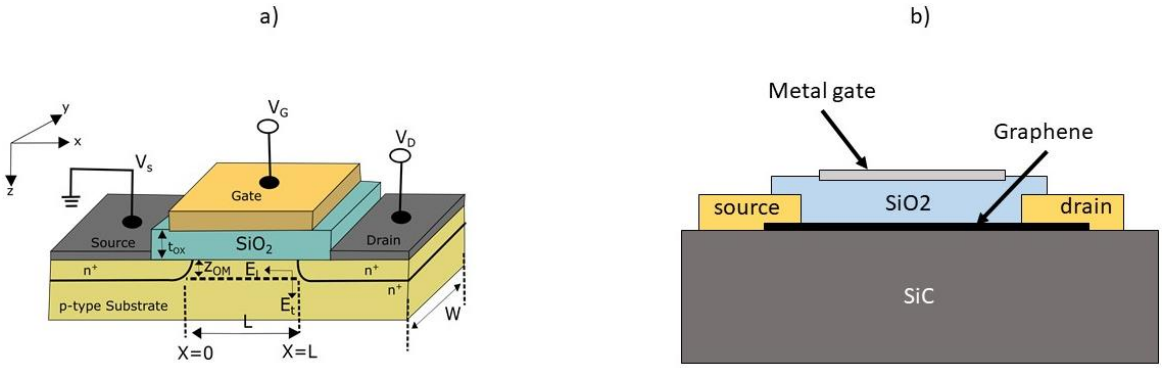

Figure 1.4: (a) Silicon-based, top-gated MOSFET design. (b) Example of graphene-based transistor, the presented design is inspired to top-gated, traditional MOSFET but it could bring some significant improvements.

1.2.2 Energy storage applications

Another important field in which graphene is having a big impact is energy storage. The diffusion of electric vehicles and wireless technology is imposing higher and more strict standards on capacitors and batteries: better yields and higher energy density is needed to reduce weight and improve battery life, allowing better performance in all vehicles and devices. Graphene based supercapacitors, for example, consist of two electrodes immersed in an electrolyte solution. They store charge by accumulating ions on the surface of the electrodes and graphene high specific surface plays the key-role in granting exceptional performances. Supercapacitor electrodes can be directly made of graphene sheets[70] or the graphene can be used to modify the surface of metal electrodes to improve their specific surface (see Figure 1.5), hence their capacitance [71]. Alternatively, graphene can be used to produce a composite together with conductive polymers obtaining a more stable polymer-based supercapacitor[72]. In all cases the presence of graphene provided a great improvement in supercapacitor capacitance and energy density, making this technology the

next generation of energy-storage devices with applications as starter for fuel efficient stop-start systems and kinetic energy recovery system.

Supercapacitors alone are not capable of solving the energy storage demand due to the relatively low energy density compared to that of batteries or fuels. Hence, another key technology that is being greatly improved in recent years are batteries. The focus with batteries is to improve the energy density, number of cycles and increase the peak current. The main used batteries for portable devices are lithium ion batteries (LIB), LIB consists of an anode, a cathode, an electrolyte and a separator. Its performances strongly depend on the structure and properties of both electrodes. In common LIB graphite is commercialized as anode material but its theoretical capacity is low and other alternatives are highly required.[73] Compared to graphite, graphene has shown a greatly higher specific capacity[74] and, combined with metals, graphene can be the base for composite materials able to improve the electrochemical performances of both electrodes in LIBs.[75–77]

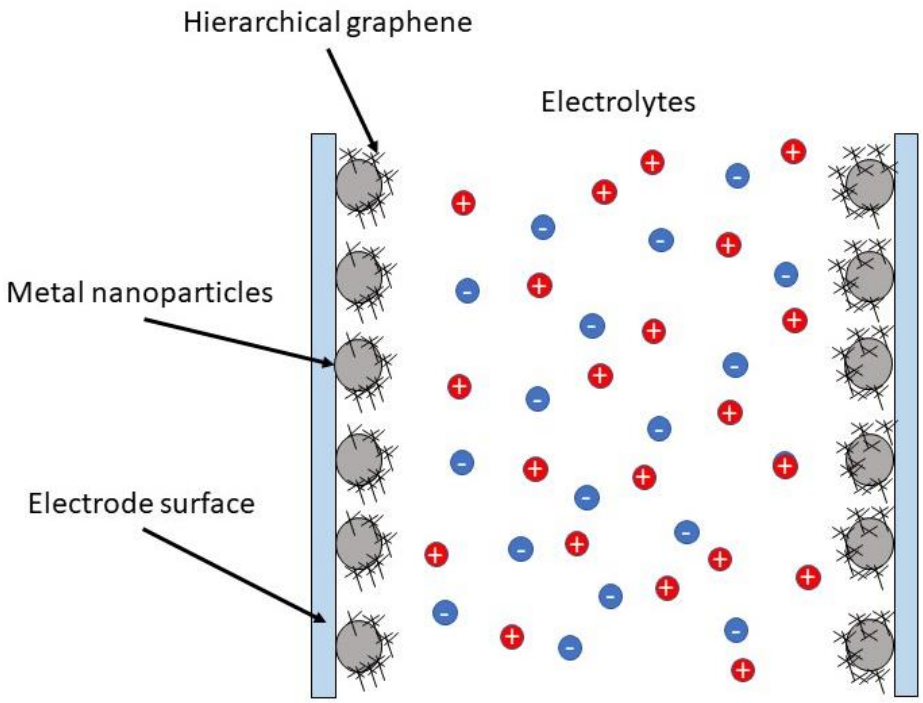

Figure 1.5: Schematic drawing of a graphene supercapacitor. To greatly improve the specific surface of the electrodes that make a supercapacitor, metallic nanoparticles are deposited on the electrode surface, then hierarchical vertical graphene is placed on top of the metallic nanoparticles causing a further increase in electrode capacitance.

1.2.3 Graphene in optoelectronics as transparent electrode

New electronic devices as smartphones, tablets, solar panels, flexible displays and touchscreen base their functioning to the presence of a transparent conductor that can collect

or distribute electrons while leaving photons passing through. The standard material for these applications is indium-tin oxide (ITO) thin films, but it is expansive scarce on earth and brittle (it is a ceramic material). The search for a cheaper, more abundant and flexible transparent conductor that might take the ITO place in the market has been going on for almost a decade, new materials as thin metal foils[78], metal grids[79], conductive polymers[80] and carbon nanotubes[81] have been explored. Thanks to recent improvement in graphene deposition technology, this new material might answer these needs answering all requirements without any catch. Although research is still in its early stages, graphene has many advantages over ITO, it is lighter, more robust, flexible, more chemically stable and potentially extremely cheaper and more abundant. All these features together make graphene extremely competitive for touch screens (See Figure 1.6) where companies as Samsung and Fujitsu are already investing and researching. Basically, depending on the method used to synthetize the graphene films, graphene offer sheet resistance down to 300 Ω and transparency up to 80-90% [82,83] providing the characteristics needed in such applications. Anyways there are some concerns related to the use of graphene, the first of which is graphene poor surface adhesion to substrates, in addition there is no perfect way to protect the films form wearing and for know their applications are limited to low wear applications. ITO needs a replacement and carbon-based systems that utilize graphene are likely to shift the paradigms in transparent conductor technology [59].

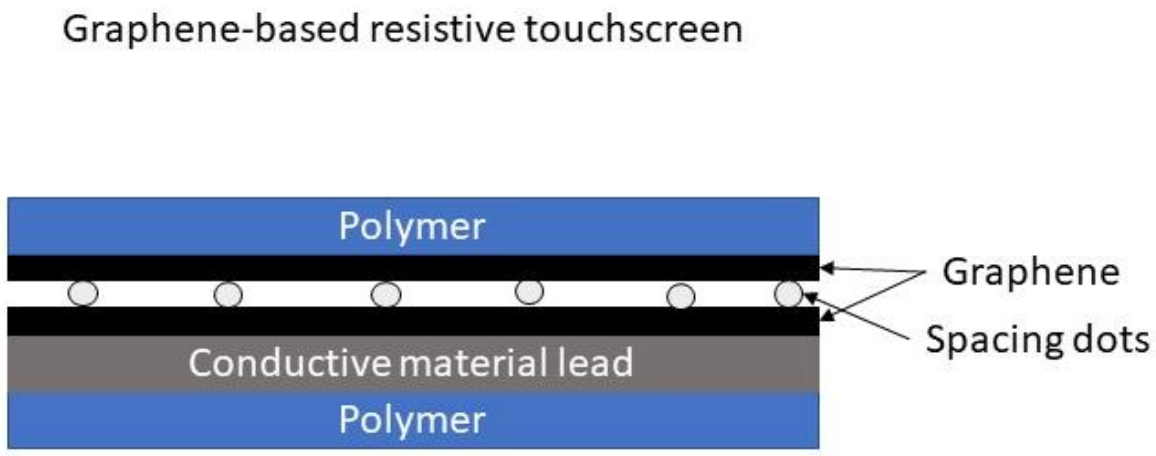

Figure 1.6: Sketch of graphene-based, resistive touchscreen design. Two graphene sheets are placed one of top of the other separated by micrometric-size spheres. When the user's finger push on the touchscreen, the two graphene sheets touch each other and close an electric circuit. The flowing current is then read by a controller circuit to determine the position of the touch on the screen.

1.2.4 Bio-applications

After entering the electronic, energy storage and composite materials fields, graphene recently entered the biology and biomedical technology research field. The most visionary technology envisioned in the recently launched Biomedical Technology Work Package[14] of the Graphene Flagship[27] concern implantable electronic devices. Such devices, as artificial retina implants or bioelectronic interfaces, are shown in Figure 1.7 (a) and would allow to treat diseases using electrical stimuli [84] but have to fulfil strict requirements in biocompatibility, comfort and durability. They have to be flexible, stable in physiological conditions and have to provide reliable electrical performances for years. Graphene has both the mechanical and electrical properties to match the required expectations but its stability *in situ* depends on many factors. In addition, whether graphene can outperform bio-sensors and bio-interfaces currently in use is also open to questions and many research groups are investigating these possibilities. Graphene has potential also in the drug delivery area and an exemplification of the use can be seen in Figure 1.7 (b) [85,86]. Many drugs can have unwanted side effects and the use of nanomaterials to slowly release the chemical only in a specific area or at a specific rate is gradually becoming a reality. Graphene can be easely chemically modified, allowing the production of nanostructures with specific binding sites on the surface that could be used to adsorb the drug and then release it only in specific conditions[4,13]. Besides, bio-applications have generally to be designed more carefully than any other. For now, there is no watertight demonstration of graphene biocompatibility and it is hard to make general statements and many studies on how this 2D material behave in contact with a complex biological system have to be done before a graphene device will be used on humans.

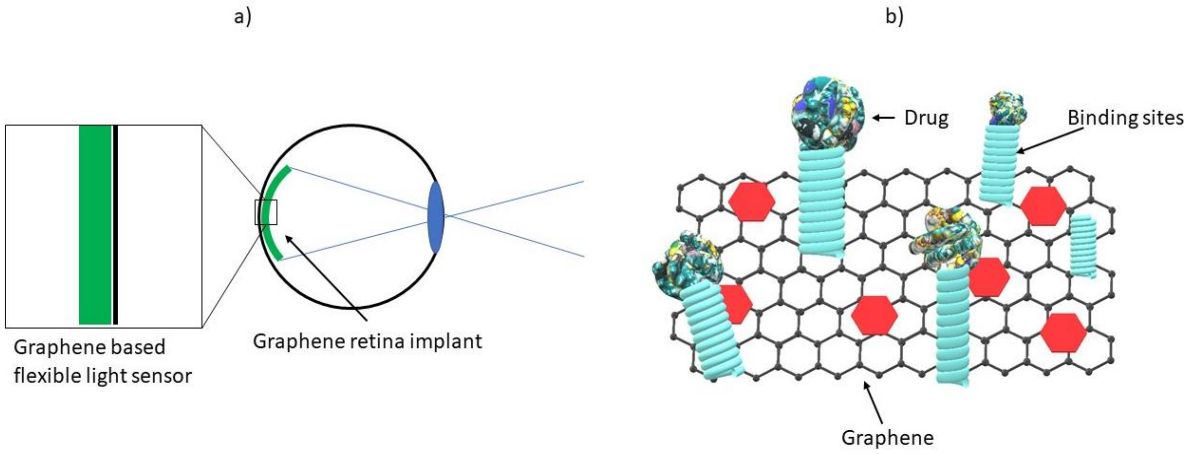

Figure 1.7: (a) Graphene would allow to produce flexible light sensor usable as synthetic retina implants. (b) Graphene functionalization allows to create nanomaterials equipped with binding sites specific to the desired drug.

1.3 Graphene synthesis and transfer

Graphene synthesis methods can be divided into two families as Figure 1.8 illustrates: top down and bottom up. Top down methods start from graphite and work by separating each graphene layer from the others. Among this technique the most well-known are mechanical exfoliation, chemical exfoliation and chemical synthesis of reduced graphene oxide. These methods are the most used when large amounts of graphene have to be produced, the raw material is graphite (abundant and cheap) and being chemical syntheses, they allow to process large quantities of material suspended in liquid. Bottom up methods, instead, start from a carbon precursor (such as a gas or a C-rich solid) and directly synthetize single or multiple layer of graphene *in situ*. The main exponents of this group of processes are epitaxial growth and chemical vapour deposition (CVD), procedures that result in high quality graphene but that have a limited production output, with this methods graphene can be deposited on insulators and metals but many means are used to adapt the process at the substrate. In addition, the substrate used for the synthesis might not be the same needed for the final device, requiring additional steps to transfer the film onto the substrate of choice. In the succeeding paragraphs each of the most important methods to synthetize graphene will be explained schematically, in conclusion a brief note on graphene transferring is provided [15].

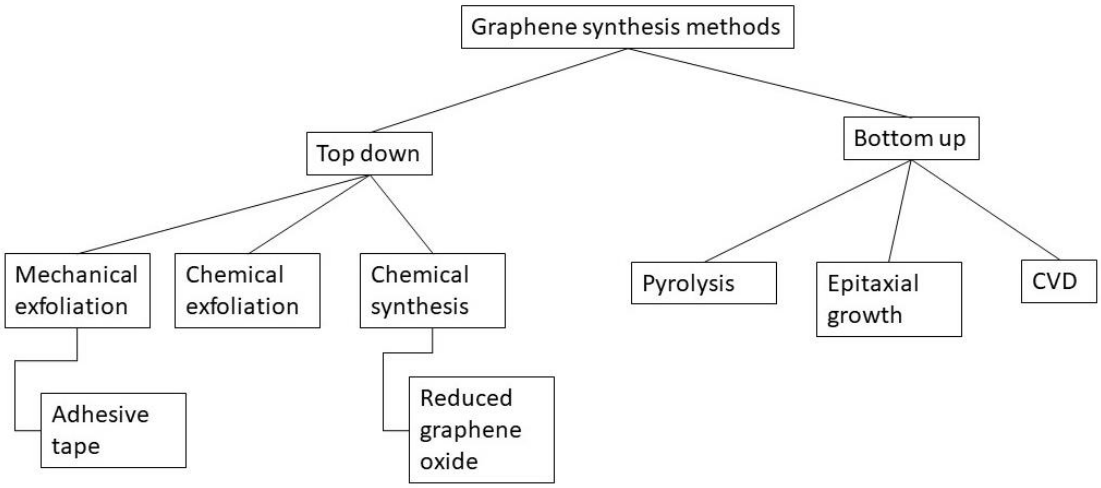

Figure 1.8: Graphene synthesis methods organized in top down and bottom up with the main representatives of each group.

1.3.1 Mechanical and chemical exfoliation

Mechanical exfoliation is the method used by Novoselov and Geim to isolate and study the first graphene in 2004 [1]. It is a top down technique where a force transversal to the layers orientation is applied on a graphite crystal in order to separate the single graphene layers by

braking the weak van der Waals forces that bind together the graphitic planes. This approach, shown in Figure 1.9 (a), usually requires the use of scotch tape or more sophisticated means to apply the mechanical force, then the graphite crystal is exfoliated repeatedly obtaining a thinner graphite nanosheet at each step, once a single- or multilayer of graphene is separated from the graphite it is usually deposited on top of another substrate to allow characterization or use of the film. This method is hard to scale for mass production, but work is being done on it. At this regard, Liang at al. come up with an interesting method of cut-and-choose based on mechanical exfoliation that would allow wafer scale graphene fabrication for integrated circuits[87]. Figure 1.9 (b), instead, displays a schematic of the principle behind chemical exfoliation of graphene. The general concept of the technique is to separate the single layers that make the graphite crystal as happens in mechanical exfoliation. In this case alkali metals (Potassium as example) are intercalated within the graphite structure. When inside the crystal, K atoms react to form the intercalated compound KC_8 (at 200°C and in He atmosphere [88]), then the compound is made react exothermically with an aqueous solution of ethanol (CH_3CH_2OH) forming potassium ethoxide ($KOCH_2CH_3$) and gaseous hydrogen which helps separating the layers (see Equation 1.1); the layers can be then collected form the suspension by filtration or evaporation of the solvent.

$$KC_8 + CH_3CH_2OH \leftrightarrow 8C + KOCH_2CH_3 + \frac{1}{2}H_2 \tag{1.1}$$

The same process can be performed with different chemicals and it is extremely versatile, low cost, scalable and not linked to a specific substrate allowing deposition on a wide variety of substrates. Together these two methods represent the dawn of graphene synthesis, effective and cheap methods offer many advantages but are not viable to produce single layer graphene offering scarce thickness control.

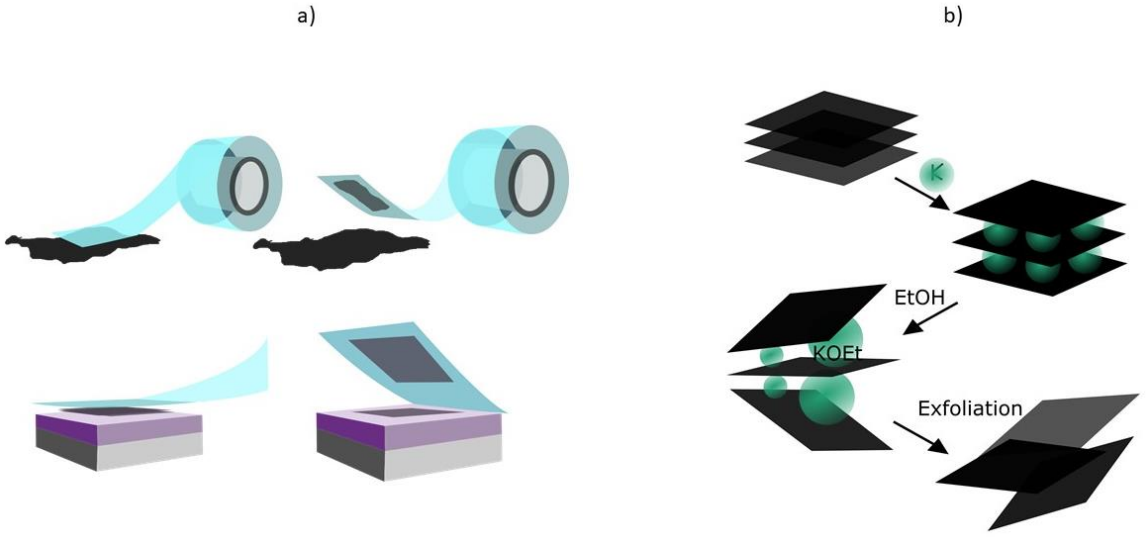

Figure 1.9: (a) Mechanical exfoliation of graphene, scotch tape is used to separate from each other the graphitic layers, when a mono- or multilayer graphene has been isolated it is deposited on the target substrate. (b) Chemical exfoliation of graphene, potassium is intercalated between different graphite layers, then expanded through chemical reaction to separate the graphene monolayers.

1.3.2 Chemically derived graphene

An alternative top down path to produce graphene consists in chemically oxidizing graphite flakes obtaining Graphene Oxide (GO) that can then be reduced getting back the original carbon structure of graphene. Graphene obtained with this method is called reduced graphene oxide (RGO). Graphite oxidation route to graphene oxide has been developed since the nineteenth century and evolved through the Brodie[89], Staudenmaier[90] and Hummers[91] methods.[92] The Brodie method involves the addition of potassium chlorate ($KClO_3$) to a slurry of graphite in fuming nitric acid (HNO_3), after the process the resulting material is composed of carbon, hydrogen and oxygen. Repeating the process sees an increase of the oxygen percentage that reach 37% at the forth repetition[89]. The German chemist Staudenmaier changed the process dividing the addition of potassium chlorate in multiple additions along the process and increased the acidity of the solution with concentrated sulfuric acid[90], the process remained the same otherwise. The most recent method is that of Hummers which developed an alternative oxidation pathway by reacting graphite with a mixture of potassium permanganate ($KMnO_4$) and sulfuric acid (H_2SO_4). The potassium permanganate is the oxidizing agent but the active species in the oxidation of graphite is dimanganese heptoxide (Mn_2O_7) a product of the reaction between the potassium permanganate and the sulfuric acid as shown in Equation 1.2 and 1.3 [91].

$$KMnO_4 + 3H_2SO_4 \rightarrow K^+ + MnO_3^+ + H_2O^+ + 3HSO_4^- \quad (1.2)$$

$$MnO_3^+ + MnO_4^- \rightarrow Mn_2O_7 \quad (1.3)$$

Today many variations of this method exist but the underlying concept is still the same. The result of this process is a brown viscous slurry which contains GO and many by-products.

To obtain pure GO suspension centrifugation, sedimentation or dialysis is used. Precipitation helps to separate heavy unoxidized graphite flakes from the GO nanoplatelets and can provide monodispersed suspensions of GO flakes. The chemical formula of GO is not perfectly known and describable but many models have been speculated, Figure 1.10 the Dékány model[93] is shown.

GO has a completely different behaviour with respect to graphene but the carbon structure of the graphene layer can be restored with thermal annealing or with chemical reduction to obtain RGO which basically is graphene. The first proposed method to reduce GO involved the use of hydrazine vapour[94] which however is highly toxic and explosive. Hence, many alternatives have been studied to provide a safer process and one of the most successful substitute is sodium borohydride ($NaBH_4$). In fact, this chemical has been demonstrate to be even better than hydrazine as reducing agent for GO[95], but has the drawback of slowly reacting with water. However, the rate at which the reaction happen is low enough that a fresh solution of sodium borohydride results unaffected by it. Another effective way to obtain RGO is via hydrogen plasma which provided results comparable with the other methods[96]. Chemically deriving graphene from graphite is today one of the most used methods, it is easily scalable and cheap, it allows a certain degree of control over the thickness of the resulting RGO but it is still difficult to remove all the chemical impurities derived from the graphite or the process itself.

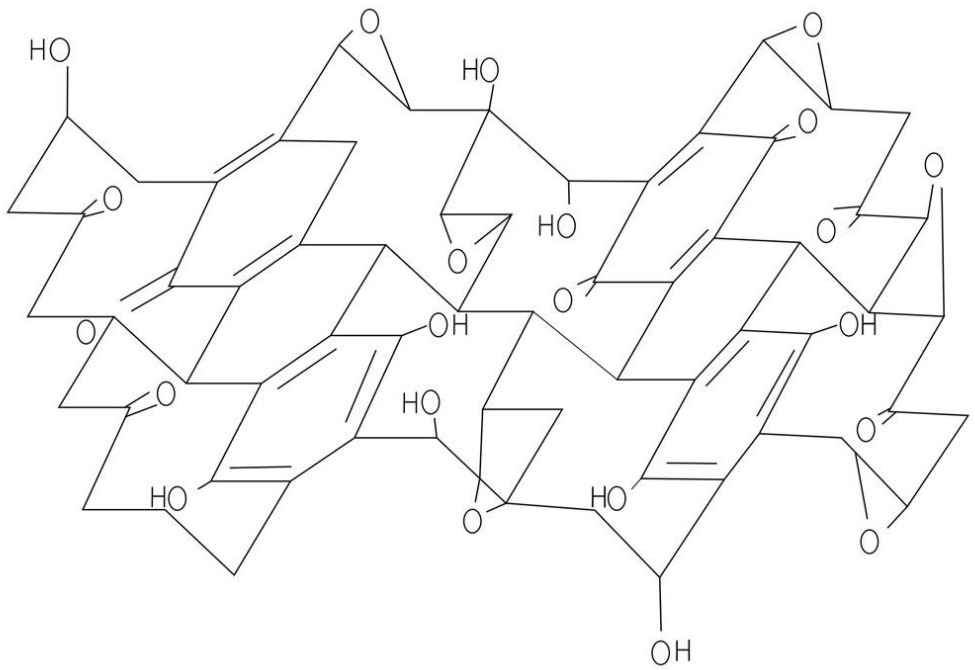

Figure 1.10: Dékány model of graphene oxide. Beside the presence of so many -O and -OH groups the honeycomb structure can still be individuated and with the proper chemical process it is possible to get back to graphene.

1.3.3 Epitaxial graphene from SiC

Top down production methods for graphene are cheap and allow to mass produce this new material, but they are not perfect for all fields of application. To make possible the use of graphene for electronic devices and other high technology applications, large scale, high quality, high reproducible graphene thin films are needed. Ideally, wafer-scale, high purity mono- or bilayer graphene have to be deposited on the desired substrate as silicon, silica, a metal or other material that can then be subjected to nanolithography techniques. At this scope, epitaxial graphene (EG), grown on silicon carbide (SiC) by thermal decomposition of the latest, is much more compatible with nanofabrication methods than exfoliation processes, and it has the required properties to be used in electronics [97]. By ultra-high vacuum (UHV) thermal decomposition of SiC, single-crystal, high-quality graphene is obtained. This process offers high control over the number of layers and does not depend too much on the SiC crystal orientation allowing high reproducibility. SiC is atomically organized in tetrahedral bonds of Si-O, these tetrahedra can be arranged in a face-centred cubic (FCC) lattice or in a hexagonal closed-packed (HCP) symmetry, these two different crystals can then expose to the surface different faces providing many polytypes with different behaviours. In addition, a crystal can terminate with a Si-rich or C-rich layer which can further influence decomposition process and graphene formation at the surface. The simplest polytype used to explain the process concept is usually a Si-terminated 6H-SiC(0001) staking sequence as shown in Figure 1.11 (a). When this polytype is subjected to high temperature, the Si on the surface begin to sublimate and leave the material. Because of the asymmetrical evaporation on the surface of the SiC, C-rich deposits start to accumulate, the carbon atoms gradually organize in a honeycomb structure resulting in EG layers (See Figure 1.11 (b)). Depending on time and temperature, these layers range from interfacial graphene to single- multilayer graphene [97]. The typical process temperature can vary from 850°C[98] and 1100°C[99] and it can involve a successive annealing, at temperatures of 1200°-1400° C or more, that helps the formation of single-crystal layers of graphene[100]. Overall, it is a costly process (expansive substrate, UHV, high temperatures) with a limited output but allows thickness control, large crystal size and it is compatible with lithography. All these features make EG a promising candidate for graphene electronic devices.

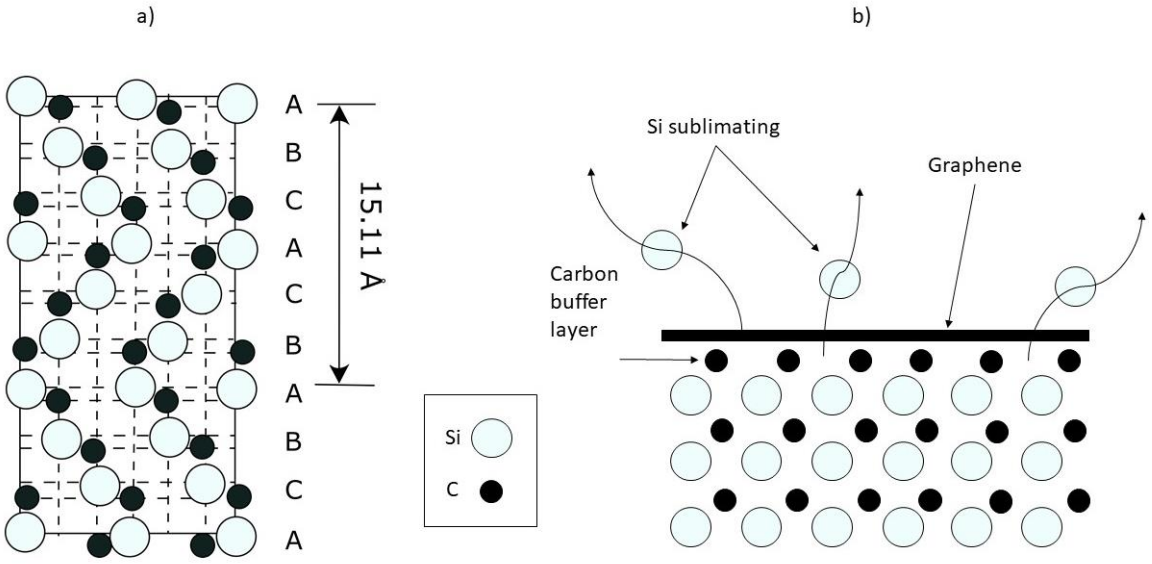

Figure 1.11: (a) Si-terminated H6-SiC(0001) crystallin orientation, the staking order is shown on the right side. (b) Schematic drawing of epitaxial graphene formation: Si atoms sublimate more often than C atoms, C atoms accumulate at the surface and organize them selves in a honeycomb structure forming graphene. The buffer layer is a layer of carbon atoms that regulate the SiC-Graphene interface.

1.3.4 Chemical vapour deposition on metals

As mentioned before, graphene production for electronic devices has many requirements and needs that only bottom-up processes can provide. Among all bottom-up method, catalytic chemical vapor deposition is the technology on which large scale graphene production for electronic devices relies [19]. Every chemical vapor deposition process sees a substrate inside a reactor chamber under high-vacuum that is exposed to high temperature while a controlled flow of a specific gas mixture is blown on the substrate itself (see Figure 1.12). In the graphene case, the gas mixture contains a carbon precursor (methane and acetylene are two examples[17]) and a catalyst (which usually happens to be the substrate as well) is used to drive the decomposition of the precursor into graphene. In addition to the carbon precursor, the gas mixture contains reducing agents as hydrogen or nitrogen which consumes any amorphous carbon that might be forming and inert gas that dilutes the gas mixture [17,101,102]. Each of these components is highly relevant and strongly influences the resulting graphene. The catalyst, usually a metal, has a special role and it is the most important and studied among the other factors.

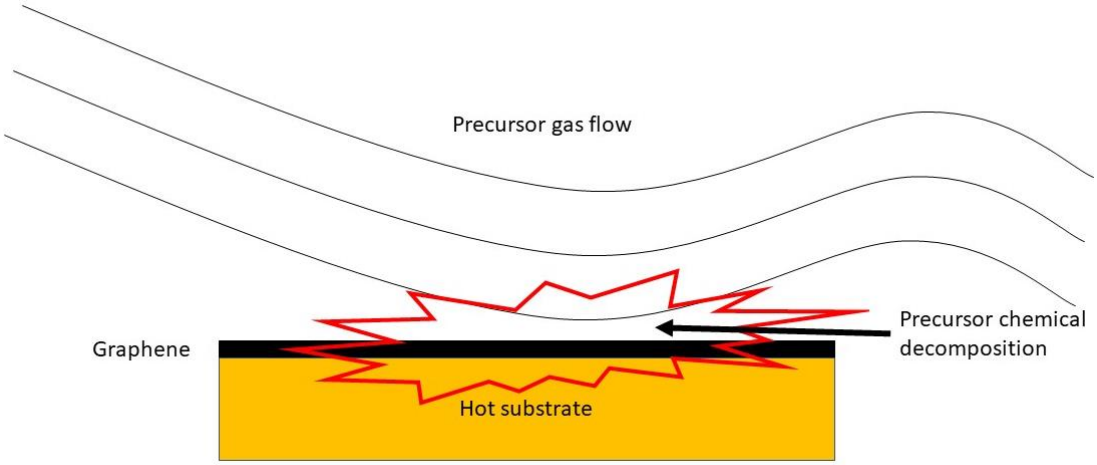

Figure 1.12: Basic concept of chemical vapour deposition. A gas mixture is blown on the hot surface of a catalyst and it decomposes. Then, the decomposition products rearrange themselves to from graphene.

Typical metallic catalyst are Cu[101], Ni[82], Pt[20] and Co[102] and depending on which catalyst is used, two main growth mechanism are identified. When using Ni (or any metal with high carbon solubility), the carbon containing precursor decomposes on the hot surface of the metallic catalyst and the resulting carbon atoms dissolve into the crystal lattice until it reaches saturation. Then the catalyst is cooled down and the carbon solubility reduced by the lower temperature, this phenomenon induces a flow of carbon atoms towards the catalyst surface and once at the surface the carbon atoms arrange themselves into graphene layers as explained in Figure 1.13 (a). Because the formation of graphene happens during the cooldown, the cooling condition are of most importance and can determine if the process will result in a single- or multilayer graphene[103]. Cu instead, has little or no carbon solubility and the decomposed precursor cannot enter the metallic solid solution, hence the precursor decomposes while forming a graphene monolayer (See Figure 1.13 (b)). This monolayer then passivates the catalyst which means the process is self-limiting and provides repeatable depositions of graphene monolayers [19].

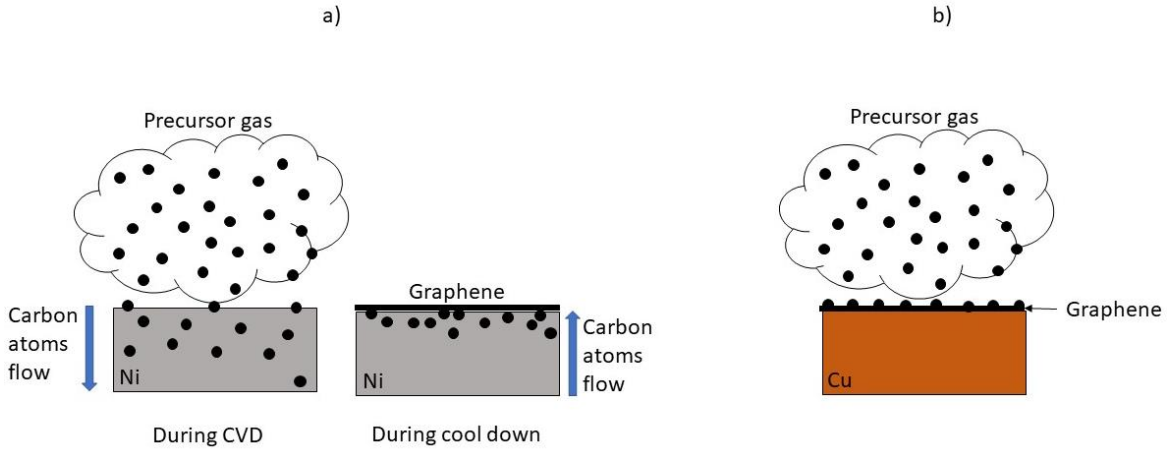

Figure 1.13: (a) Chemical vapour deposition on Ni, precursor gas decomposes on the catalyst surface and is dissolved inside the solid solution of Ni atoms, during the cooldown, the carbon solubility drops and carbon atoms are pushed outside the catalyst where they form graphene. (b) Chemical vapour deposition on Cu, precursor gas decomposes on the catalyst surface but cannot enter the solid solution due to absent carbon solubility. The carbon atoms form a graphene layer which passivates the catalyst surface ending the graphene formation.

The process results in graphene deposited on top of a metallic film. Usually for electronics an insulating or semiconductor substrate is required, hence, CVD graphene is often followed by a transferring step in which graphene is moved to the appropriate substrate. This additional step is not always convenient, reason why in the CVD field some improvements toward a transfer free deposition directly on insulator are being made. Growth on quartz, silicon, silicon oxide and silicon nitrite have been demonstrate[104,105], the resulting graphene quality was comparable with catalytic CVD graphene with the difference that direct CVD on insulators produces graphene with much smaller grain size which brings more grain boundaries and consequently lower carrier mobility overall. This method has still to be improved but it has the great advantage of not requiring any transferring step.

Feasibility of large scale production of high quality graphene, with high control over the number of deposited layers and good reproducibility is the biggest issue which limits the success of graphene and the release of graphene-based devices. CVD techniques need to be performed in vacuum and high temperature which provides a certain degree of challenge in scaling the technology but represent the most promising graphene production method for electronics.

1.3.5 Graphene transfer

As disclosed earlier, many methods of graphene production need a successive transferring of the graphene film on an appropriated substrate. In particular, catalytic CVD on metals strictly requires the graphene film to be moved on an insulating or semiconducting substrate and there are two main ways to perform this transfer: etching transfer and electrochemical transfer.

A schematic for the etching transfer is shown in Figure 1.14, this technique involves the deposition of a polymer layer on top of the grown graphene as a supporting layer, once graphene integrity is secured the metallic foil on which the film has been deposited by CVD can be chemically etched and removed freeing graphene and polymer layer from it. Once the metallic foil is removed, graphene and the polymer can be transferred on the substrate of choice and the polymer film can be dissolved using the appropriate solvent. At the end of the process the result will be graphene on top of an insulator or semiconductor. The method is well established and provide good quality graphene on any desirable substrate[106].

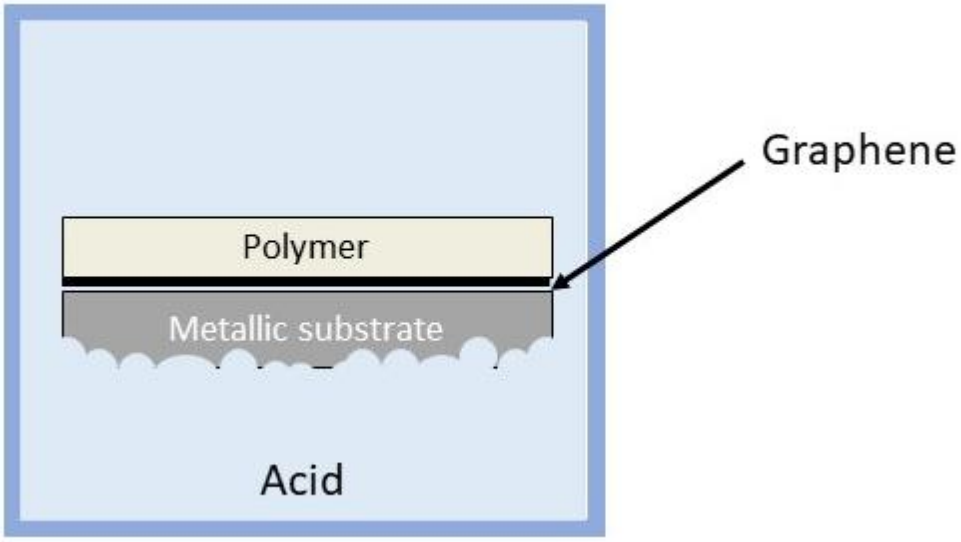

Figure 1.14: Schematic drawing of etching transfer of graphene. CVD graphene is deposited on a metallic substrate, a protective polymer coating is deposited on top of the graphene layer and then the metallic substrate is etched away using an acid solution. Once the metallic substrate has been dissolved, graphene is transferred on a new substrate and the polymer removed with the appropriate solvent.

Alternatively, electrochemical transfer can be used. Figure 1.15 contains a sketch of this technique which has the advantage to not consume the metallic catalyst making it reusable with a substantial reduction of production costs. This method is based on the electrochemical production of hydrogen at the surface of the metallic catalyst by spltting of water that detaches the graphene film from metallic foil. Hydrogen is produced by applying a voltage between the metallic foil and a platinum counter electrode while everything is immerged in NaOH water solution. To guarantee the integrity of the graphene a polymeric film is used as for the etching transfer[31].

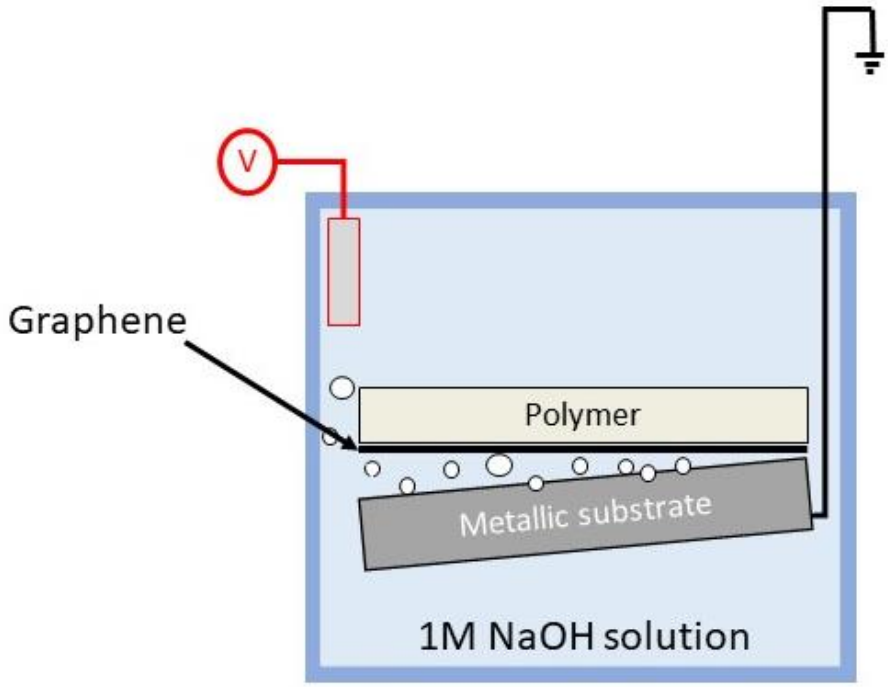

Figure 1.15: Electrochemical bubbling transfer. Graphene is deposited on a metallic substrate, a polymer coating is applied on top of it as sustain and then the complex is immerged in NaOH solution. Voltage is applied across the system and hydrogen bubbles form at the metal surface due to electrochemical splitting of water. These bubbles detach the graphene film that can be transferred. With this method the metallic substrate can be used multiple times.

1.4 Graphene characterization

Characterization techniques are fundamental in the study of graphene and its properties. Being so thin, graphene offers more than few challenges in its characterization and analysis but thanks to the advancement made in transmission electron microscopy, Raman spectroscopy, optical microscopy and other methods it is now possible to study this new material even with common laboratory tools.

1.4.1 Optical microscopy

Optical microscopy is one of the oldest imaging technologies which allowed to see microscopic details since the seventeenth century. Graphene nanometric thickness cannot be resolved by optical microscopy because the wavelength of visible light is 2-3 order of magnitude longer than graphene thickness but graphene grains have lateral sizes that can reach the centimetre scale going even further with the latest technologies[107]. In addition, a graphene film is made of many grains and there is no limitation on its lateral size.

A graphene film deposited on a substrate are sufficiently transparent to add its thickness to the optical path followed by the incident light, this additional optical path and the fact that graphene has a different refractive index with respect to most of the common insulators or

semiconductor changes the interference of reflected light and allow to identify the presence of graphene simply through colour contrast[1,106]. Graphene thickness adds to that of the substrate changing the wavelength of light that can escape the material by reflection as shown in Figure 1.16, hence the specific colour of the thin film. From this it is also possible to understand that a single layer of graphene has a different coloration than a multi-layer. This colour contrast is at the base of many studies done on graphene films, the state of the art for this method, the same used in this work, involves depositing or transferring the graphene on a silicon wafer on which was previously deposited a 300 nm thick SiO_2 film. SiO_2 thickness is chosen specifically because it provides the greatest contrast allowing for easy detection and recognition of graphene and its thickness. This method represents a quick and easy way to visually quantify the amount of deposited graphene and the number of layers. Besides, optical microscopy alone cannot provide precise data about the quality of the film or its precise number of layers and other techniques as Raman spectroscopy and transmission electron microscopy are needed.

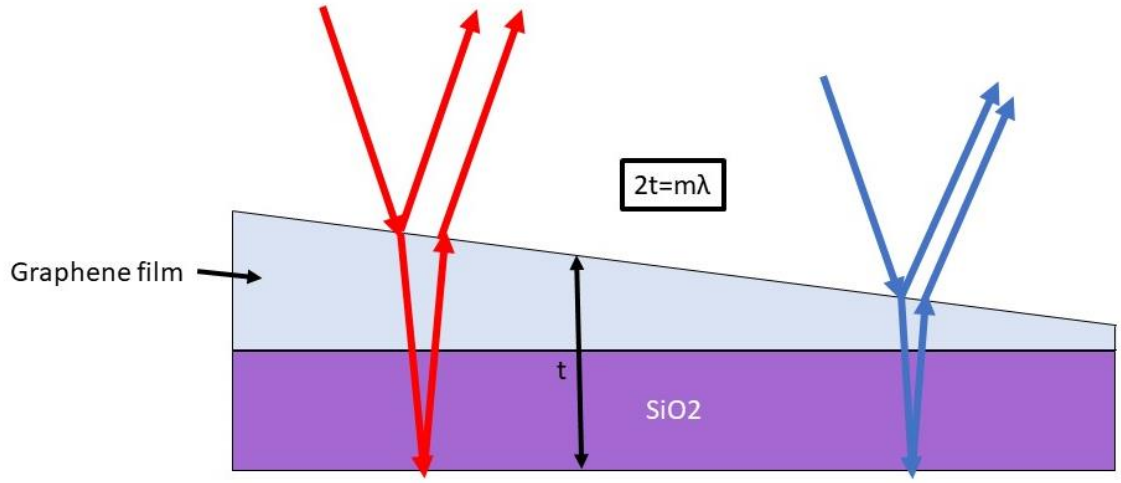

Figure 1.16: Interference effect that makes graphene visible at optical microscopy. Because of graphene transparency, is placed on top of a transparent substrate, it adds its thickness to that of the substrate changing the reflected wavelength. In the case of plain 300 nm SiO_2 the reflected light for interference effect is a specific shade of purple. When even only a single layer of graphene is added the optical path would be slightly longer and the perceived shade of reflected light would be slightly different. This phenomenon makes graphene visible.

1.4.2 Raman spectroscopy

Raman spectroscopy revealed to be one of the most useful tools to analyse graphene, it is fast, non-destructive, can be used on specific areas or can be used for mapping providing information about a wider surface of the chosen sample. This technique consists in irradiating the sample with a focused laser at a specific wavelength, the light is then partly reflected by the surface and partly adsorbed in a process called light scattering. Afterwards, the scattered light is reemitted at a different wavelength and analysed by a spectrometer

which collect data about the shift between the adsorbed and reemitted light. The reemission effect is strictly linked with photon-phonon interactions; hence the Raman shift brings a lot of information about the lattice structure and electronic, optical and phonon properties of the studied samples. Figure 1.17 contains a generalised Raman spectrum for graphene and as it is possible to see there are many different peaks which are classified with different letters as G, D, 2D, etc [108]. Each letter represents a Raman band linked to a specific phono-photon interaction, these interactions can differ in the number of phonons involved, in the presence or absence of defects and on the typology of involved phonon. For example, the G band (1583 cm^{-1}) is emitted as consequence of an interaction with phonons specific of the graphene monolayer and it is more intense when the graphene lattice is defect-free. The 2D band (2680 cm^{-1}) is related to phonons present in the graphene lattice as well but this particular band is affected by the interferences of the neighbouring layer and its intensity is decreased when many graphene layers are stacked on top of each other. In conclusion the D (1300 cm^{-1}), D' and D'' depend on the interaction with point defects in the lattice and show the degree of defectiveness of the studied film [26,109]. All these bands can be shifted due to chemical doping or mechanical stretching and some of them are also dependent on the incident wavelength. In addition, the ratios between the main peaks can provide a lot of information about thickness and overall quality of the deposited graphene. For a perfect graphene monolayer, the D peak is usually near zero, hence, the D/G ratio is near zero as well. In addition, being a monolayer means that the 2D peak is not dumped by interference and it will be extremely intense. Usually for a monolayer the 2D peak is twice intense than the G peak making easy to identify a monolayer when tested with Raman spectroscopy. Concluding, Raman spectroscopy allows to study defectiveness, thickness, doping and overall quality of the deposited graphene, it is one of the most utilized technique in graphene characterization providing many information about the electronic structure of the film. It is decently precise in identifying the number of layer but being subjected to many different influences, when used, it is also important to verify and check with other methods the obtained results.

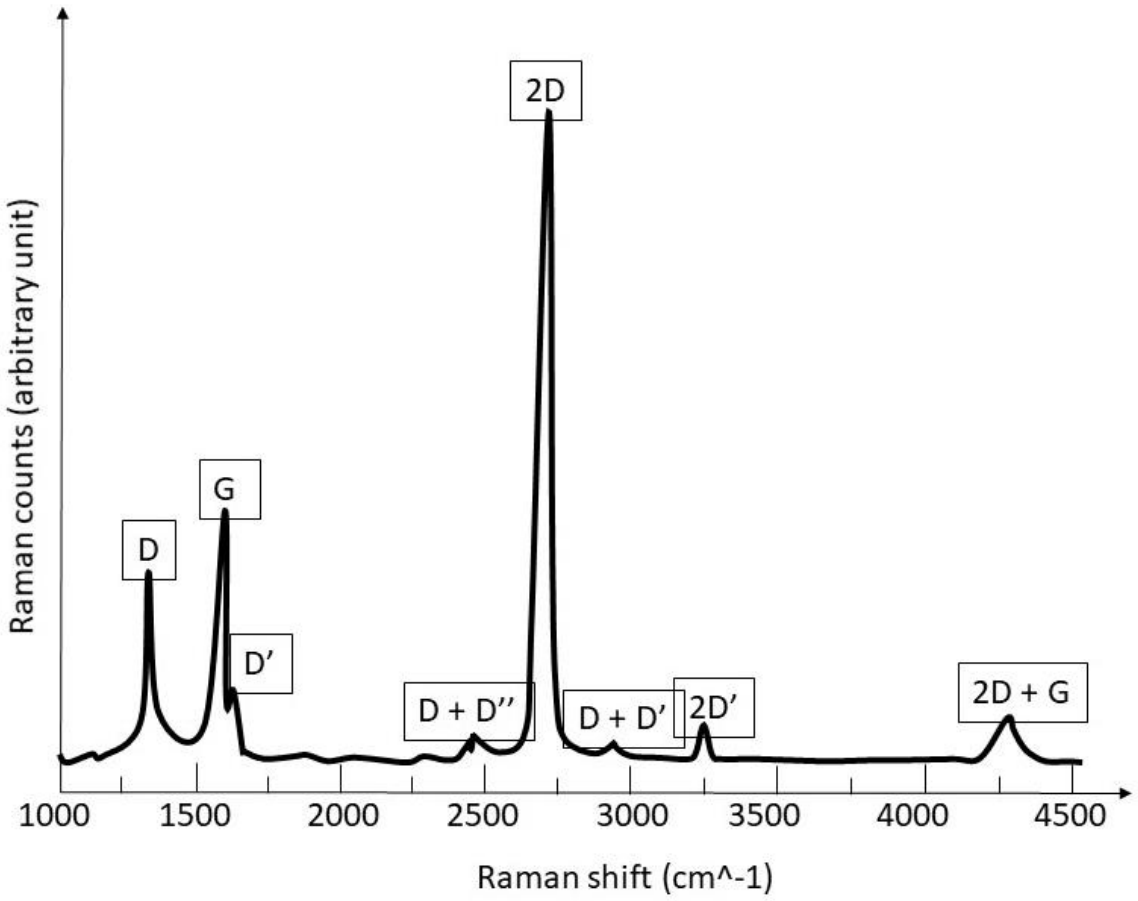

Figure 1.17: Example of Raman spectrum for a defective monolayer of graphene. This graph is fabricated and it is not obtained from real data but shows how such a spectrum could appear. 2D/G ratio around 2 or more is typical of a graphene monolayer but the intensity of the D peak is high which means high defectiveness.

1.4.3 Transmission electron microscopy

Transmission electron microscopy is one of the most expansive and complex among characterization techniques. The sample preparation involves long procedures with the aim of getting a sample few atomic layers thick and requires a lot of time. The TEM microscope have to accelerate electrons at around 100-300kV and work in UHV. The working principle on which it is based is the interaction between accelerated electrons and the extremely thin sample. In Figure 1.18 the electron beam is used to build an image of the sample morphology with resolution of the atomic scale, but the tool can be also used to obtain a diffraction pattern [110]. The first method allows to depict images of the sample while the second mode allows to study the diffraction spectrum of the sample crystallin lattice. Graphene is so thin that cannot be detected by other method than TEM imaging, and this technique represent the only way to count precisely and directly the number of layers deposited on a sample. In addition, it can provide information about the crystallin structure as additional prove about the nature of the film [111].

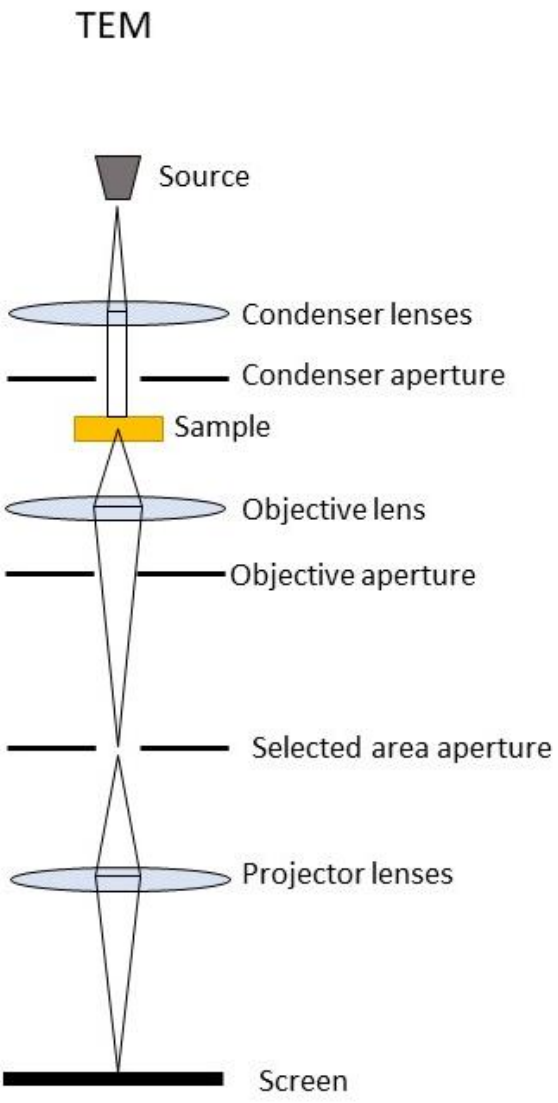

Figure 1.18: Schematic representation of electron bean path inside a transmission electron microscope in imaging mode. The lenses are electromagnetic and the actual design is much more complex, but overall the process dynamics recall that of microscopy in general.

1.5 Where can graphene improve?

Given the amazing properties of graphene, a spontaneous question to ask might be: "If Graphene is so great, why is it not already used everywhere?".

The answer to this question is related both to manufacturing limitations and graphene own nature. Despite depositing graphene is possible and widely done around the world graphene production price is still high in comparison with other materials. In addition, high quality thin films lack of reproducibility, thickness control over large areas has not been achieved

yet and large-scale transfer of graphene films is not repeatable. These issues represent the first important bottle neck that is limiting graphene availability on the market but also the most likely to be solved soon: growth technology is evolving rapidly with many innovative solutions and many companies are starting to mass produce graphene for commercial usage. On the other hand, graphene has a high intrinsic conductivity but because of is atomic thickness the resulting sheet resistance is still too high for application in electronics as substitute of silicon. Furthermore, contrarily to silicon and other semiconductors, graphene has no band gap and no native oxide that might passivate this material from the environment. Many possible solutions are being taken into consideration to solve these problems, especially regarding the band gap, and most of them might be solved in the near future. Another way to bypass the differences between graphene and other semiconductor might be to design devices specifically though around graphene properties but such a new design might need many years of tests and trial before being commercialised. Overall there is no easy answer to graphene commercialization and this process will probably take at least five to ten more years. As it is common for all new materials, the production technologies underlying graphene synthesis need to mature and the process takes time, but there are positive signs. The number of companies which main focus is graphene production is growing while the amount of published papers about graphene seems to have reached its peak, these two events lead to think that the first expectation hype has been overcome and concrete industrial endeavours are rising, bringing with them the dawn of the graphene era. [5,112,113]

2. Experiments and methods

In this study graphene is obtained through annealing of a carbon-enriched CuNi metallic film. CuNi alloy is used as catalytic substrate for graphene deposition: Cu has the ability to grow large area mono- or bi-layer graphene thin films[16] while Ni has the capability of storing carbon atoms in the solid solution[23]. Hence, Nickel allows to store and extract carbon atoms from the metallic foil while Copper catalyses the formation of graphene on the surface of the substrate. CuNi alloys have been already used in graphene synthesis and have shown good capability in producing graphene thin films[107] but in this work CuNI alloy is used to extract graphene multiple times from the same metallic sample through high-temperature annealing.

A sketch of the complete process is shown in Figure 2.1. First, a CuNi metallic foil sample is subjected to a chemical vapour deposition (CVD) process where a carbon precursor is used and decomposes on the surface of the CuNi foil that works both as a substrate and as a catalyst. During this step the precursor gas decomposes on the CuNi sample surface and carbon atoms are allowed to diffuse inside the metal. Due to the high temperature involved the carbon solubility of the alloy during the CVD is higher than at room temperature, during the length of the process the metal is saturated by the diffusing carbon atoms. Then, during the cooling down the solubility starts to drop and carbon atoms start to diffuse in the opposite direction segregating graphene and graphite nanosheets on the surface of the sample. Because a high cooling rate was used, at the end of the CVD, the system had not enough time to reach equilibrium and the carbon concentration in the metal happened to be higher than the thermodynamic one at room temperature (Figure 2.1 (a) and (b)). This first step had as object to enrich the metal alloy. After the CVD the resulting graphene and graphite nanosheets were removed to a SiO_2-Si substrate (in purple) with bubbling transferring in order to be studied and to remove all graphene form the CuNi foil (Figure 2.1 (c)). Afterwards, the carbon enriched CuNi foil can be annealed without any carbon source. During the annealing, the high temperature rises again the carbon solubility and not much is expected before the cooling. During the cooling, instead, carbon solubility in the alloy decreases rapidly and carbon atoms are pushed outside the metal lattice and diffused to the surface of the CuNi catalyst where graphene can nucleate and form. The obtained graphene is then transferred on a SiO_2-Si substrate and analysed while the CuNi foil can be annealed again repeating the process up to five times. The overall process, as depicted in Figure 2.1, contains many steps. In the following paragraphs each of the steps will be analysed in depth.

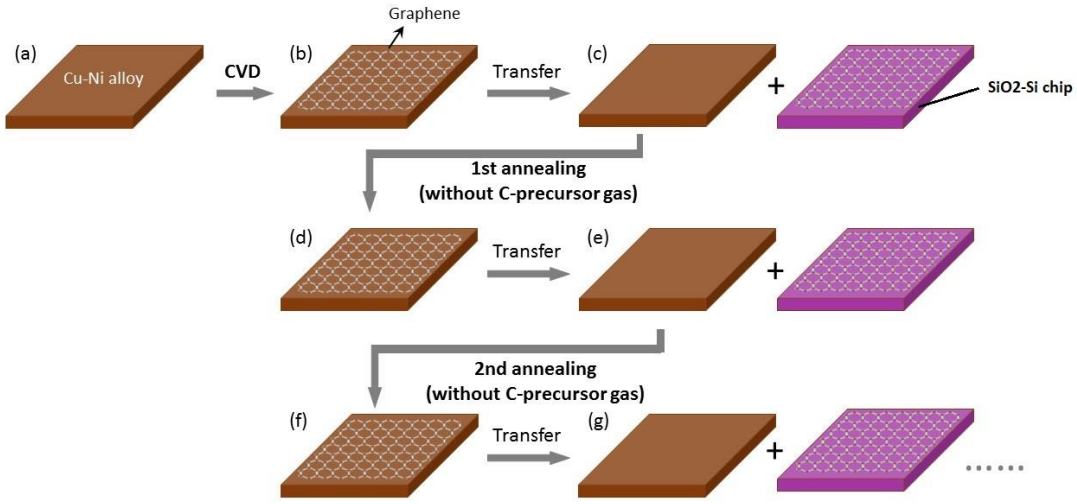

Figure 2.1: Sketch of the experimental procedures: (a) CuNi metal foil before any process; (b) CuNi metal foil covered by graphene after the thermal CVD; (c) The graphene film has been transferred on SiO2-Si substrate (purple), Now the CuNi foil is ready for the 1st annealing; (d) After the 1st annealing the CuNi foil is covered by graphene anew; (e) Again, the graphene has been transferred from CuNi to SiO2-Si substrate to prepare the CuNi metal foil for the 2nd annealing; (f) After the 2nd annealing new graphene is grown; (g) The graphene is transferred again and the whole process is repeated until the 5th annealing is reached.

2.1 Graphene synthesis

2.1.1 Substrate selection and preparation

Metallic foil made of a Copper-Nickel alloy (50% wt. Copper, 50% wt. Nickel) has been used as metallic substrate and catalyst for the graphene synthesis. The foil was 0.05 mm thick and 25 cm x 15 cm in area. For the processes the foil was cut in smaller rectangular samples 4 cm x 3 cm in size. This size was chosen to fit the CVD reactor chamber while maximising the sample surface. Each of the obtained samples was stored in its own cylindrical sample-box on top of a piece of cleanroom paper to avoid contamination between different samples or any scratching and smearing damages. The used CuNi samples are shown in Figure 2.2.

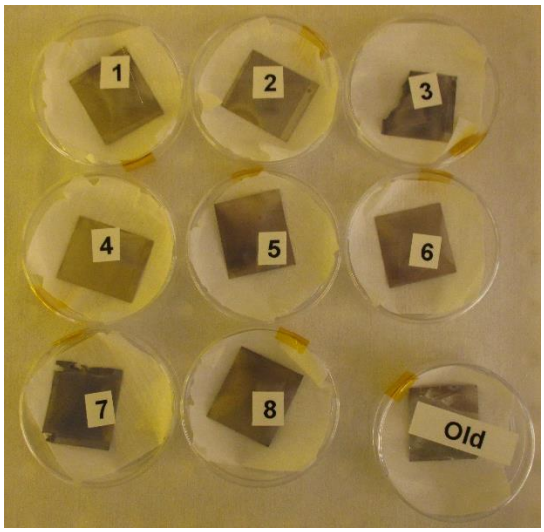

Figure 2.2: CuNi foil cut in 4 cm x 3 cm samples, each one stored in its own sample-box. The shown image has been capture after the initial CVD.

In addition to the catalytic substrate, SiO_2-Si chips were used as graphene substrate for all the analysis. These chips were obtained from a 6-inch silicon wafer which was subjected to high temperature surface oxidation and then cut with a dicing saw as shown in Figure 2.3. The thickness of the silicon wafer after the oxidative process was 0.54 mm and the SiO_2 layer on top of the silicon was around 300 nm on both sides. The SiO_2 oxidation process and the wafer cutting were done by the laboratory technicians in standardised conditions, hence, the SiO_2-Si chips are nominally the same. Still, was sometime possible to see some batch differences in colour, probably due to a slightly different SiO_2 thickness. The chips were of two different sizes, 6 mm x 6 mm and 8mm x 8mm depending on the availability.

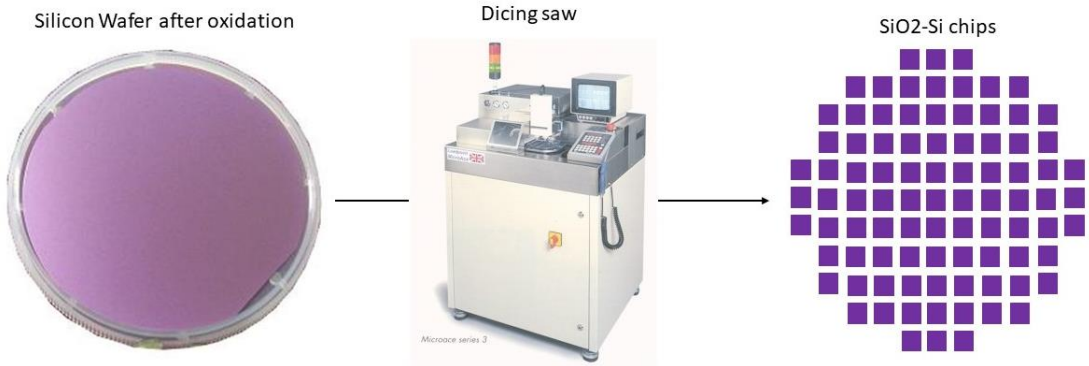

Figure 2.3: On the left a 6-inch wafer is shown, the colour is the typical purple hue that the 300 nm SiO_2 layer gives to the silicon substrate. On the right side the wafer after cutting is shown.

2.1.2 Chemical vapour deposition

As previously explained, the first step of the experiment, after sample preparation, saw the CuNi foil samples undergoing a CVD process. The CVD had the scope of dissolving carbon atoms inside the CuNi alloy with the final aim of using this carbon as a resource for future graphene synthesis by annealing. The used CVD system was a cold wall Aixtron Black

Magic 2-inch reactor (Figure 2.4). For this first step the deposition was performed from a hydrogen – argon – acetylene gas mixture of the following composition: 25 sccm H_2, 1000 sccm Ar and 40 sccm C_2H_2. Substrate temperature, process pressure and process duration were fixed respectively at 850°C, 6 mbar and 10 minutes (See Figure 2.5 (b)).

Figure 2.4: Picture of Aixtron Black Magic 2-inch CVD reactor.

In Figure 2.5 (a) and (b) the inside of the reactor is sketched. As is possible to see, the heating system is made by a rectangular graphite sheet screwed on two columns, the columns are electrically connected to a power generator and current can be let pass through the graphite heater in order to increase its temperature by resistive heating. This system is extremely precise and allows to control the reactor temperature by changing the current flow, a thermocouple in contact with the graphite heater allowed to know its temperature and to make adjustments. On top of the heater, two alumina clamps were used to hold the CuNi samples, the 1 mm thick alumina pieces that make the clamps are fundamental to electrically isolate the sample from the heater and to avoid direct contact between the two (contact which in previous tests ended up in partial melting of CuNi foil). After a sample was loaded with the explained setup, the chamber was sealed under a silica-glass bell and pumped down to 2 x 10^{-4} bar to remove all residual air, then heating (slope of 300°C/minute) and gas flow (only argon and hydrogen) were turned on until 850°C were reached. Once the process temperature was reached the system was kept stable for 1 minute before adding acetylene to the gas mixture and starting the CVD (see process conditions in the previous paragraph). After 10 minutes acetylene flow was stopped and the CVD ended, the system was then cooled as fast as possible by abruptly turning off the heating. Being a cold wall CVD reactor, the cooling rate was reasonably high and the thermocouple reported a drop in temperature from 850°C to 450°C within 5 seconds from the end of the process. Argon and hydrogen were left flowing for the entire length of the cooling. Concluding, when the sample-heater complex had cooled down to 150°C all gas flows were stopped and air was let in to allow sample unloading.

2.1.3 Notes on the carbon precursor choice

The described CVD process was done on 8 CuNi samples (4 cm x 3 cm). Acetylene was chosen as the carbon precursor for the main experiment because it has two carbon atoms per molecule and the plan was to have the highest carbon concentration at the surface of the CuNi sample during the CVD in other to dissolve a higher amount of carbon inside the alloy.

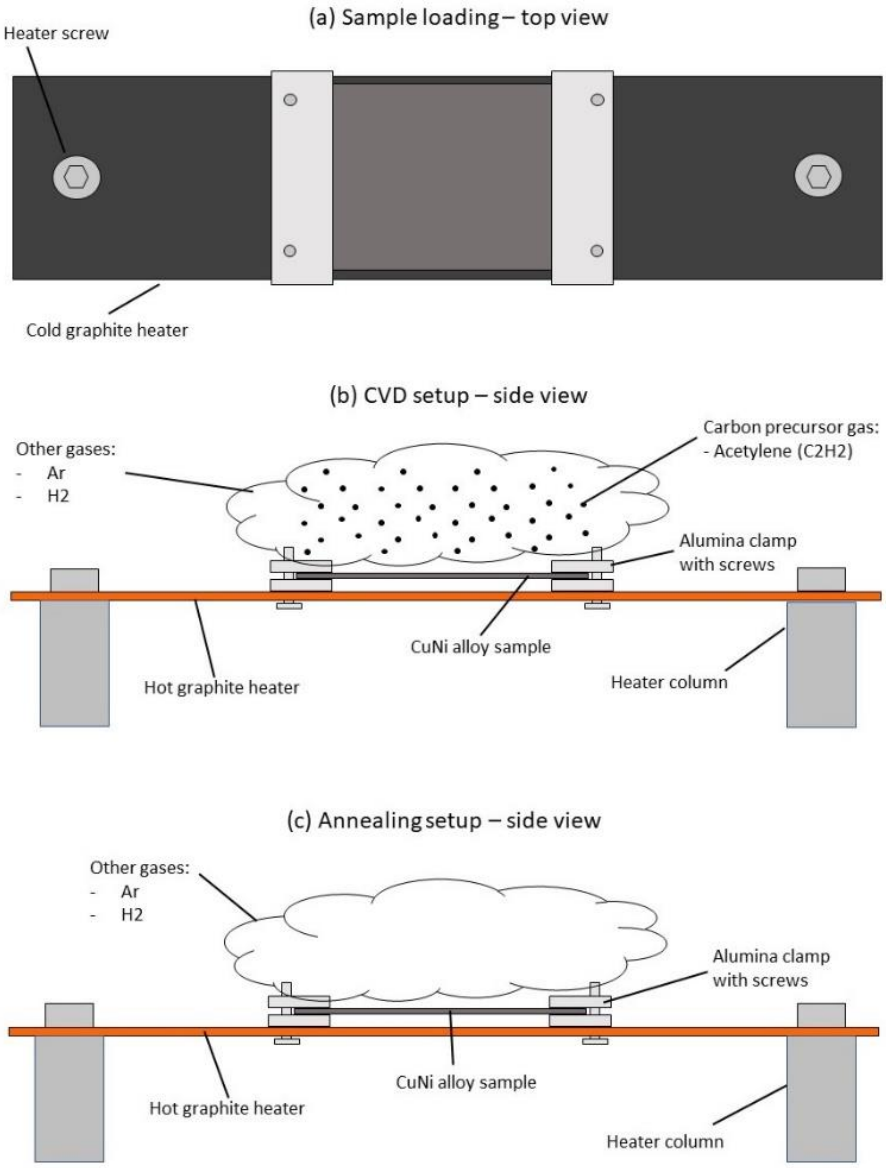

Figure 2.5: (a) Top view of the sample holder inside the CVD reactor. The graphite heater is the main support for the sample but on top of it an alumina clamping system is added to firmly hold the samples. (b) During the CVD process this setup is heated up and the gas mixture is blown on the sample surface. (c) During the annealing the same setup is used but this time there is no carbon precursor gas.

2.1.4 Graphene synthesis from pre-dissolved carbon on CuNi alloy

Carbon-enriched CuNi samples obtained from the CVD process were subjected to bubbling transferring and all graphene was removed, the now pristine CuNi alloy samples were then ready for the annealing process which is the main novelty explored in this work.

The annealing process was performed in the same reactor used for the CVD process (Aixtron Black Magic 2-inch). The samples were loaded as for the CVD (see Figure 2.5 ©). Substrate temperature, process pressure and process duration were respectively set to 850°C, 6 mbar and 10 minutes. All procedures and settings were kept the same as for the CVD process exception made for the acetylene flow which was set to zero for the whole duration of the process resulting in the following gas mixture: argon 1000 sccm and hydrogen 25 sccm. After 10 minutes of annealing the system was cooled down as fast as possible as had been done for the CVD. Then the CuNi sample could be unloaded and subjected to bubbling transferring before repeating the annealing. After the initial CVD had been done on all the CuNi samples, the combination of annealing and transferring was repeated 5 times for each metallic sample, as result graphene samples on SiO_2-Si were collected after each annealing step from each CuNi sample.

2.1.5 Notes on handling and cleaning of the alloy

All CuNi samples were kept in a separate sample-holder and always handled with extreme care to avoid any kind of damage or contamination. SiO_2-Si sample with graphene were stored in appropriated chip-holder before the analysis.

Before the CVD and each annealing, every CuNi alloy sample was cleaned to remove all grease residues and to etch away the thin film of oxide that naturally forms on the metal surface in the time between two processes. The cleaning procedure, shown in Figure 2.6, involved a 5 minutes bath in acetic acid, a 5 minutes bath in acetone, rinsing with isopropanol and blowing dry with nitrogen. The cleaning was a key step of the process because the presence of an oxide layer strongly influences the diffusion of carbon in and out the CuNi alloy changing completely the resulting carbon concentration that drives the annealing process.

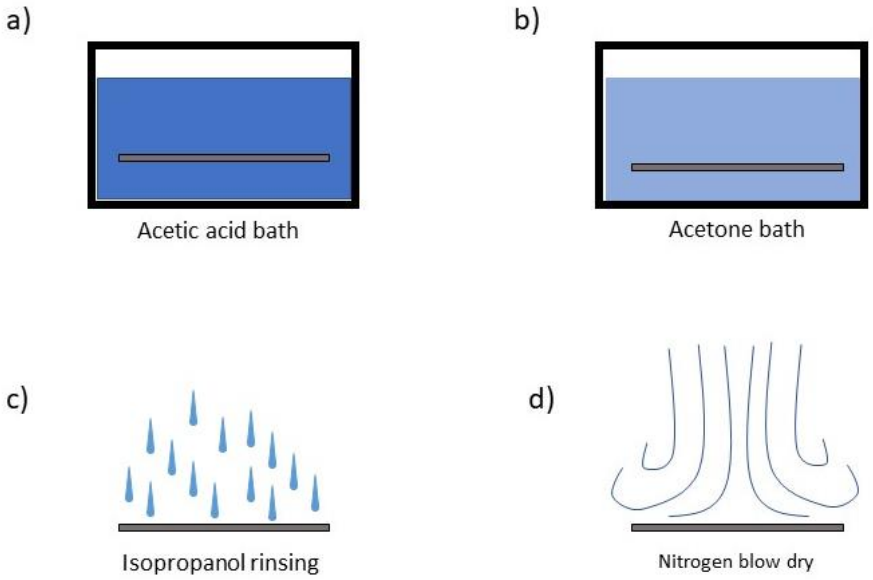

Figure 2.6: The cleaning procedure had the object of removing the oxide layer that forms on the metal surface and to remove any grease residue. First step is a 5 minutes acetic acid bath (a), followed by a 5 minutes acetone bath (b), then the samples are rinsed with isopropanol (c) and blown dry with nitrogen (d).

2.2 Frame assisted electrochemical transfer

Transferring graphene from CuNi foil samples to SiO_2-Si chips without consuming away the metallic catalyst was fundamental to allow annealing repeatability. In micro- and nanofabrication, the most common transfer methods from a metallic substrate to another substrate usually involve the chemical etching of the metallic substrate. For the case of this study, the metal catalyst chemical etch was not an available option since all the work focuses on repeated graphene synthesis from multiple annealings of the carbon-rich CuNi alloy and etching away the CuNi alloy would have resulted in the loss of the main study object. For this reason, frame assisted electrochemical transfer has been used as alternative transferring method.

An overview of all the main steps involved in frame assisted bubbling transferring is shown in Figure 2.7. First the CuNi sample with graphene on top is coated with a polymer film, then rigid squared frames are glued with the same polymer on top of all. Afterwards, the whole sample is connected to an electrical wire and submerged in 0.5M NaOH water solution where hydrogen is electrochemically produced at the interface between graphene and the metal. The hydrogen production separates the graphene film from its previous substrate and allows it to freely float in the NaOH solution sustained by the rigid frame. Now that graphene is separated from the substrate, it can be placed on top of SiO_2-Si chips and let dry before cutting away the frames and dissolving the polymer coating in hot acetone. To follow, every step of the procedures is described in detail.

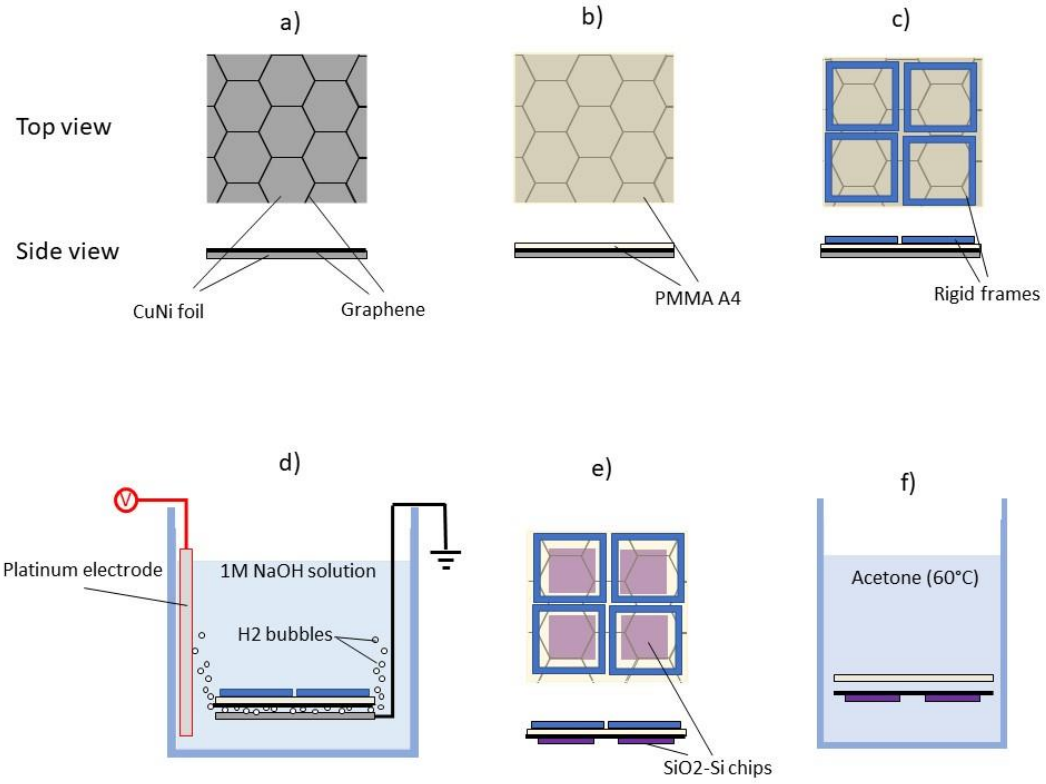

Figure 2.7: Steps involved in electrochemical bubbling transfer. CuNi catalyst with graphene on top (a) is coated with PMMA A4 (b) and plastic frames are glued on top of the polymer film (c). The obtained complex is submerged in NaOH solution and used as electrode in a electrochemical splitting of water process where hydrogen bubbles form at the surface of the catalyst separating the graphene from the CuNi foil. The graphene with polymer and frames is then taken out of the bath and placed on top of the target substrate (e). Finally the frames are cut out and the PMMA is dissolved in an acetone bath.

2.2.1 PMMA film deposition, frames utilization and substrate preparation

To safely transfer graphene thin films, it is fundamental to provide mechanical support to the graphene, in absence of any mechanical support a free-floating graphene thin film wraps and folds becoming practically unusable for any application or analysis.

To avoid these issues, the CuNi samples topsides were coated with a thin film of PMMA A4 (PMMA diluted in 4% anisole). This procedure saw the use of a spin coater operated at 1000 rpm for 1 minutes followed by a 5 minutes curing at 160°C on hot plate for 5 minutes (see Figure 2.7 (a) and (b)). PMMA film needs to be extremely thin so that can be easily removed at the end on the transferring, besides, being so thin it has not enough mechanical sturdiness to keep itself and the graphene flat and plain. For this reason, rigid frames are used. These frames had to be larger than the SiO_2-Si chips and were cut out of a plastic foil with an inner cavity of 10 mm x 10 mm. Once obtained, the frames were glued to the PMMA-coated CuNi samples with the same PMMA A4 used for the coating. The resulting complex is represented in Figure 2.7 (c). With the used CVD/annealing setup, graphene could grow on both sides of the CuNi samples, but to be allowed to effectively separate graphene from the metallic substrate with bubbling transferring it is important to have electrical contact with the metal, this allows to produce hydrogen between CuNi and

graphene separating the two of them. Hence, the graphene grown on the backside of the CuNi samples had to be removed to allow the transferring to work. To do this, after PMMA and frames were applied to the topside, all CuNi samples were laid upside-down inside a plasma reactor and exposed to 50 watts oxygen plasma for 40 seconds. Oxygen plasma etched away the graphene by oxidising the carbon atoms to carbon dioxide, leaving CuNi backsides free from any graphene.

As soon as all CuNi samples were ready for the transferring, the SiO_2-Si chips had to be prepared as well. Bubbling transferring is a wet method, when the graphene-PMMA-frame system detach from the CuNi foil it comes out of 0.5M NaOH water solution, it is washed in deionised water and it is laid on the new substrate while still wet. Therefore, the wettability of the new substrate plays a role in this process. To reduce the mechanical stresses produced by the formation of droplets on the new substrate, the SiO_2-Si chips were treated with 5 watts oxygen plasma for 40 seconds to get the highest hydrophilicity possible (contact angle approximately 180°).

2.2.2 Bubble transferring on SiO2 – Si substrate

The used electrochemical bubbling transfer setup is shown in Figure 2.7 (a). The CuNi-Graphene-PMMA-frame system is clamped with tweezers and submerged in the 0.5M NaOH water solution where has been previously inserted the anode made out of platinum (to avoid any anodic corrosion) as sketched in Figure 2.7 (d). Once both the platinum anode and the samples were inside the NaOH bath, a current generator was turned on and 1A of current was let through the system until detachment which usually occurs within 30 to 45 seconds. Equation 2.1 represents the electrochemical reaction induced at the anode where water is consumed to produce molecular oxygen and hydrogen ions. Equation 2.2, instead, contains the electrochemical reaction at the cathode which in our case is the sample. At the cathode water is consumed and molecular hydrogen is produced. This molecular hydrogen is responsible for the separation of graphene from the CuNi substrate.

$$Anode\ (oxidation): 4OH^- \rightarrow O_{2_{(g)}} + 2H_2O + 4e^- \tag{2.1}$$

$$Cathode\ (reduction): 2H_2O + 2e^- \rightarrow H_{2_{(g)}} + 2OH^- \tag{2.2}$$

NaOH electrolyte is only used to enhance the electrical conductivity of water and does not take part into the electrochemical reaction.

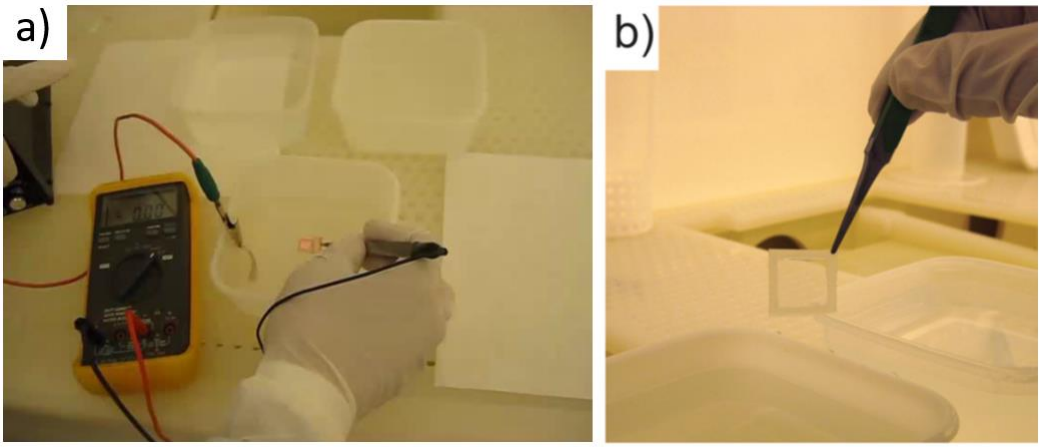

Figure 2.8: (a) Bubbling transfer in action, in the middle of the picture the substrate is visible, the current generator is captured in top-left. (b) A frame with PMMA film and graphene, once detached from the CuNi sample it is rinsed multiple times with water and then placed on top of the target substrate.

Once the bubbling hydrogen had separated graphene from CuNi, the graphene-PMMA-frame complex was picked up with tweezers and rinsed several times in deionized water to remove as much NaOH residues as was possible. In Figure 2.8 (b) the suspended graphene-PMMA film after detachment is shown. Then each frame with its graphene-PMMA was eased down on top of a SiO_2-Si chip completing this step of the transfer (see Figure 2.7 (e)).

2.2.3 Samples drying and PMMA removal

After transfer, the SiO_2-Si chips with the graphene-PMMA-frame on top were left drying for 2 hours. Then the frames were removed by carefully cutting the PMMA film in proximity of the inner edge of the frames. What was left were the SiO_2-Si chips with graphene-PMMA on top. To achieve good adhesion between the chips and graphene the samples needed to be well dried. Air drying alone would not have been enough so, in addition to that, all chips were left 2 minutes on a hot plate at 160°C. It is important to notice that leaving the samples too much at 160°C makes the PMMA removal harder but leaving them not enough time feeds the risk of having a detachment between graphene and the substrate. When all chips were correctly dried, they were put in hot acetone (60°C) for 30 minutes to dissolve the PMMA completing the polymer removal and obtaining graphene on top of SiO_2-Si chips. To complete the transfer, all samples were rinsed with isopropanol and blown dry with nitrogen.

2.3 Graphene characterisation

Graphene transfer main object was to allow the characterization of the deposited carbon thin film. The experiment started with 8 (C_2H_2) CuNi samples (4 cm x 3 cm). After the initial CVD process of those 8 treated with acetylene, two were discarded because of CVD process differences that made them inconsistent with the other samples, so only 6 (C_2H_2) CuNi samples moved to the annealings phase. From each CuNi sample up to three SiO_2-Si chips with graphene were obtained (considering a transfer success rate of 75%). After the CVD and after each annealing one of the C_2H_2-CuNi samples was put aside and saved for the

secondary ions mass spectroscopy analysis (SIMS), so the amount of annealed foils decreased by one sample each step influencing the available samples for Raman spectroscopy and Optical microscopy as shown in Table 2-1.

Table 2-1: Samples and their use throughout the whole experiment.

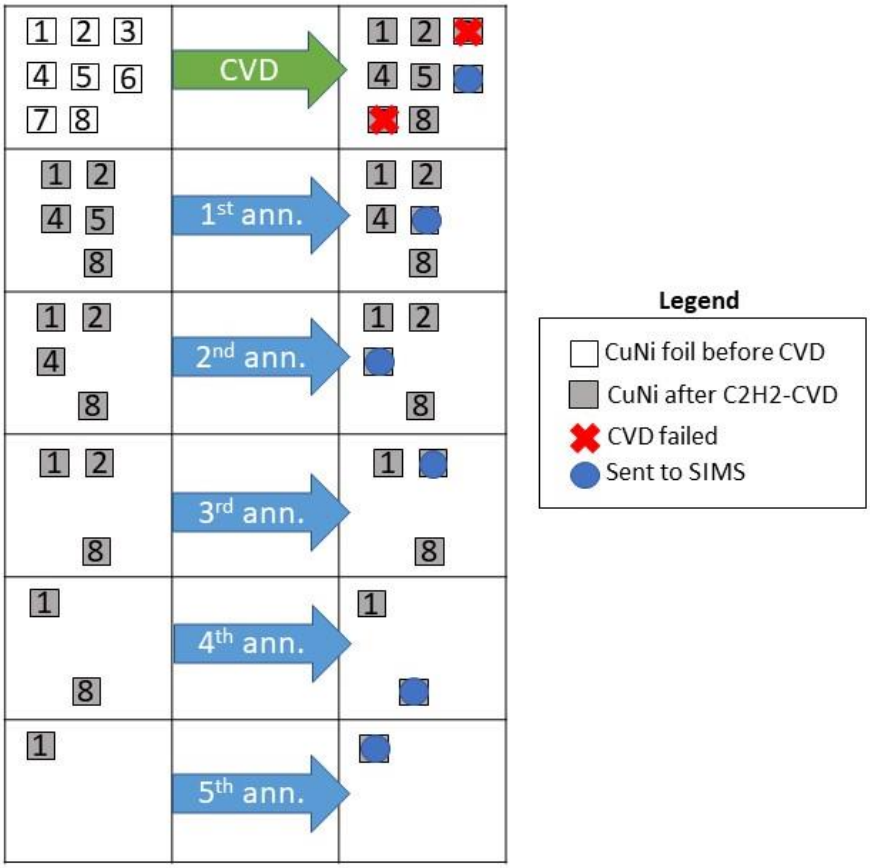

2.3.1 Optical microscopy

The most direct tool to verify the presence of graphene film on a SiO_2-Si sample is optical microscopy. The used chips were specifically chosen with 300 nm thick oxide layer on top of the silicon to allow easy individuation of thin film. On this substrate, even a single layer of graphene changes the colour and the contrast of the substrate making itself visible through optical microscopy. All images were taken with an Olympus MX50 at different magnification. Each chip was captured at 5x to have an overview of the coverage and multiple images at 10x, 20x, 50x, and 100x were captured to show specific areas and details. All photos were then analysed with ImageJ. This image processing software allows to set colour thresholds and to measure the coverage of a certain colour over the image. Figure 2.9 shows the software window, the red part is the area selected by the software based on hue, saturation and brightness filters. In this specific case, the analysed picture is a 100x image of the carbon film obtained though CVD, in red is highlighted the purple background corresponding to graphene multilayer, the area not covered in red correspond to islands made of graphite nanosheets. As it is possible to see form this figure, Imagej is a powerful

tool that allows to measure precisely the percentage of surface covered by a specific type of film.

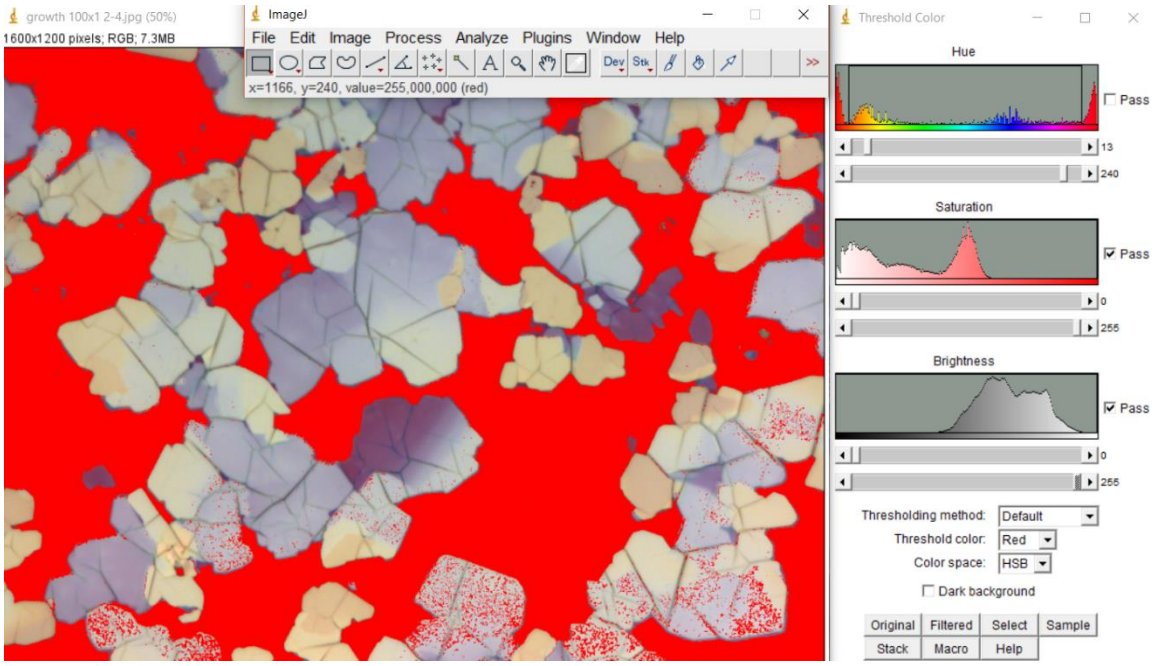

Figure 2.9: Windows of ImageJ software. The software is shown while in use, a colour threshold is set and a certain area of the analysed image is highlighted in red. The red area can then be measured and compared with areas covered in other colours obtaining the percentage of surface corresponding to each colour and hence each film type.

2.3.2 Raman spectroscopy

Optical microscopy alone cannot provide any information about the number of graphene layer or about the nature and the quality of the deposited thin film. Raman spectroscopy was used in this study in two different modalities. The used tool was a Horiba XploRA Raman spectroscope controlled by the LabSpec 6 software. This software, of which Figure 2.10 displays a window, can be used to focus the spectrometer on a small area providing precise information about the quality and the nature of a specific grain or flake. In addition, it is possible to create a Raman mapping of certain areas which allows to see the quality or thickness over a larger area. The focused analysis was used to measure the spectrum of specific areas so that to create connection between the colour of the area at the optical microscopy and its spectrum. This technique was used to confirm nature, thickness and quality of a "colour" on the sample in order to combine this data with the ImageJ analysis and obtaining the percentage of area covered by mono- or multilayer graphene. The focused spectra were collected with an acquisition time of 3 seconds and an accumulation of 3 measurements, ranging from 1100 to 3000 cm^{-1} using a variable magnification. The mapping, instead, consisted in one of this measurement for every point of a grid 20 µm x 20 µm with a knot every 5 µm for a total of 25 spectra over a 400 $µm^2$ area. Mapping was done for one sample of the CVD graphene and one sample obtained from the 5^{th} annealing.

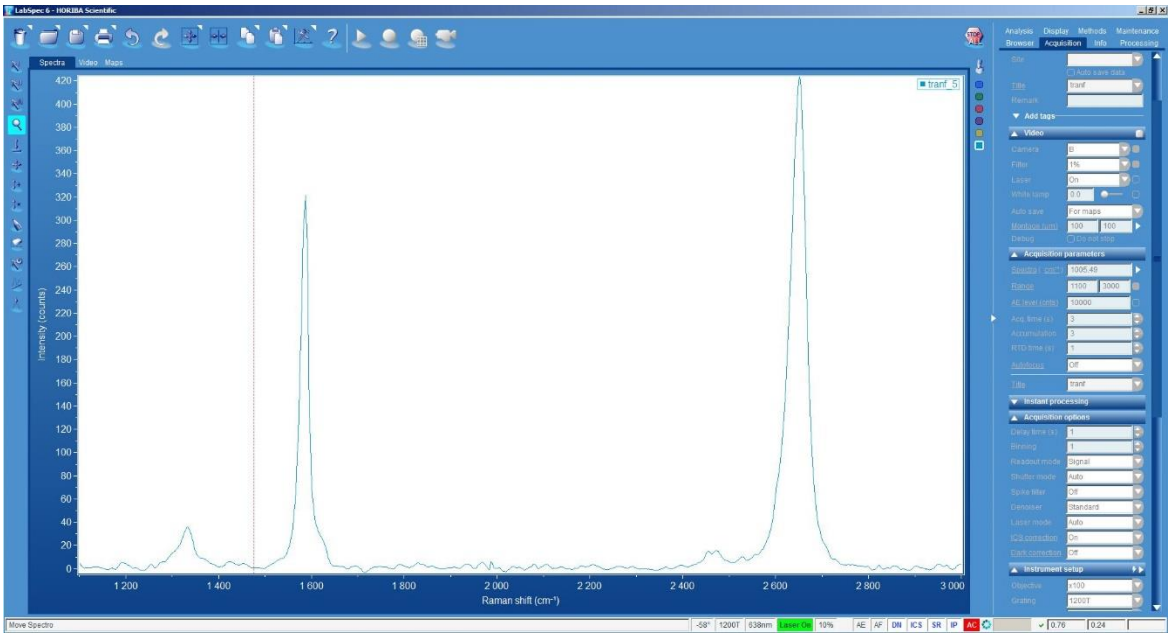

Figure 2.10: Raman spectroscopy software while performing a Raman measurement on a Graphene sample. The typical G and 2D peaks are evident. The software allows to measure the intensity and the ratios between two peaks.

2.3.3 Sheet resistance measurement

Sheet resistance of graphene is usually measured fabricating a microdevice where a small flake of graphene is laid on an insulator and connected to metallic bands that allow to safely measure graphene resistivity without scratching or ruining the film during the measurement. This process requires a lot of time and preparation in the design of the device and in its fabrication. Due to the large number of samples obtained from different annealings in this work was not possible to do such a fine work. Besides, sheet resistance is an extremely important properties and it can provide information about the quality of the graphene. Hence, a faster but less precise method was used in this study to obtain an approximation of the graphene sheet resistance. An AIT CMT-SR2000N 4-point probes system was used; the mounted probes had a tip diameter of 50 µm with a distance between the axis of two near probes of 1 mm for a total of 4 mm in length (Figure 2.11). This system analyses a large area of graphene which means the obtained results are an average sheet resistance of the graphene film with eventual scratches and grain boundaries included. In addition, while coming down to the sample, the probe tips generate a certain shear force to the underlying graphene causing some smearing. This phenomenon means that the contact between the tip and the graphene was exactly on top of the area damaged by the tip itself. For this reason, the obtained sheet resistance is an overestimation of the actual sheet resistance and cannot be fully considered in comparison with data from other studies. Still, they are really useful because they allow the comparison between two samples from different annealing steps helping to probe for trends and differences along with the proceeding of the experiment.

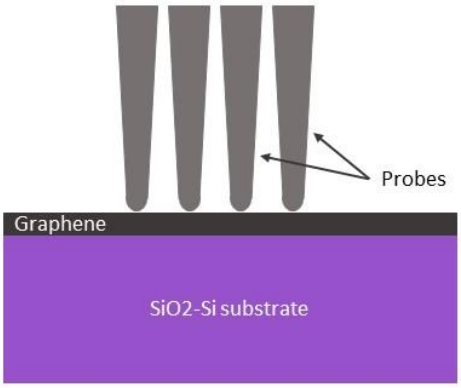

Figure 2.11: Schematic representation of the 4-point probe for sheet resistance measurements while laying on the graphene sample. Thicknesses and probe size not in scale.

2.3.4 TEM and SIMS

In addition to all previous analysis, TEM and SIMS were performed on some of the samples in another laboratory. As explained in Table 2-1, after the initial CVD and after each annealing one of the CuNi foil was sent to be analysed with SIMS. The object of the study was to verify if was possible to find a trend in the carbon concentration inside the CuNi alloy. Moreover, one sample of graphene on SiO_2-Si chip from the CVD deposition and from the fifth annealing was submitted to TEM analysis. The TEM was used to have an image of the section of the graphene film allowing to somehow count the number of layers in the CVD graphene and in the 5^{th} annealing graphene.

3. Results and Discussion

3.1 Raman spectroscopy

3.1.1 Phase identification through Raman spectroscopy

Raman spectroscopy has been used in this work to create an association among the colour of an area on the optical microscope and the nature and thickness of the deposited film. Figure 3.1 contains an optical image and the correspondent Raman spectrum for various areas selected on the carbon film obtained through CVD. Besides the CVD graphene was not interest of this study, the CVD carbon film has been characterised in order to have a comparison with the graphene obtained with the annealing processes and to understand what kind of film might be growing on the used alloy. The studied areas (highlighted by the yellow dot) shown in Figure 3.1 were selected based on their colour, in Figure 3.1 (a) the laser of the Raman spectroscope was focused on a blueish area, in Figure 3.1 (b) on a white area and in Figure 3.1 (c) on the purple background. In addition to the spectra, the values of the D/G and 2D/G ratios are listed in Table 3-1. As can be derived from the data, the blueish and white areas have an almost identical spectrum, both have high intensity G band, low intensity D band and 2D peak around half size of the G peak. From their spectra and from the values of the relative ratios it is clear that the blue and the white area are both graphite nanosheets or multilayer graphene. It is not possible to derive the number of layers that make these areas but the high intensity of the G band (typical of sp2 hybridised carbon atoms) confirm that it is graphite or graphene while the intensity of the 2D band tells it is not few layer graphene. The difference in colour has to be related to a difference in thickness, hence number of layers. The purple background, instead, shown a radically different spectrum. The G peak is still well defined but is now comparable in height with the 2D band which means this area is covered by a much thinner film, moreover the D peak is slightly more intense than the previous spectrum. D peak is associated with defects, the presence of defects breaks the lattice symmetry and the D band rises, the fact that in the purple background the D peak is higher means these areas are somehow more defective than the blue and white areas. Overall, these results suggest that on this CuNi alloy and with the selected process condition the CVD process produces a relatively thin background of graphene (probably 2-3 layers due to 0.94 2D/G ratio)[109] covered in a discontinuous layer of graphite nanosheets. The nature of graphene and graphite can be identified by the shape of the 2D peak in addition of their relative sizes, graphite 2D peak has a small secondary peak at its left side which change the shape of the resulting 2D band creating the small bump that can be seen in the spectra (a) and (b) presented in Figure 3.1 (pointed by red arrows). This bump cannot be seen in spectrum (c) of Figure 3.1 which confirm the purple background is graphene and not graphite[109]. The same method was used on samples obtained from the annealings, in this case the films presented a single homogeneous phase and the recognition was not needed.

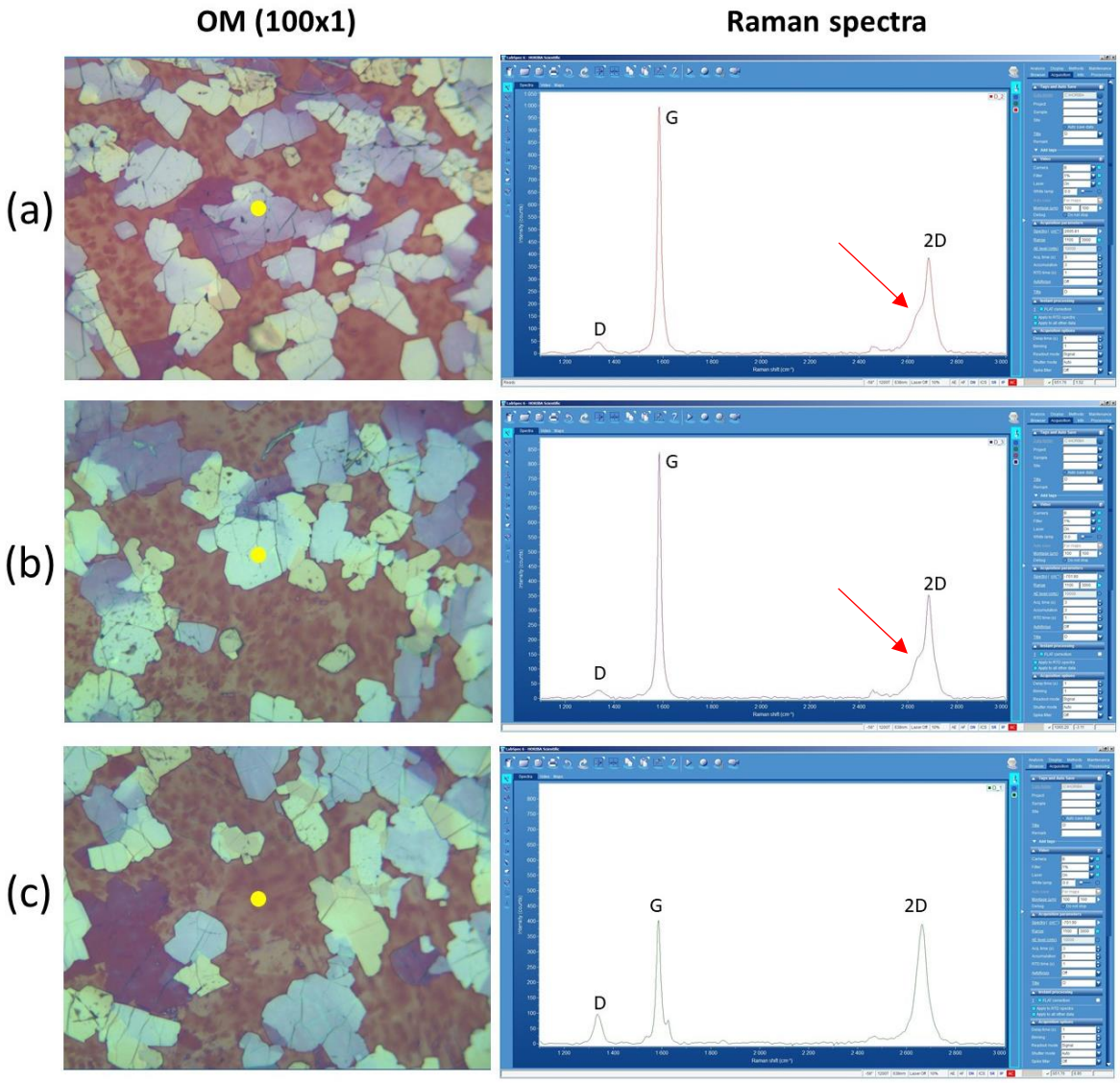

Figure 3.1: In the left column optical images taken at 100x magnification are shown, the right column instead contains the Raman spectrum corresponding to the area pointed by the yellow dot. Different areas are analysed: light blue (a), white (b) and the purple background (c).

Table 3-1: D/G and 2D/G peaks ration for the blue, white and purple area. Data taken from Figure 3.1.

	D/G	2D/G
BLUE AREA	0.086	0.41
WHITE AREA	0.078	0.43
PURPLE AREA	0.26	0.94

3.1.2 Comparison of Raman spectra from CVD and annealing samples

Graphene samples were collected after CVD and after each annealing step and all of them were analysed with Raman spectroscopy. Beside some minor differences, the graphene films obtained from CVD and from each annealing resulted similar to the other obtained in the same step. As expected, samples from the CVD process were similar even if coming from different CuNi samples and the same happened to be true for the annealing graphene. Thanks to this overall homogeneity, each group of samples had a representative spectrum which emerged in almost all cases. Figure 3.2 contains the representative spectrum of each step. The first graph was taken on CVD-graphene, as analysed before, the highly intense G band with low D is typical of good quality graphene or graphite nanosheets and shape and intensity of the 2D peak tell that the analysed film is graphite. In Figure 3.2 (b) to (f) Raman spectroscopy for graphene synthetized with the annealing process are reported (from the 1st to the 5th annealing respectively). The first thing that can be noticed is that the 2D/G ratios for these samples is much higher as displayed in Table 3-2, meaning the films obtained from the annealings are much thinner than the CVD-graphene. Beside this general observation, graphene grown in the 1st annealing is characterised by intense 2D peak but relatively feeble G peak with a D/G ratio of 0.526 which leads to think of a graphene monolayer with some defectiveness. Conversely, graphene films deposited during the 2nd, 3rd and 4th graphene are different from the film obtained in the 1st annealing and show a much healthier spectrum for a graphene monolayer. All these three samples have an almost identical spectrum, 2D peak twice intense than the G peak with 2D/G ratio around 2 and a D band a third intense than the G band resulting in a D/G ratio around 0.33. These features describe almost perfectly the spectrum of a high-quality graphene monolayer. Instead, the 5th annealing gave a graphene film with different features. The spectrum of graphene from the 5th annealing shows a D band as the most intense of all, with a split G peak (due to the presence of a D' peak) and almost absent 2D peak. If in previous samples the graphene plane structure was intact, this last sample presents a crystalline lattice disrupted and incomplete. For the first time a D' peak can be seen, this band is caused by the interaction of graphene lattice vibration with impurities and its presence suggests that beyond being incomplete, foreign atoms can be found in what remain of the lattice.

Using the data contained in Table 3-2 and summarizing the content of Figure 3.2 it is possible to create a defined picture of the overall process trend. The first important thing that can be said is that during the annealing steps the obtained graphene is completely different from the graphene obtained with the CVD process on the same substrate. Growing graphene on Ni usually ends in a multilayer graphene which sometimes overgrow to become graphite nanosheets (as happened in our case beside the presence on Cu in the alloy). This is mainly due to the fact that carbon atoms that form on the catalyst surface when the precursor decomposes can dissolve inside the Ni lattice, the growth process is a continuous one and the catalyst surface remains active for the whole process[82]. When the same CuNi alloy is annealed, the carbon atoms that forms graphene emerge from the catalyst bulk itself to form a graphene monolayer as demonstrated by the Raman results.

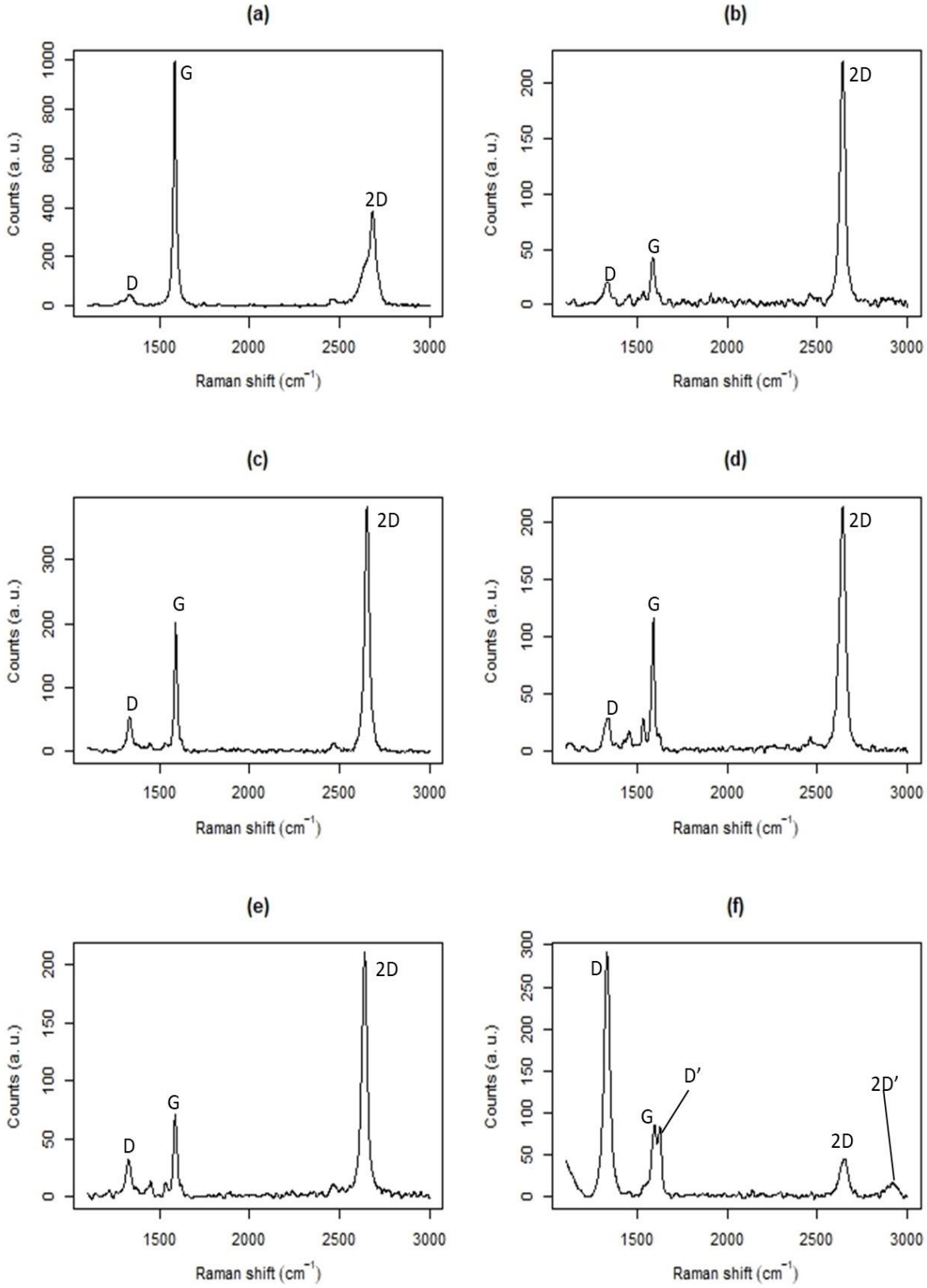

Figure 3.2: Raman spectroscopy of the transferred graphene obtained from the CVD process and from each annealing: (a) CVD, (b) 1st annealing, (c) 2nd annealing, (d) 3rd annealing, (e) 4th annealing, (f) 5th annealing.

This difference might be attributed to a less abundant carbon source but still provides a graphene monolayer, much more interesting than graphite nanosheets for technological application purpose. Once asserted the nature of graphene deposited with annealing, the Raman spectra highlight a trend within the various annealing steps. The 1st annealing provides a graphene which is overall defective and of low quality but from the 2nd to the 4th annealing the graphene quality is high and uniform. The 5th annealing instead produced the worst carbon-based film, probably an incomplete graphene film. From this trend we can speculate that during the first annealing carbon was abundant, but impurities and lattice defects were more common. From the 2nd to the 4th the carbon resource was still able to provide building blocks for the growing graphene while the repeated annealings might be the cause of the better quality. Once the process reaches the 5th and last annealing the carbon atoms were lacking and the availability of carbon was insufficient to support the growth of a complete graphene film.

Table 3-2: D/G and 2D/G peaks ratios for CVD graphene and all annealing samples. Data taken from Figure 3.2

	D/G	2D/G
CVD	0.102	0.399
1ST ANNEALING	0.526	4.344
2ND ANNEALING	0.318	1.763
3RD ANNEALING	0.338	1.710
4TH ANNEALING	0.406	2.651
5TH ANNEALING	3.561	0.616

3.1.3 Raman mapping

Raman mapping has as first aim to assert homogeneity of the substrate. In this study mapping was performed on a sample of CVD-graphene and on graphene obtained with the 5th annealing. Figure 3.3 shows a colour map of the values of D/G and 2D/G ratios. The values of these ratios are in agreement with the Raman spectra analysed in the previous section where the D/G and 2D/G ratios for CVD-graphene were found to be ~ 0.1 and ~ 0.4 respectively; and the D/G and 2D/G ratios for 5th annealing graphene were found to be ~ 3.6 and 0.6. From Figure 3.3 it is then clear that the deposited films have rather homogeneous quality over the analysed area of surface. The studied sample is not huge but it is enough to show that, at the grain scale, graphene is coherent and uniform and this is valid even for the 5th annealing sample which has the worse quality among other samples.

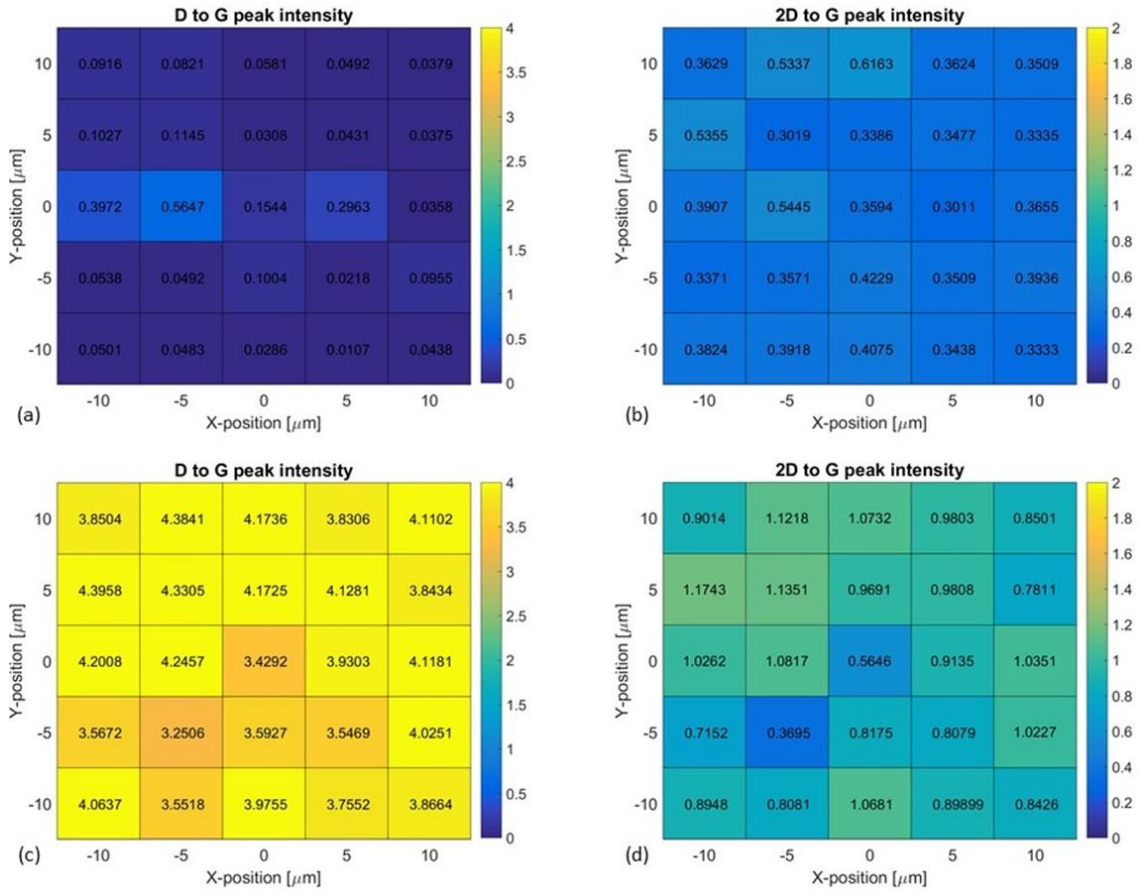

Figure 3.3: Raman mapping of the transferred graphene grown from CVD: (a) intensity ratio of D/G peaks, (b) intensity ratio of 2D/G peaks. Raman mapping of the transferred graphene from the 5th annealing: (c) intensity ratio of D/G peaks, (d) intensity ratio of 2D/G peaks.

3.2 Optical microscopy

Optical microscopy images were taken for all the obtained samples, this technique is fast, non-destructive and allowed to have an overall knowledge about the coverage and quality of graphene films. In Figure 3.4 an optical image of graphene on SiO_2-Si chip obtained from the 2nd annealing is reported, the picture was captured at 100x1 magnification. This image is not representative of the overall sample surface, but it is reported as great example of interference contrast due to atomic differences in thickness. In the background is possible to see a graphene monolayer with some scratch in the left area of the image, on top of the background graphene there is a purple island and the transition from purple to background beige is characterised by colour steps. Starting from the background is possible "to climb up-hill" towards the purple area and each colour step represent an additional graphene layer stacked on top of the previous. Each additional layer changes slightly the perceived colour and allows to count clearly the number of layers. Thanks to this method and ImageJ (image analysis software) was possible to calculate an approximation of the area coverage.

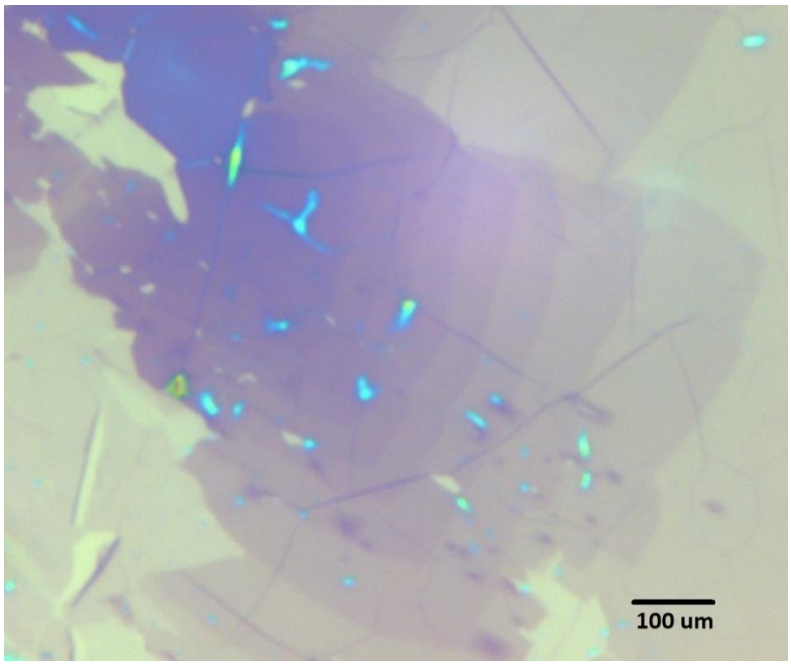

Figure 3.4: Optical image of purple island on a graphene sample obtained during the 2nd annealing. 100x magnification. In this image is possible to see how adding a single layer of graphene changes the colour of the substrate from beige to purple. Overall the number of layer that it is possible to count is around ten.

Figure 3.5 compares two optical images taken at the same magnification of 50x1. On the left an image of CVD-graphene is reported, while on the right side an image of graphene from the 5th annealing is shown. The differences are sharp and clear, the CVD graphene was extremely thick with island of graphite nanosheets while the graphene obtained from the annealing process is a monolayer of graphene. These pictures comply with the Raman results and shows how different are the films obtained from the same substrate with different processes. Additionally, what is surprising to be seen is that graphene deposited with the 5th annealing presents some wrinkles and holes, but it is almost intact. In spite of having bad Raman spectrum, the CuNi alloy was clearly able to provide enough carbon atoms to produce a 5th graphene, homogeneous and almost complete at the optical analysis. Besides, the fact that this sample had not the spectrum of a healthy graphene film leads to think that a 6th annealing process would have resulted in no graphene. Figure 3.5, on the other hand, tells how important it is to check with Raman spectroscopy, to the eye with optical microscopy the film obtained from the 5th annealing would have looked as a decent result when Raman spectrum showed how damaged the film was at the atomic level. Optical microscopy and Raman spectroscopy together provide a complete set of information, both on the crystalline structure and on the macroscopic morphology.

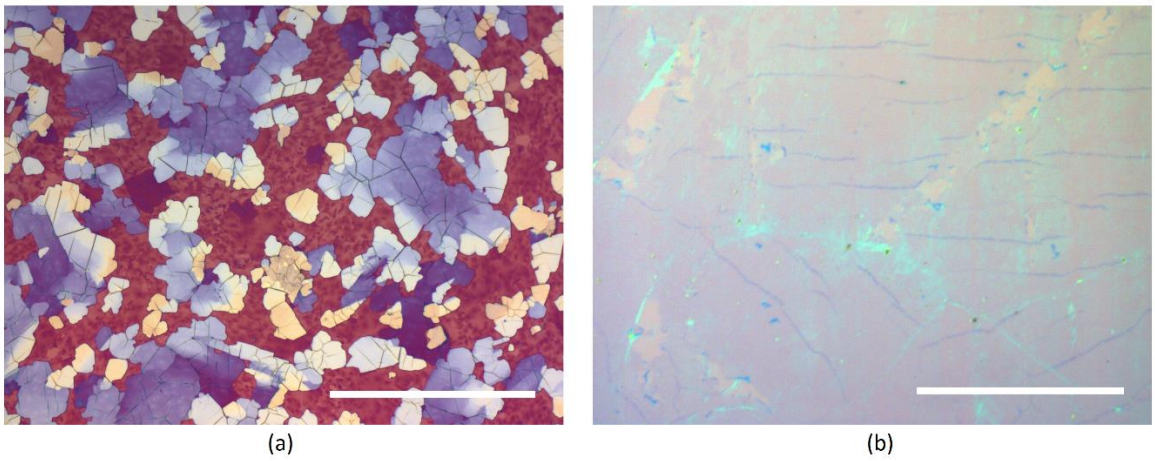

Figure 3.5: Optical microscopy images of the transferred graphene obtained from the CVD process (a) and from the 5th annealing (b). (Magnification 50X1; scale bars 100 µm).

Once collected, all images were analysed with ImageJ in order to extract the percentage of area covered in graphene monolayer, graphite nanosheets or holes. Figure 3.6 contains a visual summary of the analysis. There, it is possible to appreciate the overall trend in quality and coverage of the deposited films. The as-taken photos are displayed in column A, in column B and C part of the analysis process is shown and the red area represent the software selection. In column B the software was used to highlight the areas covered in multilayer graphene or graphite nanosheets, in column C instead the red area represents the area of substrate not covered in any film. From this overview, the difference between CVD-graphene and annealing graphene is shown. In addition, it is possible to notice how the presence of multi-layered graphene decrease along with the number of annealings. Graphene deposited in the 1st and 2nd annealing has still few areas where graphene is multi-layered, but with the 3rd annealing only monolayers are found. Presumably, the area where thicker graphene grows represent areas were carbon atoms are expelled at a faster rate out of the metallic substrate, this carbon then grows in planes creating the graphene layers. In the sample from the 3rd annealing there are no areas with multi-layered graphene but there are areas where the monolayer seems to have darker shade of pink. These darker areas might be the correspondent of the carbon emitting areas cited earlier. This time, it seems like there was not enough carbon to grow multilayer graphene on them. A theory that might explain this phenomenon involve the depletion of the driving force that pushes the carbon atoms outside the alloy: until the 2nd annealing the carbon concentration inside the CuNi catalyst is still high enough that the rate at which carbon atoms exit the metal is higher than the rate at which they are consumed. Starting from the 3rd annealing forward, this carbon concentration might be diminished sufficiently that rate at which carbon atoms exit the metal is equal or lower than the rate at which they can migrate on the whole surface forming graphene.

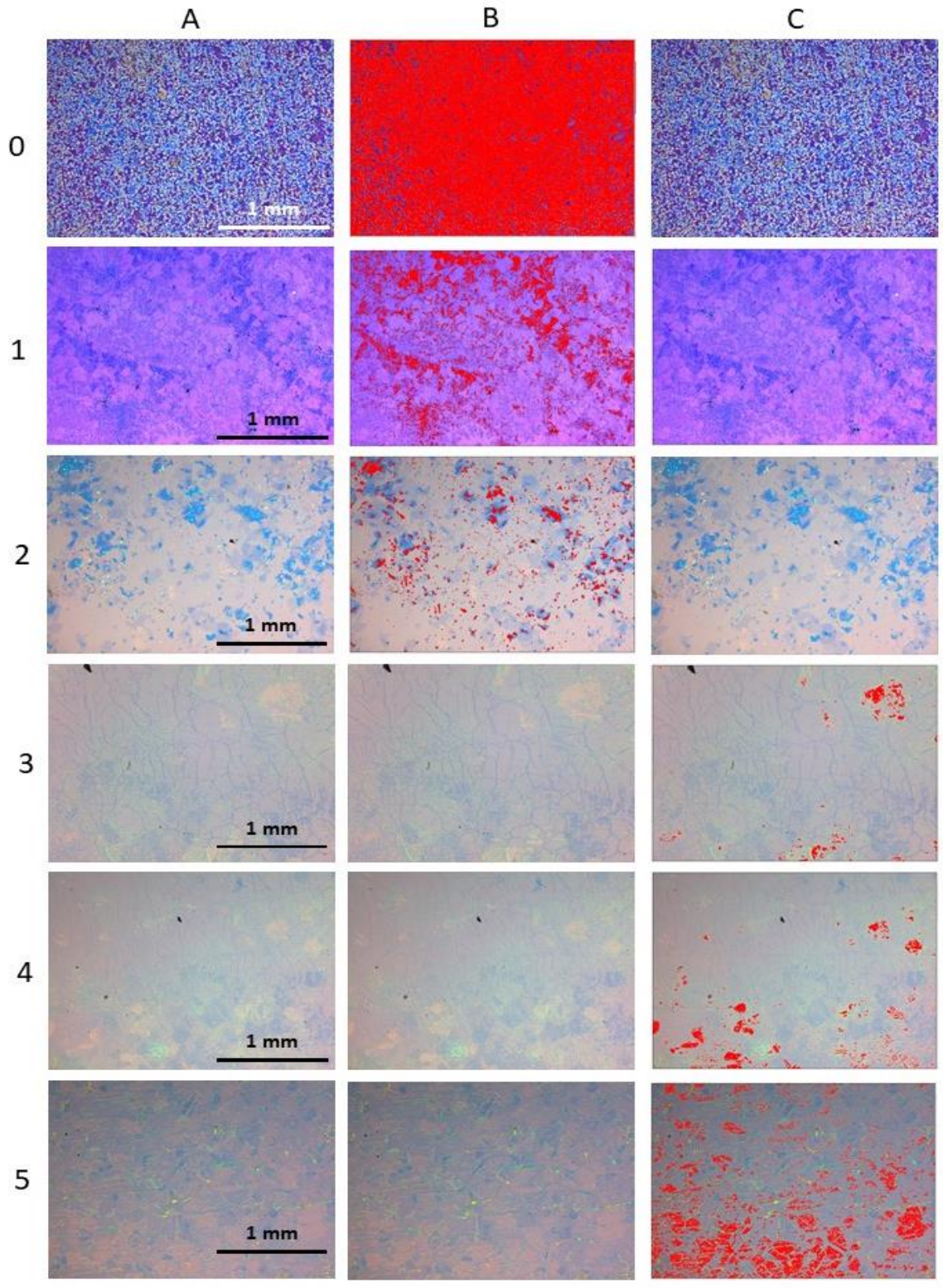

Figure 3.6: Column A – optical images, magnification 5X1; Column B – optical image, area covered by multi-layered graphene is highlighted (Red area); Column C – optical images, uncovered area is highlighted (Red area). Row 0 – Optical images from CVD; Row 1 to 5 – Optical images from annealing 1 to 5.

Continuing reading Figure 3.6 this explanation finds stronger validation, in fact the same darker areas individuated in the 3rd annealing can be seen until the 5th annealing is reached, while other areas ends up having no graphene on them. The coexistence of darker areas and holes in the same film leads to think that the availability of carbon atoms is not the same over the all metallic catalyst and that some areas needs the carbon produced in nearby areas as building blocks for the graphene. However, it is hard to assert how and why this happens, one reason could be that some of the metal grains have a higher percentage of Ni and can store a much higher amount of carbon atoms while other grains (rich in Cu) cannot store carbon but can catalyse the formation of thinner graphene. This model would explain the presence of grains where graphene is thin and other grains where it graphene is thicker. Figure 3.4 can be seen through this model as well, in fact graphene sims to expand from the central area of the picture towards the edges as if the carbon was exiting the alloy in proximity of the thicker graphene and then diffused on the nearby areas.

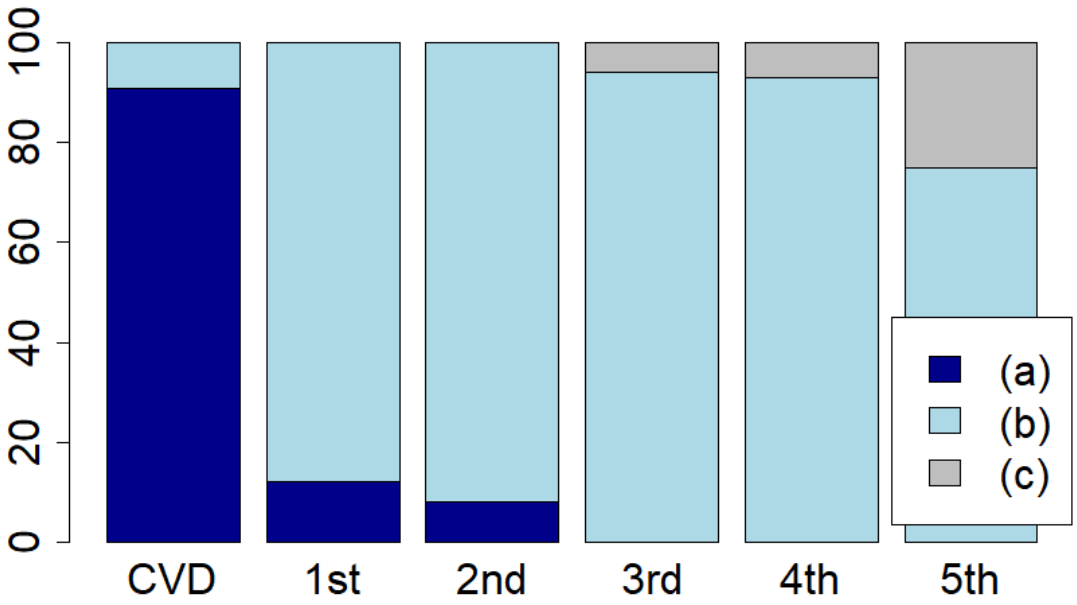

Figure 3.7: Percentage of surface covered by: (a) multilayer graphene, (b) 1-3 layers of graphene, (c) holes or scratches.

To conclude the optical images analysis, the results of ImageJ measurements are shown in Figure 3.7. This chart clarifies what has been said about the optical images and shows in a more direct way how the percentage of area covered in different film thicknesses are distributed. The CVD-graphene has the highest multi-layered graphene percentage with almost 90%. In 2nd and 3rd annealing this percentage sharply drops to 12% and then to less than 10%. Starting from the 3rd annealing the percentage of multi-layered graphene is zero but a small amount of the surface results uncovered. The amount of surface not covered by any graphene remain stable around 10% for the 3rd and 4th annealing and then rises to about

25% with the 5th annealing. Besides some of the uncovered area has to be attributed to scratches and smearing damages related to the transferring process, most of holes are probably due to the scarcity of carbon atoms that starts to become a problem in the 3rd annealing becoming unsustainable with the 5th annealing. In fact, graphene from the 3rd and 4th annealing still resulted in a good quality graphene as confirmed by Raman spectroscopy, while the 5th annealing produced only an incomplete and damaged film.

3.3 Sheet resistance

The results of the 4-probes sheet resistance measurements are shown in Figure 3.8. The chart reports the average sheet resistance in kohm/sq. The sheet resistance for the CVD-graphene is reported even if, being ~ 0.7 kohm/sq. is barely above zero in this graph. CVD-graphene was multi-layered in the background with large islands of graphite nanosheets and its resistance was expected to be much lower than that graphene deposited in the annealing processes.

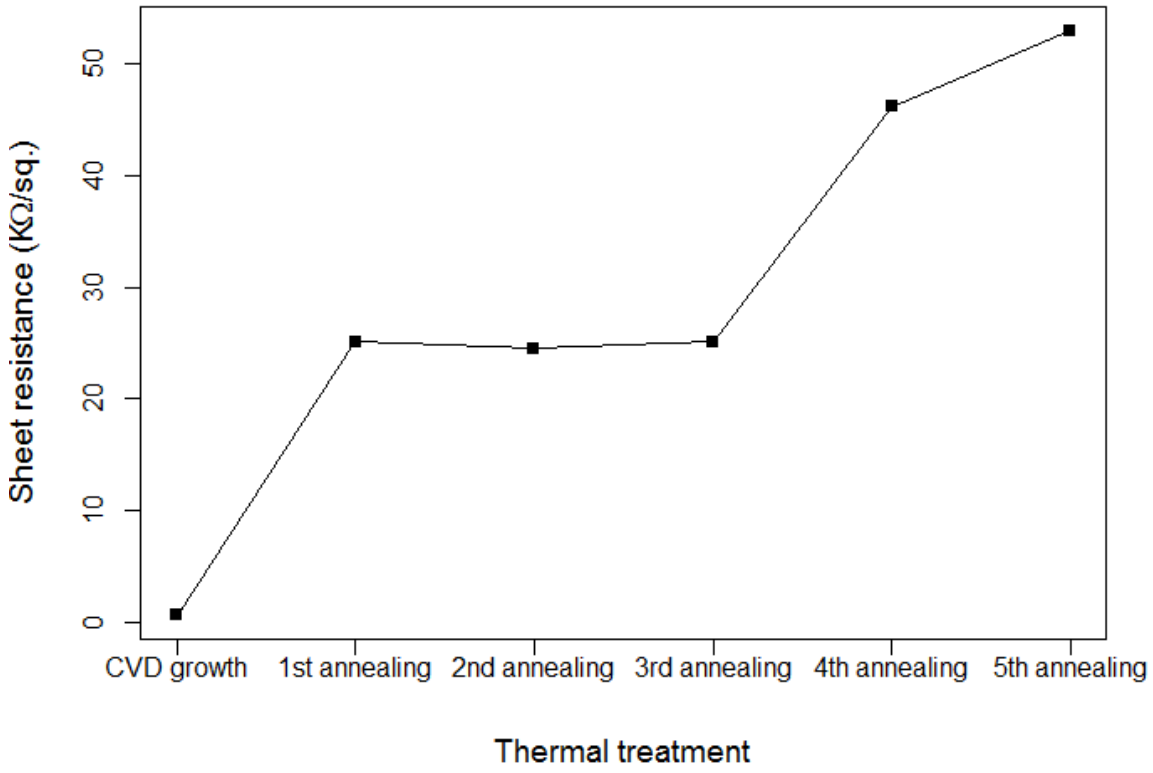

Figure 3.8: Sheet resistance measurements of the transferred graphene from the CVD and from each annealing.

The first thing that can be seen on this chart is that, CVD-graphene aside, graphene from 1st, 2nd and 3rd annealing have the same resistivity of ~ 25 kohm/sq. Once reached the 4th annealing the resistivity start to rise reaching its maximum of ~ 50 kohm/sq. at the 5th annealing. Because the graphene grown during the 1st to 3rd annealings resulted to be a

monolayer, 25 kohm/sq. is still a relatively low sheet resistance that can be associated with a high-quality graphene film. The sheet resistance of samples from 4th and 5th annealing, instead, starts to be out of the range for usable graphene. The trend shown in Figure 3.8 is of extreme importance and agrees with all the assumptions that have been made from the optical analysis and Raman spectroscopy: from the 1st to the 3rd annealing the graphene production is sustainable and repeatable with consistent properties of the film along the different steps, but once the 4th annealing is reached the formation of graphene begins to have to deal with lack of available carbon atoms at the catalyst surface. The 5th annealing in particular has to be considered the absolute limit for graphene production with this method and this specific setup. Still, it is pretty impressive that the carbon atoms stored inside the CuNi alloy were able to supply the graphene formation for 4 successive annealings.

3.4 Transmission electron microscope

Figure 3.9 display a TEM image of a CVD-graphene and 5th annealing graphene samples. In this view the film is depicted in section and it is possible to directly visualise the substrate covered in graphene. On the left CVD-graphene is shown and the number of graphene layers can be counted around 20. This image together with Raman spectroscopy and optical microscopy is a final confirmation of the nature of the film. The boundary between multi-layered graphene and graphite nanosheets is conventionally set at 5-10 layers, hence, the analysed film is definitely in the graphite nanosheet field. It is important to say that the area which has been selected for TEM imaging was one of the blue areas treated in the Raman section and it was already identified as graphite nanosheet through its Raman spectrum. On the right side of Figure 3.9 a sample from the 5th annealing is analysed.

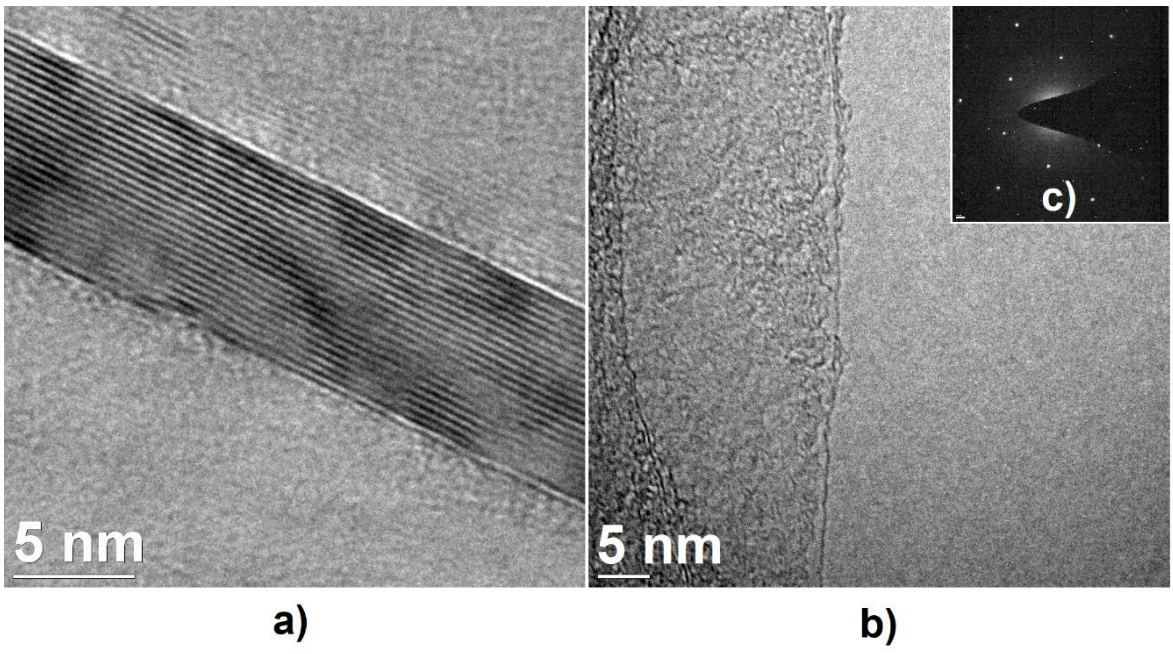

Figure 3.9: TEM imaging of multilayer graphene from the CVD (a) and monolayer graphene from the 5th annealing (b). Diffraction pattern of a graphene monolayer (c).

Here it is immediately clear that the deposited layer is much thinner than the CVD-graphene. In this image the substrate is on the left side and on top of it an uneven layer can be noticed. This uneven layer is the graphene obtained during the 5th annealing and it appears highly damaged and incomplete as was expected by the Raman spectroscopy. To complete the TEM study a diffraction pattern was measured for the CVD-graphene, the pattern results to be the typical pattern for graphene and brings an additional confirmation on the film nature.

3.5 Secondary ions mass spectroscopy

One of the final analysis performed in this study is the secondary ions mass spectroscopy on the metal foils used for the experiment. Before analysing the results, it is important to understand what is the amount of carbon that would have saturated the used CuNi alloy (50% wt. Cu, 50% wt. Ni). The solubilities of carbon in Cu and Ni are 0.0027 at.%[104] and 1.26 at.%[23] at around 1000° C, respectively. Therefore, the nominal maximum carbon concentration in the 50% Cu 50% Ni alloy is (1.26×0.5+0.0027×0.5) at.%=0.6313. The initial CVD process was performed at 850°C, at this temperature the nominal concentration of equilibrium would be slightly lower but still in the same range of concentration. At room temperature the carbon solubility is much lower which means carbon should diffuse outside the metal during the cooling down: carbon concentration is higher than the maximum thermodynamically stable at room temperature, it is an oversaturated solid solution. From this consideration, the atomic concentration of carbon was expected to be slightly below 0.6313 % at. after the CVD process. Then the concentration is expected to decrease towards a minimum annealing after annealing. This minimum represents the carbon solubility of the used alloy at room temperature: when the carbon concentration is at this value, during the cooling down the alloy would not result in an oversaturation and carbon would have no reason to diffuse outside becoming graphene.

Figure 3.10 contains the SIMS results, as it is shown the values and the trend of the graph are in complete accordance with the previous assumptions. After CVD the ally had a 0.58% at. of carbon concentration which is just below the theoretical value for the same alloy at 1000°C. After the 1st annealing this value drops to 0.54% at. and it keep diminishing annealing after annealing. What it is interesting to highlight is the size of the steps the carbon concentration undergoes, if from the 1st to the 2nd and from the 2nd to the 3rd the steps are quite big, in the following annealing the carbon concentration diminishes more slowly until it reaches a plateau at 0.41 % at. From the 4th to the 5th annealing there is almost any drop in carbon concentration which explains why graphene obtained in the 5th annealing was incomplete and damaged. Nevertheless, the fact that some carbon film formed during the 5th annealing tells that even when the carbon concentration inside the alloy has reached its plateau some carbon diffuses towards the surface anyway. This happens because at the surface the carbon concentration is virtually zero, hence, even if the solid solution is not oversaturated, some diffusion still happens due to the concentration gradient.

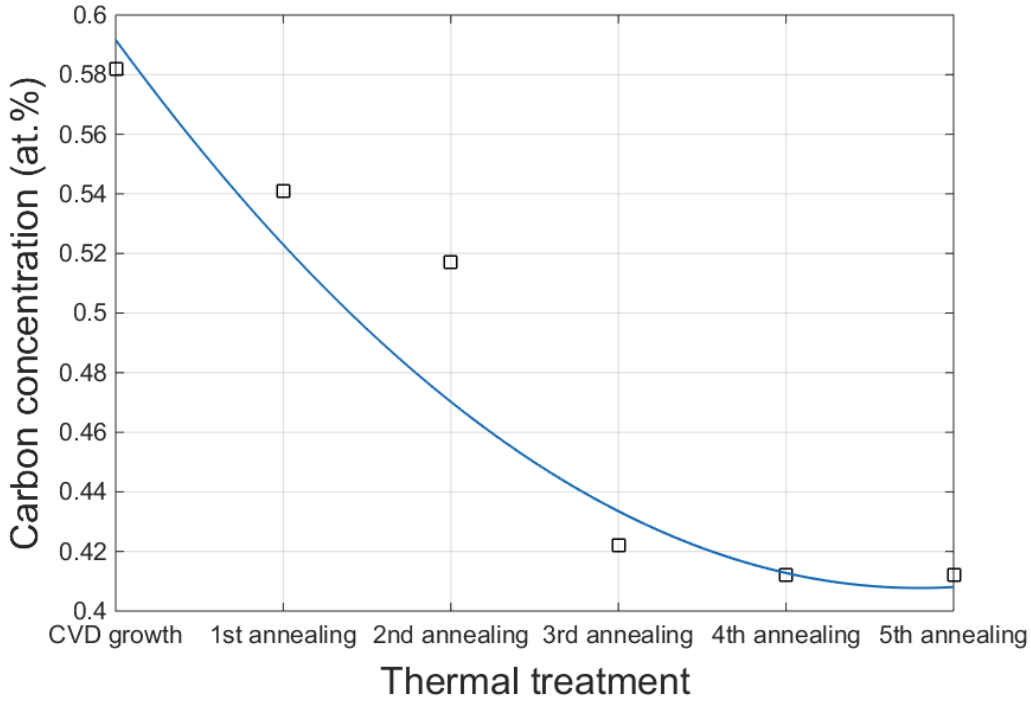

Figure 3.10: Results from the SIMS analysis on the CuNi metal foils after the CVD and after each annealing.

3.6 Proposed growth-model

To conclude this section, it is now important to collect all the main information obtained from various analysis and try to have some insight about the growth dynamics for the proposed annealing method. Raman spectroscopy and optical microscopy confirmed that all annealing processes led to a successful graphene deposition. All steps provided with high-quality graphene exception made for the 5th annealing which gave an incomplete graphene monolayer. SIMS analysis demonstrated that the carbon responsible for the graphene growth was coming from the CuNi alloy and that this reservoir of carbon atoms actually depletes over time. In our setup this reservoir became unable to feed the synthesis of a complete graphene film after 4 annealings but, changing some conditions, the number of possible annealings is likely to be improved. From the collected data a growth-model is proposed and Figure 3.11 contains a sketch of this model. During the CVD acetylene decomposes in carbon atoms on the hot surface of the catalyst, once the carbon atoms are on the surface a concentration gradient between the surface and the bulk of the metal is generated and carbon atoms start to diffuse towards the core of the CuNi catalyst. In this phase the carbon concentration at the surface is saturated and kept constant by the acetylene flow. Because of the almost perfect fit between the 0.58% at. obtained from the SIMS and the 0.63% at theoretically calculated, it looks like during the CVD process there is enough time to reach the thermodynamic equilibrium. Hence, the obtained concentration is the maximum reachable for the tested alloy. During the cooldown the acetylene flow is stopped,

the equilibrium concentration gradually decreases with the alloy temperature and carbon starts to diffuse outside the substrate but because of the high cooling rate there is not enough time to brings the final carbon concentration inside the catalyst to the equilibrium value at room temperature. Therefore, at the end of the CVD process, at room temperature, the solid solution of Ni, Cu and C is supersaturated. During the annealing the alloy is heated up again at 850°C and mobility inside the alloy is restored, atoms can now diffuse again but due to the high temperature (which brings up the maximum concentration of carbon atoms) only a small amount of carbon atoms diffuse to the surface. Then, the cooling starts and the equilibrium concentration drops, carbon atoms are rapidly pushed to diffuse outside the CuNi foil and manage to escape preferentially from certain grains (purple island individuated with optical microscopy) this sudden flow of carbon atoms to the surface of the CuNi foil is activated by the CuNi catalyst itself and arranged to form graphene. This is the most important step and it happens quickly. Immediately after, the carbon flow is stopped by the low temperature which obstructs the diffusion. Because of the cooling rate, one annealing is not sufficient to deplete all the carbon surplus and after the first annealing the final concentration is still higher than the maximum carbon concentration at room temperature. This means the process can be repeated.

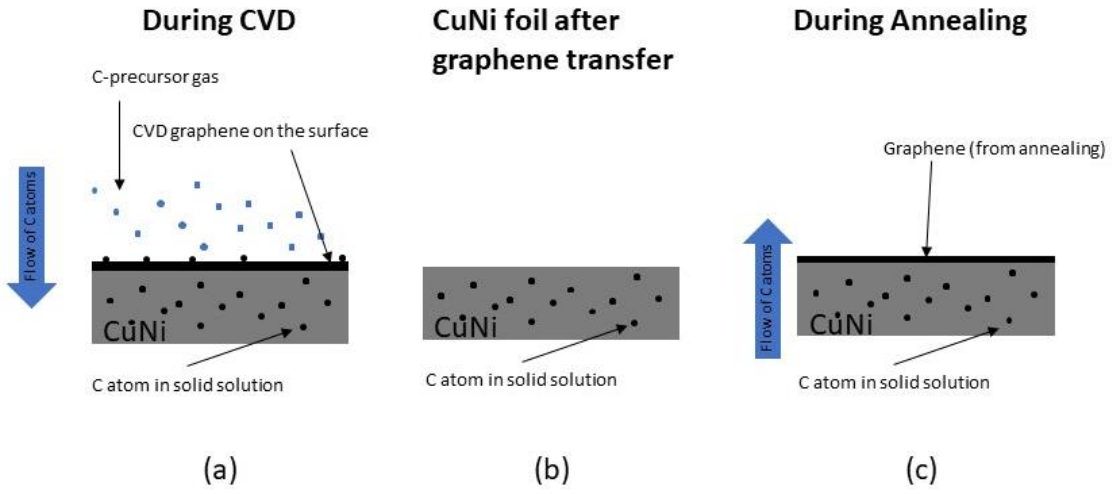

Figure 3.11: A schematic for the process dynamics is presented. (a) During the CVD the precursor gas decomposes in carbon atoms on the surface of the CuNi metal foil, some of the carbon atoms form CVD graphene on the surface, some enter the metal foil. (b) Once the graphene is removed from the surface of the CuNi metal foil, the only carbon remaining is in the forms of atoms inside the crystal lattice. (c) During the annealing the high temperature increase the diffusion rate of the carbon atoms trapped in the crystal lattice and set them free to migrate towards the surface to form a new layer of graphene.

This model is clearly a simplification of what is really happening inside the metallic foil, but it is helpful to understand what are the main forces in play and might be useful to drive further studies in the right direction. For example, from what has been assumed, having a thicker metallic foil keeping the same surface area might improve linearly the number of

successful annealing synthesis; besides, a thicker foil might need longer CVD times to be fully saturated. Moreover the alloy composition can be adjusted changing the Cu/Ni ratio in order to improve carbon solubility or the catalytic effect of Cu, the alloy itself can be changed to other metals in order to test the same process with different catalysts and even the grown film can be changed from graphene to any other thin film which has a precursor that can be dissolved inside a solid solution. This method is rather new and unexplored, it might open many innovative ways to deposit graphene and other 2D materials, changing the way graphene is stored and even making it more available for industrial processes. In addition, it provides a lot of information about graphene growth dynamics helping to explore the role of different metallic catalysts and their use.

4. Conclusions

4.1 Experimental results

This work allowed to safely conclude that it is possible to grow high-quality graphene monolayers annealing a CuNi metallic foil which was previously enriched with carbon atoms. The innovation of this method is that it does not involve any external carbon source and uses the carbon atoms dissolved inside the metallic lattice as only resource for graphene formation. Not having to deal with precise concentration of carbon precursor gases greatly reduce the complexity of the growth process making it easier and cheaper.

In addition, the same CuNi foil could be used multiple time to successfully grow graphene. In this study the annealing process was repeated 5 time on each of the CuNi samples and it resulted in graphene monolayer for all annealing but the 5^{th}. In particular, graphene obtained with the 2^{nd}, 3^{rd} and 4^{th} annealing resulted to be of exceptional high-quality and all three films were found amazingly similar moth in morphology (optical microscopy) and in electronic structure (Raman spectroscopy). The used setup and method provided an overall good reproducibility, in particular during the central annealings.

Investigating the alloy composition throughout the different process steps was possible to extrapolate the carbon concentration trend, which gave deep insight about the synthesis dynamics and the role of dissolved carbon as carbon precursor for graphene production.

Bubbling transferring method demonstrated to be an effective way to safely transfer graphene from the CuNi foils to the target substrate, this technique saved the graphene integrity and consented to clean the metal surface between two steps. Without bubbling transfer would have not be possible to reiterate the annealings multiple time making impossible to proceed with this project.

4.2 Further studies

From the theoretical point of view, this set of experiments provides a lot of information about graphene growth dynamics with particular focus on the roles of metallic catalysts and carbon precursor. This process is pretty simple and does not involve any new or expansive technology which means it can be easily studied and adopted in almost any research or industrial environment. The possibility to grow graphene multiple times from the same catalyst without depleting it, simply through thermal annealing, is new and interesting by itself but it can be improved in many ways with further studies.

For example, this very method can be applied to many other metals and alloy compositions and graphene quality can be improved even further optimizing the metal mix. Moreover,

changing the metal catalyst composition it could be possible to selectively deposit multi- or monolayer graphene.

Beside the alloy, the annealing process can be improved as well. For this work, the annealing temperature was chosen to be less than the metal melting point, it had to be reproducible inside the used reactor chamber and was kept in line with temperatures used in common CVD deposition of graphene to avoid adding to many new factors to the study. In future studies, different temperatures might be tested to find the ideal annealing temperature. Also, the process duration was selected to be 10 minutes just to mimic common CVD duration, but, as far as our understanding goes, during the annealing itself not much is happening hence the time could probably be reduced greatly without experiencing much differences. Furthermore, what is thought to be one of the most important features of the process is the cooling rate, with the used setup the cooling rate was not tuneable beyond a small degree. This means it would be interesting to try different cooling rate in order to understand which condition best suits graphene formation.

On top all these, also the carbon-enriching system can be rethought. There is nothing bounding this method to use CVD to enrich the CuNi alloy, as a matter of facts the CVD was used only because there were no other available systems to obtain a carbon-rich CuNi foil, and metallurgy can borrow many cheaper technologies to achieve the same result in much easier ways.

Finally, from the obtained results, the proposed technology might work at atmospheric pressure as well. Graphene synthesis still needs a reducing agent to consume amorphous carbon and the metal foil needs to be protected from oxidation, but the same gases can work at atmospheric pressure without any additional issue. Avoiding a direct need for vacuum would reduce drastically costs and needed instrumentation. In this case as reducing agent nitrogen would be a better fit than hydrogen, it is much safer and can be used in an industrial environment without safety issues. In conclusion, this method opens to many innovation and improvement and might help graphene industrialization process drawing closer and closer the day when graphene will be used in the everyday life by all of us.

4.3 Outlooks

This method is based on a new concept that has not been reported before. Being free from the use of carbon precursor gas and giving as result CVD-quality graphene, the proposed technology can radically change the way graphene is integrated into industrial processes. One of the main outlooks for this technology is to be used as long-term storage mean for graphene. CuNi foil, independently of its chemical composition can be easily stored for years in common warehouse without deterioration, many other metal alloys can be stored in the same way and the use of grease could improve even further the shelf-life of the carbon-enriched metal. In this prospective, a metallic foil of the chosen alloy can be carbon-enriched by a graphene production company, coated with some grease and rolled in the form of a coil. The obtained coil can then be sold and shipped to the device manufacturing

company. Once arrived at the manufacturing company, the coil can be stored in the company warehouse until needed. When graphene is needed the coil can be unrolled and subjected to thermal treatment where graphene is formed on its surface. The grown graphene can then be transferred to the target substrate and used for any micro- or nanofabrication purpose. If bubble transferring is used, the same metallic foil might be used multiple times greatly reducing raw material and shipping costs, while allowing a more efficient storage yield. As exposed in the previous section, this method is for now only an embryo and many studies should be done on the argument, but in future the whole annealing process might be done at atmospheric pressure using already existing controlled atmosphere heat treatment ovens. These ovens are considered an expensive solution for thermal treatment in the metallurgy industry but, compared to the average costs that the semiconductor industry must face, it would be considered an extremely cheap solution for a highly technological product. In conclusion, this new technology has all the feature needed to have a significant impact on the graphene market. By reducing the risks of long-term storage, such as chemical or physical adsorption of substances that might change graphene properties, and subdividing the graphene making between the alloy producer and the device manufacturer this method might allow higher company specialization, be overall more efficient and more suitable for todays industry.

5. Acknowledgement

I want to acknowledge the support of prof. Jie Sun and prof. Yifeng Fu of Chalmers University of Technology (Sweden) for their support in all the lab procedures and in providing me guidance and the necessary training for the completion of my thesis work.

In addition, I have to be grateful to the Erasmus program and all the connection that Politecnico di Torino has across Europe and the world for giving me the possibility to study abroad in a prestigious university as Chalmers.

In conclusion, I am thankful to prof. Marco Sangermano who helped me through my period abroad and followed my progress making sure I had all I needed.

6. References

[1] Novoselov K S, Geim A K, Morozov S V, Jiang D, Zhang Y, Dubonos S V, Grigorieva I V and Firsov A A 2004 Electric Field Effect in Atomically Thin Carbon Films *Science* **306** 666–9

[2] Frank I W, Tanenbaum D M, van der Zande A M and McEuen P L 2007 Mechanical properties of suspended graphene sheets *J. Vac. Sci. Technol. B Microelectron. Nanometer Struct. Process. Meas. Phenom.* **25** 2558–61

[3] Castro Neto A H, Guinea F, Peres N M R, Novoselov K S and Geim A K 2009 The electronic properties of graphene *Rev. Mod. Phys.* **81** 109–62

[4] Kuila T, Bose S, Mishra A K, Khanra P, Kim N H and Lee J H 2012 Chemical functionalization of graphene and its applications *Prog. Mater. Sci.* **57** 1061–105

[5] Novoselov K S, Fal′ko V I, Colombo L, Gellert P R, Schwab M G and Kim K 2012 A roadmap for graphene *Nature* **490** 192–200

[6] Geim A K and Novoselov K S 2007 The rise of graphene *Nat. Mater.* **6** 183–91

[7] Schwierz F 2010 Graphene transistors *Nat. Nanotechnol.* **5** 487–96

[8] Lee X, Yang T, Li X, Zhang R, Zhu M, Zhang H, Xie D, Wei J, Zhong M, Wang K, Wu D, Li Z and Zhu H 2013 Flexible graphene woven fabrics for touch sensing *Appl. Phys. Lett.* **102** 163117

[9] Gao Z, Zhang Y, Fu Y, Yuen M M F and Liu J 2013 Thermal chemical vapor deposition grown graphene heat spreader for thermal management of hot spots *Carbon* **61** 342–8

[10] Subrina S, Kotchetkov D and Balandin A A 2009 Heat Removal in Silicon-on-Insulator Integrated Circuits With Graphene Lateral Heat Spreaders *IEEE Electron Device Lett.* **30** 1281–3

[11] Wu J, Agrawal M, Becerril H A, Bao Z, Liu Z, Chen Y and Peumans P 2010 Organic Light-Emitting Diodes on Solution-Processed Graphene Transparent Electrodes *ACS Nano* **4** 43–8

[12] Yin Z, Zhu J, He Q, Cao X, Tan C, Chen H, Yan Q and Zhang H 2014 Graphene-Based Materials for Solar Cell Applications *Adv. Energy Mater.* **4** 1300574

[13] Georgakilas V, Tiwari J N, Kemp K C, Perman J A, Bourlinos A B, Kim K S and Zboril R 2016 Noncovalent Functionalization of Graphene and Graphene Oxide for Energy Materials, Biosensing, Catalytic, and Biomedical Applications *Chem. Rev.* **116** 5464–519

[14] E. Maine P S 2016 Graphene steps into biomedicine *Nat. Mater.* **15** 485

[15] Wonbong Choi, Jo-won Lee 2011 Graphene: Synthesis and Applications *CRC Press*

[16] Li X, Colombo L and Ruoff R S 2016 Synthesis of Graphene Films on Copper Foils by Chemical Vapor Deposition *Adv. Mater.* **28** 6247–52

[17] Frank O and Kalbac M 2014 2 - Chemical vapor deposition (CVD) growth of graphene films *Graphene* ed V Skákalová and A B Kaiser (Woodhead Publishing) 27–49

[18] Seah C-M, Chai S-P and Mohamed A R 2014 Mechanisms of graphene growth by chemical vapour deposition on transition metals *Carbon* **70** 1–21

[19] Li X, Cai W, An J, Kim S, Nah J, Yang D, Piner R, Velamakanni A, Jung I, Tutuc E, Banerjee S K, Colombo L and Ruoff R S 2009 Large-Area Synthesis of High-Quality and Uniform Graphene Films on Copper Foils *Science* **324** 1312–4

[20] Gao L, Ren W, Xu H, Jin L, Wang Z, Ma T, Ma L-P, Zhang Z, Fu Q, Peng L-M, Bao X and Cheng H-M 2012 Repeated growth and bubbling transfer of graphene with millimetre-size single-crystal grains using platinum *Nat. Commun.* **3** 699

[21] Liu X, Fu L, Liu N, Gao T, Zhang Y, Liao L and Liu Z 2011 Segregation Growth of Graphene on Cu–Ni Alloy for Precise Layer Control *J. Phys. Chem. C* **115** 11976–82

[22] Zhang Y, Fu Y, Edwards M, Jeppson K, Ye L and Liu J 2017 Chemical vapor deposition grown graphene on Cu-Pt alloys *Mater. Lett.* **193** 255–8

[23] Lander J J, Kern H E and Beach A L 1952 Solubility and Diffusion Coefficient of Carbon in Nickel: Reaction Rates of Nickel-Carbon Alloys with Barium Oxide *J. Appl. Phys.* **23** 1305–9

[24] de la Rosa C J L, Sun J, Lindvall N, Cole M T, Nam Y, Löffler M, Olsson E, Teo K B K. and Yurgens A 2013 Frame assisted H2O electrolysis induced H2 bubbling transfer of large area graphene grown by chemical vapor deposition on Cu *Appl. Phys. Lett.* **102** 022101

[25] Blake P, Hill E W, Castro Neto A H, Novoselov K S, Jiang D, Yang R, Booth T J and Geim A K 2007 Making graphene visible *Appl. Phys. Lett.* **91** 063124

[26] Wu J-B, Lin M-L, Cong X, Liu H-N and Tan P-H 2018 Raman spectroscopy of graphene-based materials and its applications in related devices *Chem. Soc. Rev.* **47** 1822–73

[27] Graphene Flagship - https://graphene-flagship.eu/

[28] Hirsch A 2010 The era of carbon allotropes *Nat. Mater.* **9** 898-871

[29] Lee I, Park H-Y, Park J, Yoo G, Lim M-H, Park J, Rathi S, Jung W-S, Kim J, Kim S-W, Roh Y, Kim G-H and Park J-H 2014 Poly-4-vinylphenol and poly(melamine-co-formaldehyde)-based graphene passivation method for flexible, wearable and transparent electronics *Nanoscale* **6** 3830–6

[30] Shen J, Zhu Y, Yang X, Zong J, Zhang J and Li C 2012 One-pot hydrothermal synthesis of graphene quantum dots surface-passivated by polyethylene glycol and their photoelectric conversion under near-infrared light *New J. Chem.* **36** 97–101

[31] Balog R, Jørgensen B, Nilsson L, Andersen M, Rienks E, Bianchi M, Fanetti M, Lægsgaard E, Baraldi A, Lizzit S, Sljivancanin Z, Besenbacher F, Hammer B, Pedersen T G, Hofmann P and Hornekær L 2010 Bandgap opening in graphene induced by patterned hydrogen adsorption *Nat. Mater.* **9** 315–9

[32] Chan K T, Neaton J B and Cohen M L 2008 First-principles study of metal adatom adsorption on graphene *Phys. Rev. B* **77** 235430

[33] Leenaerts O, Partoens B and Peeters F M 2008 Adsorption of H2O, NH3, CO and NO on graphene: A first-principles study *Phys. Rev. B* **77** 125416

[34] Petroski H 1990 *The Pencil: A History of Design and Circumstance* (Knopf)

[35] Wallace P R 1947 The Band Theory of Graphite *Phys. Rev.* **71** 622–34

[36] Kresse G and Furthmüller J 1996 Efficient iterative schemes for ab initio total-energy calculations using a plane-wave basis set *Phys. Rev. B* **54** 11169–86

[37] Kresse G and Furthmüller J 1996 Efficiency of ab-initio total energy calculations for metals and semiconductors using a plane-wave basis set *Comput. Mater. Sci.* **6** 15–50

[38] Perdew J P, Ruzsinszky A, Csonka G I, Vydrov O A, Scuseria G E, Constantin L A, Zhou X and Burke K 2008 Restoring the Density-Gradient Expansion for Exchange in Solids and Surfaces *Phys. Rev. Lett.* **100** 136406

[39] Reich S, Maultzsch J, Thomsen C and Ordejón P 2002 Tight-binding description of graphene *Phys. Rev. B* **66** 035412

[40] Stolyarova E, Rim K T, Ryu S, Maultzsch J, Kim P, Brus L E, Heinz T F, Hybertsen M S and Flynn G W 2007 High-resolution scanning tunneling microscopy imaging of mesoscopic graphene sheets on an insulating surface *Proc. Natl. Acad. Sci.* **104** 9209–12

[41] Saito R, Dresselhaus G and Dresselhaus M S 1998 *Physical Properties of Carbon Nanotubes* (Imperial College Press - World Scientific)

[42] Novoselov K S, Geim A K, Morozov S V, Jiang D, Katsnelson M I, Grigorieva I V, Dubonos S V and Firsov A A 2005 Two-dimensional gas of massless Dirac fermions in graphene *Nature* **438** 197–200

[43] Haldane F D M 1988 Model for a Quantum Hall Effect without Landau Levels: Condensed-Matter Realization of the "Parity Anomaly" *Phys. Rev. Lett.* **61** 2015–8

[44] Greiner W 1985 Quantum electrodynamics of strong fields *Hadrons and Heavy Ions* Lecture Notes in Physics (Springer, Berlin, Heidelberg) 95–226

[45] Katsnelson M I, Novoselov K S and Geim A K 2006 Chiral tunnelling and the Klein paradox in graphene *Nat. Phys.* **2** 620–5

[46] Piscanec S, Lazzeri M, Mauri F and Ferrari A C 2007 Optical phonons of graphene and nanotubes *Eur. Phys. J. Spec. Top.* **148** 159–70

[47] Charlier J-C, Eklund P C, Zhu J and Ferrari A C 2007 Electron and Phonon Properties of Graphene: Their Relationship with Carbon Nanotubes *Carbon Nanotubes* Topics in Applied Physics (Springer, Berlin, Heidelberg) pp 673–709

[48] Bolotin K I, Sikes K J, Jiang Z, Klima M, Fudenberg G, Hone J, Kim P and Stormer H L 2008 Ultrahigh electron mobility in suspended graphene *Solid State Commun.* **146** 351–5

[49] Hwang E H and Das Sarma S 2008 Acoustic phonon scattering limited carrier mobility in two-dimensional extrinsic graphene *Phys. Rev. B* **77** 115449

[50] Rosa Axet M, Bacsa R R, Machado B F and Serp P 2013 Adsorption on and Reactivity of Carbon Nanotubes and Graphene *Handbook of Carbon Nano Materials* World Scientific Series on Carbon Nanoscience vol Volume 5 & 6 (World Scientific) pp 39–183

[51] Radovic L R 2009 Active Sites in Graphene and the Mechanism of CO2 Formation in Carbon Oxidation *J. Am. Chem. Soc.* **131** 17166–75

[52] Ataca C, Aktürk E, Şahin H and Ciraci S 2011 Adsorption of carbon adatoms to graphene and its nanoribbons *J. Appl. Phys.* **109** 013704

[53] Robertson A W, Bachmatiuk A, Wu Y A, Schäffel F, Rellinghaus B, Büchner B, Rümmeli M H and Warner J H 2011 Atomic Structure of Interconnected Few-Layer Graphene Domains *ACS Nano* **5** 6610–8

[54] Georgakilas V, Otyepka M, Bourlinos A B, Chandra V, Kim N, Kemp K C, Hobza P, Zboril R and Kim K S 2012 Functionalization of Graphene: Covalent and Non-Covalent Approaches, Derivatives and Applications *Chem. Rev.* **112** 6156–214

[55] Dmitriev S V, Baimova J A, Savin A V and Kivshar Y S 2012 Ultimate strength, ripples, sound velocities, and density of phonon states of strained graphene *Comput. Mater. Sci.* **53** 194–203

[56] Scarpa F, Adhikari S and Phani A S 2009 Effective elastic mechanical properties of single layer graphene sheets *Nanotechnology* **20** 065709

[57] Balandin A A 2011 Thermal Properties of Graphene, Carbon Nanotubes and Nanostructured Carbon Materials *Nat. Mater.* **10** 569–81

[58] Balandin A A, Ghosh S, Bao W, Calizo I, Teweldebrhan D, Miao F and Lau C N 2008 Superior Thermal Conductivity of Single-Layer Graphene *Nano Lett.* **8** 902–7

[59] Wassei J K and Kaner R B 2010 Graphene, a promising transparent conductor *Mater. Today* **13** 52–9

[60] Bonaccorso F, Sun Z, Hasan T and Ferrari A C 2010 Graphene Photonics and Optoelectronics *Nat. Photonics* **4** 611–22

[61] Bussy C, Ali-Boucetta H and Kostarelos K 2013 Safety Considerations for Graphene: Lessons Learnt from Carbon Nanotubes *Acc. Chem. Res.* **46** 692–701

[62] Baccarani G, Wordeman M R and Dennard R H 1984 Generalized scaling theory and its application to a 1/4 micrometer MOSFET design *IEEE Trans. Electron Devices* **31** 452–62

[63] S. I. Association 2007 The International Technology Roadmap for Semiconductors

[64] Liang G, Neophytou N, Nikonov D E and Lundstrom M S 2007 Performance Projections for Ballistic Graphene Nanoribbon Field-Effect Transistors *IEEE Trans. Electron Devices* **54** 677–82

[65] Cheli M, Michetti P and Iannaccone G 2010 Model and Performance Evaluation of Field-Effect Transistors Based on Epitaxial Graphene on SiC *IEEE Trans. Electron Devices* **57** 1936–41

[66] Wang H, Hsu A, Kong J, Antoniadis D A and Palacios T 2011 Compact Virtual-Source Current 2013; Voltage Model for Top- and Back-Gated Graphene Field-Effect Transistors *IEEE Trans. Electron Devices* **58** 1523–33

[67] Chico L, Crespi V H, Benedict L X, Louie S G and Cohen M L 1996 Pure Carbon Nanoscale Devices: Nanotube Heterojunctions *Phys. Rev. Lett.* **76** 971–4

[68] Schwierz F 2015 Graphene and beyond: two-dimensional materials for transistor applications Micro- and Nanotechnology Sensors, Systems, and Applications VII vol 9467 (International Society for Optics and Photonics) p 94670W

[69] Lin Y-M, Jenkins K A, Valdes-Garcia A, Small J P, Farmer D B and Avouris P 2009 Operation of Graphene Transistors at Gigahertz Frequencies *Nano Lett.* **9** 422–6

[70] Fan L-Z, Liu J-L, Ud-Din R, Yan X and Qu X 2012 The effect of reduction time on the surface functional groups and supercapacitive performance of graphene nanosheets *Carbon* **50** 3724–30

[71] Chen S, Zhu J, Wu X, Han Q and Wang X 2010 Graphene Oxide−MnO2 Nanocomposites for Supercapacitors *ACS Nano* **4** 2822–30

[72] Bose S, Kim N H, Kuila T, Lau K and Lee J H 2011 Electrochemical performance of a graphene–polypyrrole nanocomposite as a supercapacitor electrode *Nanotechnology* **22** 295202

[73] Liang M and Zhi L 2009 Graphene-based electrode materials for rechargeable lithium batteries *J. Mater. Chem.* **19** 5871–8

[74] Yoo E, Kim J, Hosono E, Zhou H, Kudo T and Honma I 2008 Large Reversible Li Storage of Graphene Nanosheet Families for Use in Rechargeable Lithium Ion Batteries *Nano Lett.* **8** 2277–82

[75] Zhou G, Wang D-W, Li F, Zhang L, Li N, Wu Z-S, Wen L, Lu G Q (Max) and Cheng H-M 2010 Graphene-Wrapped Fe3O4 Anode Material with Improved Reversible Capacity and Cyclic Stability for Lithium Ion Batteries *Chem. Mater.* **22** 5306–13

[76] Cao F-F, Deng J-W, Xin S, Ji H-X, Schmidt O G, Wan L-J and Guo Y-G 2011 Cu-Si Nanocable Arrays as High-Rate Anode Materials for Lithium-Ion Batteries *Adv. Mater.* **23** 4415–20

[77] Mahmood N, Zhang C, Yin H and Hou Y 2014 Graphene-based nanocomposites for energy storage and conversion in lithium batteries, supercapacitors and fuel cells *J. Mater. Chem. A* **2** 15–32

[78] Meiss J, Riede M K and Leo K 2009 Towards efficient tin-doped indium oxide (ITO)-free inverted organic solar cells using metal cathodes *Appl. Phys. Lett.* **94** 013303

[79] Lee J-Y, Connor S T, Cui Y and Peumans P 2008 Solution-Processed Metal Nanowire Mesh Transparent Electrodes *Nano Lett.* **8** 689–92

[80] Patra A, Wijsboom Y H, Zade S S, Li M, Sheynin Y, Leitus G and Bendikov M 2008 Poly(3,4-ethylenedioxyselenophene) *J. Am. Chem. Soc.* **130** 6734–6

[81] Wu Z, Chen Z, Du X, Logan J M, Sippel J, Nikolou M, Kamaras K, Reynolds J R, Tanner D B, Hebard A F and Rinzler A G 2004 Transparent, Conductive Carbon Nanotube Films *Science* **305** 1273–6

[82] Li X, Cai W, Colombo L and Ruoff R S Evolution of graphene growth on Cu and Ni studied by carbon isotope labelling *Nano Lett.* Vol. 12 **9** 4268-4272

[83] Kim K S, Zhao Y, Jang H, Lee S Y, Kim J M, Kim K S, Ahn J-H, Kim P, Choi J-Y and Hong B H 2009 Large-scale pattern growth of graphene films for stretchable transparent electrodes *Nature* **457** 706–10

[84] Famm K, Litt B, Tracey K J, Boyden E S and Slaoui M 2013 Drug discovery: A jump-start for electroceuticals *Nature* **496** 159

[85] Goenka S, Sant V and Sant S 2014 Graphene-based nanomaterials for drug delivery and tissue engineering *J. Controlled Release* **173** 75–88

[86] Liu J, Cui L and Losic D 2013 Graphene and graphene oxide as new nanocarriers for drug delivery applications *Acta Biomater.* **9** 9243–57

[87] Liang X, Fu Z and Chou S Y 2007 Graphene Transistors Fabricated via Transfer-Printing In Device Active-Areas on Large Wafer *Nano Lett.* **7** 3840–4

[88] Viculis L M, Mack J J, Mayer O M, Hahn H T and Kaner R B 2005 Intercalation and exfoliation routes to graphite nanoplatelets *J. Mater. Chem.* **15** 974–8

[89] Brodie B C 1859 On the Atomic Weight of Graphite *Philos. Trans. R. Soc. Lond.* **149** 249–59

[90] Staudenmaier L 1898 Verfahren zur Darstellung der Graphitsäure *Berichte Dtsch. Chem. Ges.* **31** 1481–7

[91] Hummers W S and Offeman R E 1958 Preparation of Graphitic Oxide *J. Am. Chem. Soc.* **80** 1339–1339

[92] Sundaram R S 2014 3 - Chemically derived graphene *Graphene* ed V Skákalová and A B Kaiser (Woodhead Publishing) pp 50–80

[93] Szabó T, Berkesi O, Forgó P, Josepovits K, Sanakis Y, Petridis D and Dékány I 2006 Evolution of Surface Functional Groups in a Series of Progressively Oxidized Graphite Oxides *Chem. Mater.* **18** 2740–9

[94] Stankovich S, Dikin D A, Piner R D, Kohlhaas K A, Kleinhammes A, Jia Y, Wu Y, Nguyen S T and Ruoff R S 2007 Synthesis of graphene-based nanosheets via chemical reduction of exfoliated graphite oxide *Carbon* **45** 1558–65

[95] Shin H-J, Kim K K, Benayad A, Yoon S-M, Park H K, Jung I-S, Jin M H, Jeong H-K, Kim J M, Choi J-Y and Lee Y H 2009 Efficient Reduction of Graphite Oxide by Sodium Borohydride and Its Effect on Electrical Conductance *Adv. Funct. Mater.* **19** 1987–92

[96] Gómez-Navarro C, Weitz R T, Bittner A M, Scolari M, Mews A, Burghard M and Kern K 2007 Electronic Transport Properties of Individual Chemically Reduced Graphene Oxide Sheets *Nano Lett.* **7** 3499–503

[97] Huang H, Chen S, Wee A T S and Chen W 2014 1 - Epitaxial growth of graphene on silicon carbide (SiC) *Graphene* ed V Skákalová and A B Kaiser (Woodhead Publishing) pp 3–26

[98] Chen W and Wee A T S 2007 Self-assembly on silicon carbide nanomesh templates *J. Phys. Appl. Phys.* **40** 6287

[99] Kim S, Ihm J, Choi H J and Son Y-W 2008 Origin of Anomalous Electronic Structures of Epitaxial Graphene on Silicon Carbide *Phys. Rev. Lett.* **100** 176802

[100] Huang H, Chen W, Chen S and Wee A T S 2008 Bottom-up Growth of Epitaxial Graphene on 6H-SiC(0001) *ACS Nano* **2** 2513–8

[101] Mattevi C, Kim H and Chhowalla M 2011 A review of chemical vapour deposition of graphene on copper *J. Mater. Chem.* **21** 3324–34

[102] Ago H, Ogawa Y, Tsuji M, Mizuno S and Hibino H 2012 Catalytic Growth of Graphene: Toward Large-Area Single-Crystalline Graphene *J. Phys. Chem. Lett.* **3** 2228–36

[103] Reina A, Jia X, Ho J, Nezich D, Son H, Bulovic V, Dresselhaus M S and Kong J 2009 Large Area, Few-Layer Graphene Films on Arbitrary Substrates by Chemical Vapor Deposition *Nano Lett.* **9** 30–5

[104] Sun J, Lindvall N, Cole M T, Teo K B K and Yurgens A 2011 Large-area uniform graphene-like thin films grown by chemical vapor deposition directly on silicon nitride *Appl. Phys. Lett.* **98** 252107

[105] Kim K-B, Lee C-M and Choi J 2011 Catalyst-Free Direct Growth of Triangular Nano-Graphene on All Substrates *J. Phys. Chem. C* **115** 14488–93

[106] Kang J, Shin D, Bae S and Hong B H 2012 Graphene transfer: key for applications *Nanoscale* **4** 5527–37

[107] Wu T, Zhang X, Yuan Q, Xue J, Lu G, Liu Z, Wang H, Wang H, Ding F, Yu Q, Xie X and Jiang M 2016 Fast growth of inch-sized single-crystalline graphene from a controlled single nucleus on Cu–Ni alloys *Nat. Mater.* **15** 43–7

[108] Hulman M 2014 7 - Raman spectroscopy of graphene *Graphene* ed V Skákalová and A B Kaiser (Woodhead Publishing) pp 156–83

[109] Ferrari A C 2007 Raman spectroscopy of graphene and graphite: Disorder, electron–phonon coupling, doping and nonadiabatic effects *Solid State Commun.* **143** 47–57

[110] Meyer J C 2014 5 - Transmission electron microscopy (TEM) of graphene *Graphene* ed V Skákalová and A B Kaiser (Woodhead Publishing) pp 101–23

[111] Meyer J C, Geim A K, Katsnelson M I, Novoselov K S, Obergfell D, Roth S, Girit C and Zettl A 2007 On the roughness of single- and bi-layer graphene membranes *Solid State Commun.* **143** 101–9

[112] Bae S, Kim S J, Shin D, Ahn J-H and Hong B H 2012 Towards industrial applications of graphene electrodes *Phys. Scr.* **2012** 014024

[113] Park S 2016 The puzzle of graphene commercialization *Nat. Rev. Mater.* **1** 16085